The Influence of *Escherichia coli* Metabolism on Antibiotic Resistance

Dissertation

der Mathematisch-Naturwissenschaftlichen Fakultät

der Eberhard Karls Universität Tübingen

zur Erlangung des Grades eines

Doktors der Naturwissenschaften

(Dr. rer. nat.)

vorgelegt von

Paul Lubrano

aus Paris, Frankreich

Tübingen

2024

Gedruckt mit Genehmigung der Mathematisch-Naturwissenschaftlichen Fakultät der Eberhard Karls Universität Tübingen.

Tag der mündlichen Qualifikation:	24.09.2024
Dekan:	Prof. Dr. Thilo Stehle
1. Berichterstatter/-in:	Prof. Dr. Hannes Link
2. Berichterstatter/-in:	Prof. Dr. Heike Brötz-Oesterhelt

Acknowledgment

Long years of work finally come to an end. It is with great emotion that I am writing these words. Looking back on my life, I can safely say that I have been immensely privileged to know exceptional people that guided me and permitted me to reach this far.

I was blessed with supervisors which taught me well how to become a scientist, and ignited the spark that drives my thirst for knowledge. How could I forget Dr. Agnès Saint-Pol, who took me under her wings as I was full of doubt, and made me understand that I could find my place in science? How not to mention the amazing team of Biosyntia and my mentors Luisa, Nils, Lasse and Carlos? It is Carlos which advised me to join the Max Planck Institute of microbiology. While I was preparing the application process, I was gifted by the kindness of Dr. Yanyan Li which offered me yet another thrilling experience and a short return to my home country. Finally, I joined Marburg and the Link Lab. Of all the supervisors I could have had for this adventure, Hannes was probably the best. Hannes provided me with his knowledge, and helped me to become a scientist and finish my formation. Your patience and honesty have been inspiring. I will miss our fiery yet fruitful discussions. Thank you for everything.

I would also like to thank Dr. Ilka Bischofs-Pfeifer, Prof. Heike Brötz-Oesterhelt, Prof. Tobias Erb, Prof. Lisa Maier and Prof. Klaus Hantke for their guidance and time, as well as the IMPRS and IGIM doctoral schools. Finally, I cannot omit Dr. Vanessa Proux for her work as head of Sup'Biotech, a place where I have built many of the foundations for my work.

Wherever I went, I was also happy to find amazing colleagues, many of which became my friends. I would like to thank the entirety of the Link Lab which made this thesis such a special experience. I would like to specifically thank Elisabeth, Nils and Amelie for being such capable and awesome students which I was happy to supervise.

It is France towards which my eyes are turned now. As I owe my country, I also owe Germany. I chose it as I believed that I should finish my formation where science has such a prestigious history. I received much, and I will never forget what Germany has done for me. However, my place is with my people, friends and family.

Car oui, je n'oublie pas ce que mon pays, mes amis et mes parents ont fait pour moi. Quels que soient mes choix, ils m'ont toujours supporté. J'avais un monde derrière moi. Merci à vous tous. Papa, Maman, je ne suis pas le plus expressif, mais j'espère que ce travail démontre mon amour pour vous. Cette thèse est aussi la vôtre. Merci.

Table of content

Abbreviations

Abbreviation	Meaning
ESKAPE	*Enterococcus faecium*, *Staphylococcus aureus*, *Klebsiella pneumoniae*, *Acinetobacter braumanii*, *Pseudomonas aeruginosa* and *Enterobacter* species
UPEC	Uropathogenic *E. coli*
PBP	Penicillin binding protein
AG	Aminoglycoside
RNA	Ribonucleic acid
DNA	Desoxyribonucleic acid
PMF	Proton motive force
ARB	Antibiotic resistant bacteria
MIC	Minimal inhibitory concentration
MDK	Minimal duration for killing
MBC	Minimal bactericidal concentration
TK	Time-kill
CFU	Colony forming unit
OD	Optical density
LB	Lysogeny broth
RC	Respiratory chain
ETC	Electron transport chain
TCA	Tricarboxylic acid
HPLC	High-pressure liquid chromatography
TQ	Triple-quadrupole
FI	Flow injection
TOF	Time-of-flight
MS	Mass spectrometer
m/z	Mass over charge
ROS	Reactive oxygen species
CREATE	CRISPR-enabled trackable genome engineering
CRISPR	Clustered regularly interspaced short palindromic repeats
sgRNA	Single-guide RNA
bp	Base pair
PAM	Protospacer adjacent motif
DSB	Double-strand break
dsDNA	Double-stranded DNA
aTc	Anhydrotetracycline
NGS	Next generation sequencing
GC	Guanine-cytosine
CRISPRi	CRISPR interference
dCas9	Deactivated Cas9

PCR	Polymerase chain reaction
tRNA	Transfer RNA
DWP	Deep-well plate
RPM	Rotation per minute
AMR	Antimicrobial resistance
PTS	Phosphotransferase system
MALDI	Matrix-assisted laser desorption/ionisation
SOC	Super optimal medium with catabolic repressor
6-MP	6-mercaptopurine
AEC	Adenylate energy charge
FC	Fold-change
qPCR	Real-time polymerase chain reaction
mRNA	Messenger RNA

Metabolite abbreviations

Note: in the text, capital letters abbreviations are used for metabolites when needed. Figures use BiGG abbreviations for convenience. If any metabolite is present in the text and figures, both abbreviations are indicated in bracket.

Abbreviation	Meaning	BiGG
NADH	β-nicotinamide adenine dinucleotide, reduced	nadh
ATP	Adenosine-triphosphate	atp
NAD+	β-nicotinamide adenine dinucleotide, oxydised	nad
ADP	Adenosine-biphosphate	adp
IMP	Inosine-monophosphate	imp
XMP	xanthosine-monophosphate	xmp
	Adenylosuccinate	dcamp
GMP	Guanosine-monophosphate	gmp
AMP	Adenosine-monophosphate	amp
GDP	Guanosine-biphosphate	gdp
PRPP	5-phosphoribosylpyrophosphate	prpp
PRA	5-phospho-β-D-ribosylamine	pram
	phosphoribosyl-ATP	prbatp
AICAR	5-amino-1-(5-phospho-D-ribosyl) imidazole-4-carboxamide	aicar
FAICAR	5-formamido-1-(5-phospho-D-ribosyl)-imidazole-4-carboxamide	fprica
MEP	Methylerythrol-phosphate	2me4p
FAD	Flavin adenine dinucleotide	fad
FGAM	2-(formamido)-N1-(5-phospho-β-D-ribosyl)acetamidine	fpram
	Hisitidinol	histd
PEP	Phosphoenolpyruvate	pep
	Succinate	succ
G6P	β-D-glucose-6-P	g6p
5-ALA	5-aminolevulinic acid	5aop
AIR	5-amino-1-(5-phospho-β-D-ribosyl)imidazole	air
	Histidinol-phosphate	hisp
	Cystathionine	cyst

Abstract

Antibiotics are important tools to fight bacteria in complement to vaccines and public hygiene regulation. Antibiotics are molecules that interfere with key bacterial processes, ranging from translation and transcription to cell wall synthesis. This results in arrest of bacterial proliferation. Because of the selective pressure antibiotics impose on microbes, they are challenged by the formidable capacities of evolution. Indeed, bacteria have been shown to counteract antibiotics through multiple strategies, either at population or clonal levels. This is notably the case for ESKAPE pathogens (*Enterococcus faecium*, Staphylococcus aureus, *Klebsiella pneumoniae*, *Acinetobacter braumannii*, *Pseudomonas aeruginosa* and species of the genus *Enterobacter*). These bacterial species quickly evolve escape mechanisms to currently used antibiotics as well as new-to-market antibiotics.

Two main routes of antibiotic escape are resistance and tolerance. Antibiotic tolerance permits to withstand antibiotic treatment for a longer period of time while antibiotic resistance allows to grow in the presence of the antibiotic at normally non-permissive concentrations. Resistant or tolerant pathogens often require the use of last-resort antibiotics or longer and heavier treatments to be eradicated. However, these alternatives are also met with evolutionary escape while the development of new antibiotics takes a substantial time. This leads to a sharp decrease of new antibiotic development and ever-increasing pressure on health authorities. Therefore, it is pressing to understand evolutionary strategies employed by bacterial pathogens to escape antibiotic treatment in order to anticipate and counter them.

One key evolutionary weapon is the acquisition of genomic mutations that confer antibiotic resistance or tolerance. Some of these mutations have relatively trivial effects. Mutations in the direct target of an antibiotic alter binding interactions and nullify antibiotic effects. Efflux pumps regulators can also be mutated to affect antibiotic import or export towards their targets.

More recently, mutations in core metabolic genes have been shown to affect antibiotic treatments. However, how these mutations affect metabolism and lead to antibiotic treatment failure remains poorly understood. It is generally assumed that antibiotic treatments could be globally affected by a general "metabolic state", or metabolic-

dependent phenomenon such as growth rate. However, these observations were made while studying antibiotic tolerance and not antibiotic resistance. Whether a general "metabolic state" could confer resistance to multiple antibiotics remains unknown.

Here is presented a body of work that investigates the link between metabolism and antibiotic treatment in the ESKAPE pathogen *Escherichia coli* with a focus on antibiotic resistance. The following question is formulated for this thesis: **Do mutations in metabolic genes of *E. coli* have a general impact on antibiotic resistance?**

This thesis will first present a general introduction of its scientific **framework**. **Chapter 1** discusses the elaboration of the main tool used in the thesis: a library of *E. coli* strains each with a genomic mutation in an essential gene. **Chapter 2** covers the main body of work done in this thesis and present its most important findings. **Chapter 3** further discusses findings made in Chapter 2 and provides additional experiments and hypothesis.

Zusammenfassung

Antibiotika sind wichtige Instrumente zur Bekämpfung von bakteriellen Infektionen und ergänzen Impfstoffe sowie öffentliche Hygienevorschriften. Diese Moleküle zielen auf wichtige bakterielle Prozesse ab, von der Translation und Transkription bis zur Zellwandsynthese. Sie bewirken häufig eine Unterbrechung dieser essentiellen Prozesse, was zu einer Hemmung des bakteriellen Wachstums führt. Durch den selektiven Druck, den die Antibiotika auf die Mikroorganismen ausüben, werden diese durch die Kapazitäten der Evolution herausgefordert. Bakterien können Antibiotika durch verschiedene Strategien entgegenwirken, entweder auf Populations- oder auf klonaler Ebene. Dies ist insbesondere bei ESKAPE-Erregern (*Enterococcus faecium*, *Staphylococcus aureus*, *Klebsiella pneumoniae*, *Acinetobacter braumanii*, *Pseudomonas aeruginosa* und Arten der Gattung *Enterobacter*) der Fall. Diese Bakterienarten entwickeln schnell Mechanismen, um den derzeit verwendeten Antibiotika zu entkommen.

Es gibt dabei zwei Hauptwege: Resistenz und Toleranz. Die Toleranz ermöglicht es einer Antibiotikabehandlung über einen längeren Zeitraum standzuhalten. Die Antibiotikaresistenz hingegen ermöglicht den Mikroorganismen in Gegenwart von normalerweise tödlichen Antibiotikakonzentrationen zu wachsen. Resistente oder tolerante Erreger erfordern häufig den Einsatz von sogenannten ‚Last-Resort' Antibiotika,als letzte Mittel, sowie längere oder stärkere Behandlungen, um die Erreger in ihrem Wachstum zu hemmen. Aber auch diese alternativen Behandlungen können zu Resistenz- oder Toleranzentwicklungen der Bakterien führen. Zudem nimmt die Erforschung neuer Antibiotika zusätzlich viel Zeit in Anspruch. Dies führt zu einem starken Rückgang der Entwicklung neuer antimikrobieller Wirkstoffe und zu einem immer größeren Druck auf die Gesundheitsbehörden. Daher ist es dringend erforderlich, die evolutionären Strategien der Mikroorganismen zu verstehen, damit sie bekämpft werden können.

Eine wichtige evolutionäre Waffe ist der Erwerb von Genommutationen, die eine Antibiotikaresistenz oder -toleranz vermitteln können. Einige dieser Mutationen können triviale Auswirkungen haben. Mutationen in der direkten Zielstruktur eines Antibiotikums verändern die Bindungsinteraktionen und heben die Wirkung des

Antibiotikums auf. Auch die Regulatoren von Effluxpumpen können mutiert werden und somit den Import oder Export von Antibiotika in Richtung ihrer Ziele beeinflussen.

In der Vergangenheit hat sich gezeigt, dass auch Mutationen in Genen des zentralen Stoffwechsels die Antibiotikabehandlung beeinflussen können. Wie sich diese Mutationen auf den Stoffwechsel auswirken und zu einer reduzierten Wirksamkeit der Antibiotika führen können, ist jedoch nach wie vor kaum erforscht. Im Allgemeinen wird davon ausgegangen, dass Antibiotikabehandlungen durch einen allgemeinen "Stoffwechselzustand" oder durch stoffwechselabhängige Eigenschaften wie die Wachstumsrate beeinflusst werden könnten. Diese Beobachtungen wurden jedoch bei der Untersuchung der Antibiotikatoleranz und nicht der Antibiotikaresistenz gemacht. Ob ein allgemeiner "Stoffwechselzustand" eine Resistenz gegen mehrere Antibiotika bewirken kann, ist nach wie vor unbekannt.

In dieser Arbeit wird der Zusammenhang zwischen Stoffwechsel und Antibiotikabehandlung bei dem ESKAPE-Erreger *Escherichia coli* mit dem Schwerpunkt Antibiotikaresistenz untersucht. Für diese Arbeit wurde die folgende Frage formuliert: **Haben Mutationen in Stoffwechselgenen von *E. coli* einen generellen Einfluss auf die Antibiotikabehandlung?**

Zunächst wird eine allgemeine Einführung in den wissenschaftlichen **Rahmen** gegeben. **Kapitel 1** behandelt die Ausarbeitung des wichtigsten Instruments, das in dieser Arbeit verwendet wird: eine ‚Library' von *E. coli*-Stämmen, die jeweils genomische Mutationen in wichtigen Genen aufweisen. Das **Kapitel 2** umfasst den Hauptteil der durchgeführten Experimente und stellt die wichtigsten Ergebnisse vor. **In Kapitel 3** werden weitere Erkenntnisse aus Kapitel 2 erörtert und zusätzliche Experimente und Hypothesen vorgestellt.

__Thesis framework__

Escherichia coli

The bacteria *Escherichia coli* is a facultative anaerobe estimated to be present in the intestinal microbiome of more than 90% of humans, either as pathogen or commensal[1]. It has been shown to represent less than 0.1 % of the total human gut microbiota bacterial population[2]. *E. coli* is one of the most studied and understood organism to date[3]. Because of its high robustness, versatility, and amenability for genetic manipulation, it has become a crucial model for microbiology and a key workhouse for industrial biotechnology[4]. Currently, hundreds of thousands of *E. coli* genomes are available on public databases such as EnteroBase[5] and contribute to an extensive knowledge on population structures and dynamics. *E. coli* is a polyclonal species which contains multiple phylogroups[a] adapted to various ecological niches[1,6]. Indeed, this species can colonise multiple environments other than the gut and contributes to multiple diseases[7]. Most of *E. coli* pathotypes[b] (enteropathogenic *E. coli*, enterotoxigenic *E. coli* …) are human gut pathogens that cause severe diarrhoea. *E. coli* can also colonise the urinary tract (uropathogenic *E. coli*, UPEC)[8] or the blood and the meninges (sepsis — meningitis-associated *E. coli*)[9], which makes it a key human pathogen.

However, *E. coli* is also a powerful ally for human research. This is notably the case for laboratory strains such as *E. coli* BW25113. This strain is a derivative of *E. coli* K-12 and was originally used for lambda-red mediated genome editing[10] (see later section). It was the host chosen for the Keio collection, a library of more than 4000 *E. coli* mutants each with a gene knock-out[11] and its genome has been sequenced[12].

E. coli K-12 is a member of the A phylogroup[1,13], and *E. coli* strains can very highly within and between phylogroups[14]. As a consequence, *E. coli* K-12 is a model organism and extrapolation of findings made in this strain to other *E. coli* strains and other organisms remains challenging. Nevertheless, it was chosen for this thesis

---

[a] "Groups of organisms that belong to a large phylogenetic entity within the species. There are at least eight phylogenetic groups within the *Escherichia coli* species, named A, B1, B2, C, D, E, F and G."[6]

[b] "Groups of organisms that have the same pathogenicity on a specified host."[6]

because it is easy to handle and to genetically modify. This is especially important when using libraries (see later sections). Chapter 2 notably covers the extension of findings made in *E. coli* BW25113 to pathogenic *E. coli*.

Antibiotics

Antibiotics are molecules capable of interfering with various bacterial processes. This can result in the lysis of the target bacteria (bactericide antibiotics) or the arrest of its division (bacteriostatic antibiotics), although debates exist in the literature on the clinical relevance of this mechanistic opposition[15,16]. On Earth, antibiotics are produced by multiple organisms (from fungus to bacteria) and thought to be used as a weapon to compete for ecological niches[17,18]. Due to their effects on bacterial growth, antibiotics are used by the human species to fight diseases since 1910 and the commercialisation of salvarsan to treat syphilis[19,20]. As such, they are of prime importance for public hygiene although their accessibility and consumption has been shown to be uneven between countries[21].

In general, antibiotics bind a cellular target (generally an essential protein) and inhibit its functions, leading to severe consequences. Antibiotics belong to multiple classes which are chemically different in their structure as well as their modes of actions. Here will be described the two antibiotic families involved in this thesis: β-lactams and aminoglycosides.

β-lactams share a common molecular backbone named β-lactam ring. They are used to combat an extensive number of bacterial pathogens, either gram-positive (*Streptococcus spp.*, *Staphylococcus aureus*…) or gram-negative (*Acinetobacter spp.*, *E. coli*, *Pseudomonas aeruginosa*…)[22]. The first β-lactam to be industrially produced was penicillin in 1940 and was discovered in the fungi *Penicillium notatum* by Alexander Fleming in early 1930's[23]. The β-lactams family is divided into several subclasses (penam, penem, carbapenem, cefem and monobactam) which differ in their structure through various moieties attached to the β-lactam ring, with exception for monobactams[24]. β-lactams bind and inhibit penicillin binding proteins (PBPs), a family of proteins essential for the synthesis of peptidoglycan through their transpeptidase activity[25]. In gram-negative bacteria such as *E. coli*, peptidoglycan is assembled in the periplasm, which is the space between the outer and inner

membranes[26]. Therefore, to bind gram-negative PBPs, β-lactams need to pass the outer membrane with passive transport relying on porins like OmpF[27].

The peptidoglycan is crucial for preserving cell shape. Its perturbation leads to destabilisation of bacterial cell wall integrity, which has been proposed to be the main cause of β-lactam-mediated cell lysis, although this remains poorly understood[28–31]. Several studies have shown that β-lactams, depending on their structure, more favourably bind one PBP over others[32–34]. Since PBPs do not have the same role in peptidoglycan synthesis[35], β-lactams may induce different morphological changes[36,37]. For example, cephalexin and ampicillin induce cell elongation through their affinity to PBP3 which leads to septation arrest[38]. Cefsulodin targets PBP1 and induces bulging without blocking cell septation, a property shared with imipenem which targets PBP2[39]. It has also been proposed that β-lactams could lead to futile cycles in peptidoglycan assembly which could deplete cell resources and contribute to killing[40].

Another key family of antibiotics used in this thesis is the aminoglycosides (AGs) family. In early 1940's, Albert Schatz was the first to isolate an AG, called Streptomycin from *Streptomyces griseus*[41]. AGs mostly bind the A-site of the 30S ribosome subunit, responsible for the docking of charged t-RNA which ensures translational fidelity[42]. AGs binding leads to protein synthesis destabilisation, which is thought to cause cell death through accumulation of faulty polypeptides damaging the cell[43,44]. Because they target the ribosome, AGs have a broad spectrum of activity against multiple pathogens from *E. coli* to *S. aureus*[45]. The AGs family is composed of multiple members which share a core amino sugars structure linked with glycosidic linkages and aminocyclitol moieties, the nature of which classifies them in four subclasses[45]. Because they target ribosomes, AGs require to be transported in the bacterial cytosol. In gram-negative bacteria, this transportation relies on ionic binding to the outer membrane, followed by a respiratory chain and proton motive force (PMF) mediated import to reach the cytosol owing to the polycationic nature of AGs [46–48].

The antibiotics used in this dissertation are three β-lactams (carbenicillin, aztreonam, meropenem) and two AGs (gentamicin and tobramycin), with a strong focus on carbenicillin and gentamicin (**Table 1**).
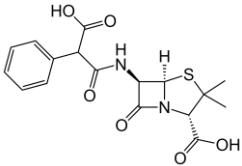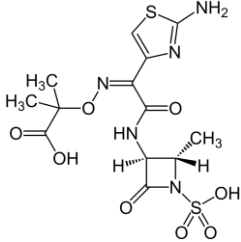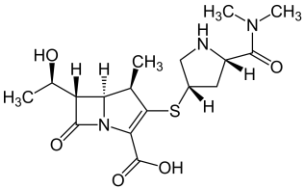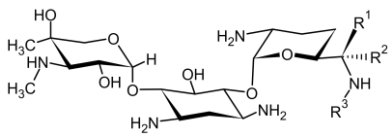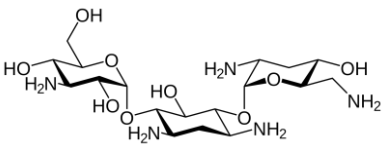
Name	Class	Target	Critically important medicines[49]/ essential medicines[50]	Structure[c]
Carbenicillin	β-lactams	Preferably binds PBP3 and PBP4 in *P. aeruginosa*[51,52]	Yes/No	
Aztreonam	β-lactams	Binds PBP3 in *P. aeruginosa*[51] and *E. coli*[53]	Yes/No	
Meropenem	β-lactams	High affinity for PBP4 but also binds all other PBPs except PBP1b in *P. aeruginosa*[51]. Preferably binds PBP4 and PBP2 in *E. coli* [53]	Yes/Yes	
Gentamicin	Aminoglycosides	Binds the 30S subunit of bacterial ribosome on the A-site[54]	Yes/Yes	d
Tobramycin	Aminoglycosides	Same as gentamicin[56]	Yes/Yes	

Table 1: Antibiotics used in this thesis (Chapters 2 and 3)

Antibiotic resistance

Antibiotic resistance has been defined as **"the inherited ability of microorganisms to grow at high concentrations of an antibiotic"**[57]. Antibiotic resistance manifests from multiple evolutionary paths[58,59]. It can be acquired through the expression of genes coding for proteins hindering drug efficiency. For example, β-lactamases hydrolyse β-lactams[60], methyltransferases protect the ribosomal target site of

---

[c] All structures shown originate from the Wikipedia (https://en.wikipedia.org) page of the respective antibiotics and were checked using PubChem (https://pubchem.ncbi.nlm.nih.gov/).

[d] Gentamicin « R » groups refer to the multiple forms C1, C1a, C2, C2a and C2b[55]

aminoglycosides[61], or multidrug efflux pumps transport drugs from the cytosol to the periplasm or outside the cell[62]. Some bacterial species are also inherently resistant to several classes of antibiotic due to their physiology. For instance, the low proportion of anionic phospholipids in Gram-negative bacterial membrane drastically reduces the efficiency of the lipopeptide daptomycin[63].

Additionally, resistance can be caused by random genomic mutations (**Fig. 1**). This is assumed to be the result of an evolutionary strategy involving the generation of mutator phenotypes in response to drug stress. This encourages the faulty replication of DNA which may lead to mutations that permit to resist drug treatment[64]. Genomic mutations have varied effects. The most intuitive are mutations affecting direct drug targets. For instance, the mutation RpoB^{D516V} prevents binding of rifampicin to the RNA polymerase and restores transcription upon treatment[65,66]. Mutations in the PBP3-encoding gene *ftsI* confer ampicillin resistance to *Haemophilus influenza*[67]. The modification of the ribosome structure by mutations also permits evasion of aminoglycoside treatments[68]. Mutations can also happen in regulators involved in the expression control of drug efflux pumps. This is the case for the regulator MepR of *Staphylococcus aureus*, in which the mutation A103V leads to overexpression of the tetraphenylphosphonium bromide efflux pump MepA[69]. A later section will discuss the role of mutations in metabolic genes in acquiring antibiotic resistance.
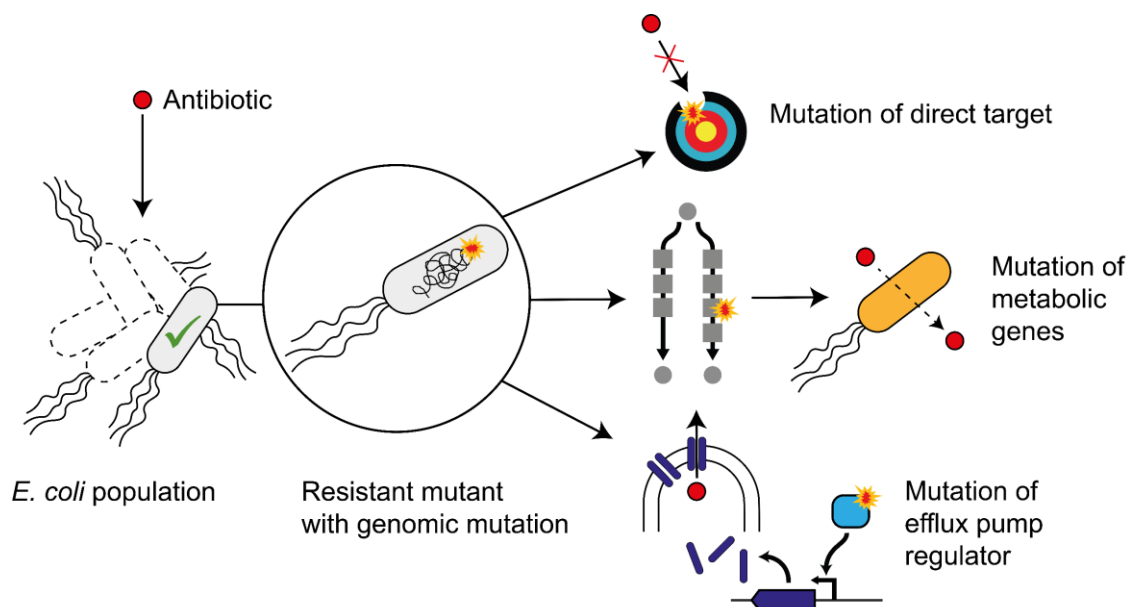

Figure 1: Various paths taken by *E. coli* to acquire antibiotic resistance with genomic mutations. The relationship between antibiotics and metabolic mutations is explored in a later section.

In 2019, Antibiotic Resistant bacteria (ARBs) were estimated to be responsible for more than a million deaths worldwide, with *Escherichia coli* being listed as the deadliest pathogen[70]. The spearhead of antimicrobial resistance is embodied by the ESKAPE pathogens. It is a category of life-threatening bacteria species which have evolved resistance against multiple classes of antibiotics, including last resort antibiotics[71]. They are *Enterococcus faecium*, *Staphylococcus aureus*, *Klebsiella pneumoniae*, *Acinetobacter braumannii*, *Pseudomonas aeruginosa* and species of the genus *Enterobacter*, in which *E. coli* is included. The high evolvability of these bacteria, coupled with decreasing research efforts in developing new antibiotics[72], highlights the need for new research in understanding antibiotic resistance to anticipate and combat it. In Europe, most infections carried by ARBs happen in healthcare settings and can also lead to high amount of disability-adjusted life years[73]. Moreover, considerable economical loss is driven by infections carried by ARBs as they lead to increased treatment cost as well as prolonged length of stay in hospitals[74]. The 2022 report of the Global Antimicrobial Resistance and Use Surveillance System from the World Health Organisation notes either stable or increasing proportion of infections caused by ARBs from 2017 to 2020, demonstrating that the problem is yet to be solved[75].

In this thesis, a variation of the previously given definition for antibiotic resistance is used and designates **the ability of a microbial strain to grow in the presence of a higher concentration of antibiotic than a control strain**. Therefore, this definition includes a necessary comparison with other bacterial strains to claim resistance and does not exclude any antibiotic concentration.

The parameter generally used to quantify resistance in a bacterial strain is the minimal inhibitory concentration (MIC), which is the first concentration of antibiotic at which growth of the tested strain is not observed. MIC determination is usually done *in vitro* using cultivation medium which do not reflect *in vivo* conditions[76]. However, MIC is easy and fast to determine and provide important information on the tested bacteria. In this thesis, agar and broth dilution assays are used to determine MIC of tested strains and follow an established protocol[77]. Technical details are provided in the Material and methods section of Chapter 2.

Antibiotic tolerance

Antibiotic tolerance is another strategy adopted by bacteria to counteract antibiotic treatments. It is known as " **the ability of a bacterial population to survive a transient exposure to antibiotics […], even at concentrations that far exceed the MIC**"[57]. Because it is a population-level phenomenon which does not involve growth but survival, tolerance differs from resistance (**Fig. 2**). As a consequence, tolerance is not always genetically inherited, and can depend on environmental factors[57,78]. For example, β-lactam tolerance has been shown to be proportional to growth rate[79] which is affected by nutrient availability[80]. Tolerance to ampicillin and norfloxacin have also been shown to be caused by extended lag phases which keep bacteria dormant and reduce killing[81]. Tolerance is challenging to quantify and publications have proposed multiple indicators mirroring the MIC, such as the MDK_{99} (Minimal Duration for Killing 99% of the bacterial population)[81] or the MBC (Minimal Bactericidal Concentration for killing 99% of the bacterial population).
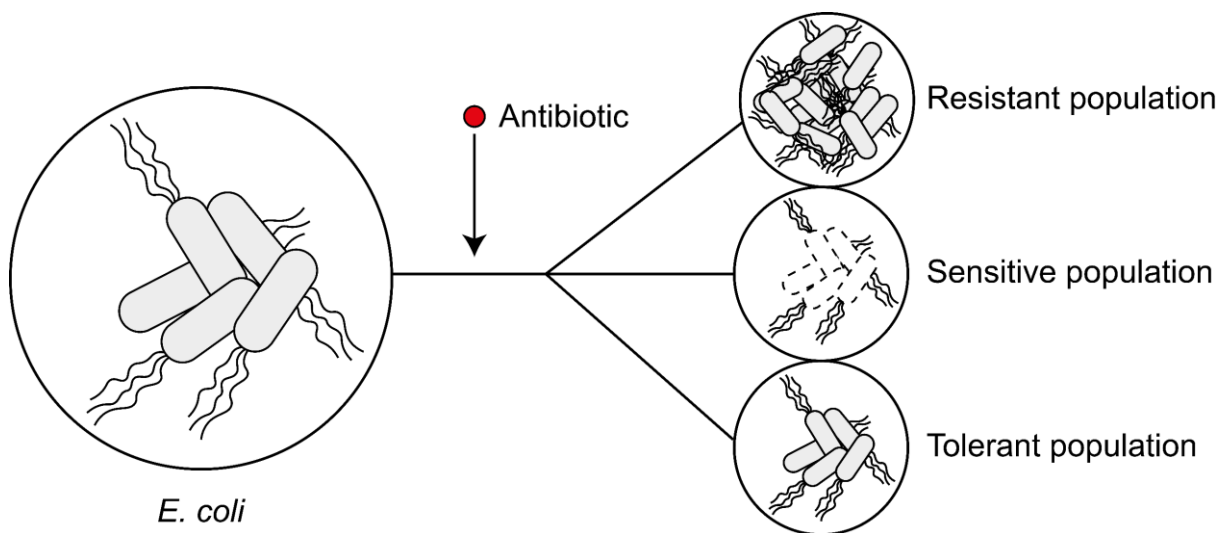

Figure 2: The difference between antibiotic resistance and antibiotic tolerance. A resistant bacterial strain is capable of growing at non-permissive antibiotic concentrations while tolerance involves transient antibiotic survival.

In this work, tolerance is defined as the **capacity of a bacterial population to survive antibiotic treatment over a time period longer than that of a control population**. Tolerance will be evaluated by using time-kill (TK) curves. Technical details are provided in the Material and methods section of Chapter 2.

Metabolism

Metabolism is the ensemble of chemical reactions happening inside a cell which drives the synthesis of essential building blocks for life. In *E. coli*, these building blocks are fatty-acids (for inner and outer membranes synthesis), nucleotides (for DNA and RNA synthesis), amino-acids (for protein synthesis) and polysaccharides (energy storage and peptidoglycan synthesis)[82]. Metabolism is modelized as a complex network of chemical reactions, many catalysed by proteins called enzymes. The EcoCyc database, which summarises available knowledge on *E. coli* metabolism, lists more than 1600 enzymes and thousands of chemical reactions[83]. Enzymes catalyse the conversion of a substrate into a product. Any molecule that is either a substrate or a product of an enzymatic reaction is called a metabolite. Enzymes often rely on co-factors such as reduced β-nicotinamide adenine dinucleotide (NADH) or adenosine-triphosphate (ATP, atp). Co-factors provide energy and electrons for catalysis. They are often converted to other molecules during catalysis (for example, NAD+ or adenosine-biphosphate (ADP, adp)) and require to be regenerated. This is another role fulfilled by metabolism.

Metabolism is divided into multiple branches, or "metabolic pathways", which are subsequent enzymatic reactions leading to the synthesis of key building blocks[84]. Examples are the *de novo* leucine pathway, which synthetises L-leucine, or the *de novo* pyrimidine pathway, which synthetises UTP and CTP. Often, a single substrate can be converted into different products. This is well exemplified by the metabolite inosine-monophosphate (IMP, imp) of the *de novo* purine pathway. IMP is converted either to xanthosine-monophosphate (XMP, xmp) or adenylo-succinate (dcamp) by the enzymes GuaB or PurA respectively[85]. Another example is carbamoyl-phosphate, which can be used for the *de novo* pyrimidine or arginine pathways by the enzyme complex PyrIB or the isoenzymes ArgI and ArgF[85] respectively.

Because it depends on key parameters such as enzymatic reaction speed, enzyme abundance and metabolite concentrations, metabolism is highly dynamic[86,87]. Equilibrium between metabolic pathways is required so that a cell would not lack important building blocks or waste energy for its growth[82,88]. This is generally achieved through transcriptional control and allosteric regulation[89]. They are complementary and ensure resource distribution and optimal building block synthesis with regards to

available resources. In *E. coli* this is well exemplified by regulation of *de novo* proteinogenic amino-acid pathways. Indeed, 16 out of 20 of these pathways are allosterically regulated and 19 out of 20 are genetically controlled by transcription factors[90]. This ensures that the pool of amino-acids available for protein synthesis is equilibrated. Any suppression of transcriptional control or allosteric regulation can have drastic consequences. For example, arginine can inhibit the enzyme ArgA by binding its H15 residue[91]. Transcription of all enzymes of the arginine pathway is under the control of the transcription factor ArgR[92], itself allosterically activated by arginine[93]. Simultaneously mutating ArgA to supress allosteric control from arginine and deleting *argR* from *E. coli* genome led to severe pathway dysregulation, arginine overproduction, and fitness defect[94].

Because of metabolism dynamics, any dysfunction or insufficient abundance of an enzyme can cause severe accumulation of its substrate and low levels of its products, which can have consequences for the cell. This accumulation profile is termed "metabolic bottleneck" (**Fig. 3**). Although *E. coli* generally prevents fluctuation in enzyme levels by synthesising more enzymes that needed[95], it is still sensitive to perturbations resulting from antibiotic treatments or genetic engineering[96]. For example, trimethoprim inhibits the enzyme FolA of the tetrahydrofolate biosynthesis pathway and affects cell growth[97]. Metabolic bottlenecks are central to this thesis and will be caused by implemented mutations using genetic engineering (see later sections).
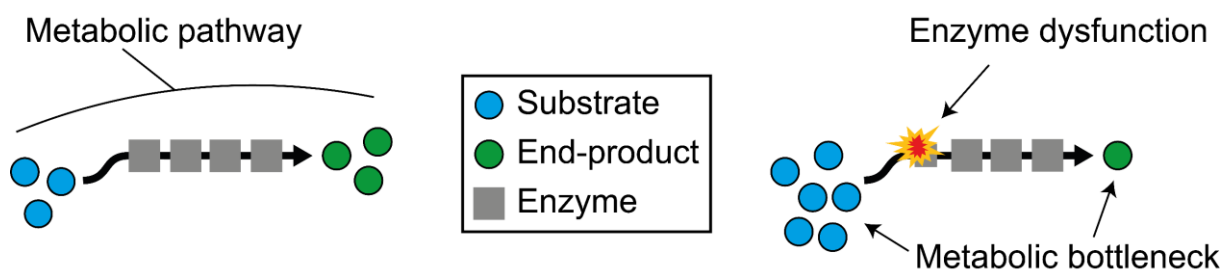

Figure 3: Representation of a metabolic bottleneck. Any dysfunction in an enzyme of a metabolic pathway can lead to accumulation of its substrate and lower levels of downstream products. Enzyme dysfunction may be caused by mutations or external perturbations.

Depending on the cultivation medium of *E. coli*, many metabolic pathways can become obsolete[98,99]. Indeed, because they require the synthesis of multiple enzymes and participate in the competition for cell resources, metabolic pathways are energy costly

to use[100,101]. As a consequence, the transcription of metabolic pathway genes is repressed in rich medium where essential building blocks are directly provided[102,103]. For example, Lysogeny Broth (LB) contains nucleotides and amino acids. *E. coli* can salvage nucleobases like adenine from its environment and convert them to purine nucleotides[104,105]. As a consequence, the transcription factor PurR, allosterically activated by the salvage nucleobase hypoxanthine, inhibits the transcription of *de novo* purine pathway genes[106].

Therefore, studying metabolism requires the use of a cultivation medium providing *E. coli* with a single defined carbon source at the branching point of all metabolic pathways in the cell. This is why, in this thesis, we use minimal medium (M9 medium) supplemented with glucose. The exact composition of M9 medium can be found in material and methods sections of each chapter relating its use.

The *de novo* purine and L-histidine pathways, as well as metabolic pathways involved in the respiratory chain (RC) will be extensively mentioned in this thesis. Their role in antibiotic resistance will be explored in Chapters 2 and 3. Following is a description of these pathways.

De novo purine and histidine pathways

The *de novo* purine nucleotide pathway is composed of 11 enzymatic reactions that convert 5-phosphoribosylpyrophosphate (PRPP, prpp) to IMP. IMP is then converted by PurA/PurB or GuaB/GuaA to AMP or GMP[107] (**Fig. 4**). Various enzymatic reactions (oxidative phosphorylation, kinases…) add phosphate atoms to AMP and GMP which forms ADP/ATP or guanosine-biphosphate (GDP, gdp)/GTP[85]. Purine nucleotides are essential as building blocks for DNA and RNA. They are also important signalling molecules, like guanosine tetraphosphate[108] or cyclic-AMP[109]. They are used as co-factors for a considerable number of enzymatic reactions.

L-histidine, like any other proteinogenic amino-acid, is used for the synthesis of proteins and peptides. Its synthesis requires 9 enzymatic reactions[85]. The *de novo* purine and L-histidine pathways share two metabolites. They start with the same metabolite, PRPP, which is either converted to 5-phospho-β-D-ribosylamine (PRA, pram) by PurF for the *de novo* purine pathway, or phosphoribosyl-ATP (prbatp) by

HisG for the *de novo* L-histidine pathway. Furthermore, the metabolite 5-amino-1-(5-phospho-D-ribosyl) imidazole-4-carboxamide (AICAR, aicar) is the product of either the heterodimer HisFH or the enzyme PurB. To which extent each pathway contributes to the AICAR pool has been studied in *Saccharomyces cerevisae*[110] but is currently uncharacterised in *E. coli*.

Hence, the *de novo* L-histidine and purine pathways are tightly associated. The regulation of the two pathways is complex and will not be covered here. They are notably regulated by different transcription factors[106,111]. AICAR, ADP, and AMP have been shown to be allosteric regulators of HisG[112] which suggests that the *de novo* purine pathway metabolites influence the synthesis of L-histidine.

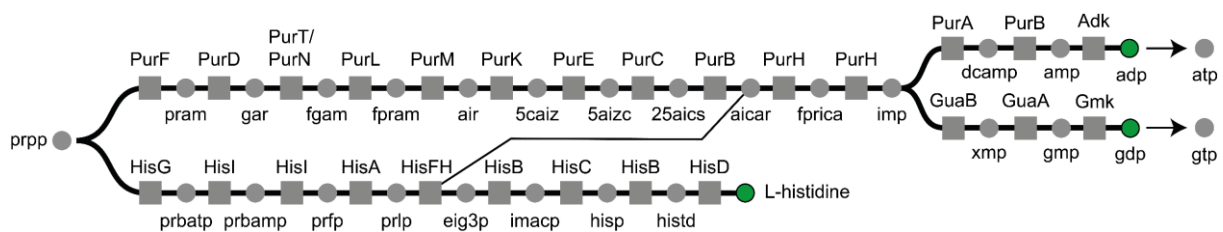**Figure 4:** The *de novo* metabolic pathways of L-histidine and purine nucleotides. Metabolites names are given using the BiGG models as reference[113].

The respiratory chain

In aerobic conditions, *E. coli* is able to use oxygen as electron acceptor to generate an electrochemical potential across its inner membrane. This is called the proton motive force (PMF) and is used by the enzymatic complex ATP synthase to phosphorylate ADP to ATP (oxidative phosphorylation). Oxidative phosphorylation is an efficient way to regenerate ATP pools in the cell depending on available resources[114,115]. The PMF components are the ΔpH (the difference of proton concentration between the periplasm and the cytosol), as well as the Δψ (the difference of electric potential across the inner membrane[116]). To generate a PMF, *E. coli* relies on proteins and metabolites associated in what is called a respiratory chain (RC), or electron transport chain (ETC). The RC transfers electrons from a donor (like NADH) to a final acceptor (oxygen)[117]. Importantly, the RC of *E. coli* relies on various electron donors or acceptors depending on environmental conditions[118,119]. In this thesis, the focus is made on electron donors and acceptors relevant in aerobic conditions.

Because it employs a wide variety of metabolites for electron transfer and redox reactions, the RC is dependent on metabolic pathways that synthesise and regenerate these metabolites. Important in Chapter 2, the methylerythrol-phosphate (MEP), flavin, tetrapyrrole and cardiolipin metabolic pathways as well as glycolysis and the tricarboxylic acid (TCA) cycle are described here (**Table 2**):

Pathway	Starting metabolite(s)	End metabolite(s)	Role in RC	Number of genes
MEP[85,120]	Pyruvate/ glyceraldehyde 3-phosphate	Isopentenyl-pyrophosphate/ prenyl diphosphate	Furnishes precursors for the isoprenoid moiety of menaquinone, dimethylmenaquinone and ubiquinone, three electron shuttles[121]. Furnishes the isoprenoid moiety for heme o, which binds to terminal ubiquinol oxidases that carry electron transfers[122].	8
Flavin[85]	GTP/ D-ribulose 5-phosphate	Flavin adenine dinucleotide (FAD)	Flavin mononucleotide and FAD are used as cofactors by multiple enzymes[119].	8
Tetrapyrrole[85,123]	L-glutamate	Protoheme	Furnishes the tetrapyrrole moiety of various heme compounds which binds to cytochromes enzymes that carry electron transfers[124].	10
Cardiolipin[85]	Cytidine biphosphate - diacylglycerol	Cardiolipin	Complexes with RC enzyme members and creates a proton trap which helps to maintain the proton gradient[125].	7
Glycolysis and TCA cycle[85]	D-glucose	Pyruvate (glycoslysis) None (TCA cycle)	Regenerates the electron donors succinate and NADH[119] and furnishes essential precursors for other pathways aforementioned.	44[e]

Table 2: Summary of RC-related metabolic pathways of interest in this thesis

Antibiotics and metabolism

Because they target essential bacterial processes and often enzymes, antibiotics efficiency is tightly connected to metabolism. The link between metabolism and antibiotics has been the topic of multiple studies in recent years[126]. One main reason

---

[e] Including the phosphotransferase system and glyoxylate shunt.

is that antibiotics-mediated death is not fully understood, as discussed for β-lactams and amino-glycosides. Metabolism might be the missing link explaining how antibiotic treatments result in cell death.

An interesting model involves reactive oxygen species (ROS) hypothesis. This hypothesis states that antibiotics of various classes induce generation of ROS as side-effect of their mode of action mainly due to interactions with central carbon metabolism[127,128]. Since ROS are lethal to many bacterial species such as *E. coli*, this could explain the reason why antibiotics ultimately induce cell death. However, this hypothesis has faced numerous contradictions, as it failed to explain multiple observations, such as the fact that many antibiotics are efficient in anaerobic conditions[129,130]. However, studies involving ROS-mediated killing never claimed that they were the sole responsible for antibiotic lethality, but instead contributed to it[131,132]. An interesting part of this model is the correlation between antibiotic lethality and levels of energy co-factors influencing "metabolic activity" such as ATP or NADH[133,134]. The lower the metabolic activity, the lower the antibiotic lethality. The importance of ATP in antibiotic efficiency has put a focus on the *de novo* purine nucleotide pathway. It was suggested that antibiotic stress could induce "adenine limitation" which drives an increase in respiration as compensation, leading to ROS production and subsequent lethality[135,136]. Therefore, a lower metabolic activity may reduce ROS generation and shield from antibiotic treatments. Overall, this model highlights the tight relationship between antibiotics and metabolism and show that (i) metabolism can impact antibiotics and (ii) antibiotics can impact metabolism.

One major caveat of all of these studies is that they describe antibiotic tolerance and not resistance. They consistently use the term "antibiotic killing" and rely on tolerance assays[128,133–135]. They attempt to generalise killing from many antibiotic classes with a single generic "metabolic state" which would depend solely on energy available to the treated cells. While this may be true for antibiotic tolerance, few approaches have explored the relationship between antibiotic resistance and metabolism[137]. Hence, a complete landscape of bacterial metabolic strategies to counteract antibiotic treatments is missing. New approaches that include antibiotic resistance are needed.

One such approach, adaptive laboratory evolution, was recently adopted[137]. In this study, *E. coli* BW25113 was evolved with antibiotics of three different classes (the β-lactam carbenicillin, the amino-glycoside streptomycin and the quinone ciprofloxacin)

with a cultivation constraint to encourage metabolic adaptations[137]. This led to mutations in metabolic genes such as *sucA*/*icd* (TCA cycle), *gltA* (glutamate synthesis) or *dxs*/*ubiF* (isoprenoids) that conferred resistance. Interestingly, no mutations in the purine pathway were enriched during this evolution experiment, probably because of potential fitness defect resulting in mutations in purine genes (see Chapter 2). Furthermore, while some mutated genes overlapped between antibiotics, no unifying metabolic strategy that would confer resistance to the three antibiotics was observable. Nevertheless, this study suggested that mutations in metabolic gene could confer low-level (2X-8X MIC increase) antibiotic resistance, although the metabolic consequences of these mutations was not further characterised. Specific antibiotic-metabolic pathway relationships have also been shown. For example, mutations in metabolic pathways involved in the respiratory chain can cause AGs resistance[138,139].

These studies indicate that metabolism could have a more intimate link with antibiotic resistance than with antibiotic tolerance. The extent and the nature of these specific associations remains to be investigated and fully characterised. One key result of such research is that a deep understanding of the relationship governing antibiotics and metabolism can help supplementing antibiotic treatments with adjuvants that contribute to killing and alleviate bacterial escape strategies[140,141]. This thesis aimed at complementing current knowledge and furnish a better picture of this relationship, mainly by using metabolomics and sets of genetic tools which allowed metabolic control. This is shown in Chapters 2 and 3.

Metabolomics

Metabolomics is the quantification and the study of metabolites[142]. The "omics" suffix (from Latin "ome" – many, mass)[143] refers to simultaneous measurement and analysis of large amounts of metabolites. Metabolomics is of high interest for the understanding of biological systems[89,90,96,144]. Metabolites can be extracted and analysed by using a wide variety of methods[145]. A presentation of the methods used in this thesis follows (**Fig. 5**).

To quantify metabolites, they must be first extracted and stored. Metabolite extraction and storage are crucial for analysis and influence the reliability of the conclusions drawn from data analysis[142]. Here, a quenching solution was used for extraction and

storage of metabolites[146]. It serves multiple purposes: (i) stopping all enzymatic reactions in the cell, (ii) lysing the cell membranes to release their content and (iii) providing a stable environment for metabolite storage. Technical details on the metabolite sampling and storage protocols can be found in material and methods sections of Chapter 2.

Metabolite extracts were measured either with a triple-quadrupole mass spectrometer coupled with a high-pressure liquid chromatographer (**HPLC-TQ**)[146] or a quadrupole time-of-flight mass spectrometer coupled with a flow-injector (**FI-TOF**)[147]. Mass spectrometers (MS) are machines that utilise the mass and charge properties of molecules for their identification and quantification[148]. Briefly, upon measurement, metabolites hit the ion detector of the MS and generate a signal of which the intensity is proportional to the metabolite abundance. Depending on the MS used and the mass and charge of the metabolites (m/z), they may hit the ion detector at different time, which permits their identification. Deeper technical specificities of the HPLC-TQ and FI-TOF will not be covered here.

In this thesis, HPLC-TQ was used for **targeted metabolomics, the measurement of a defined subset of already annotated and characterised metabolites**[149]. On the other hand, FI-TOF was used for **untargeted metabolomics, the simultaneous measurement of a large amount of metabolites**, generally with lower confidence than with targeted metabolomics[150]. Untargeted metabolomics is used for discovery while targeted metabolomics is suited for hypothesis-driven research[151]. As a result, both approaches are complementary.
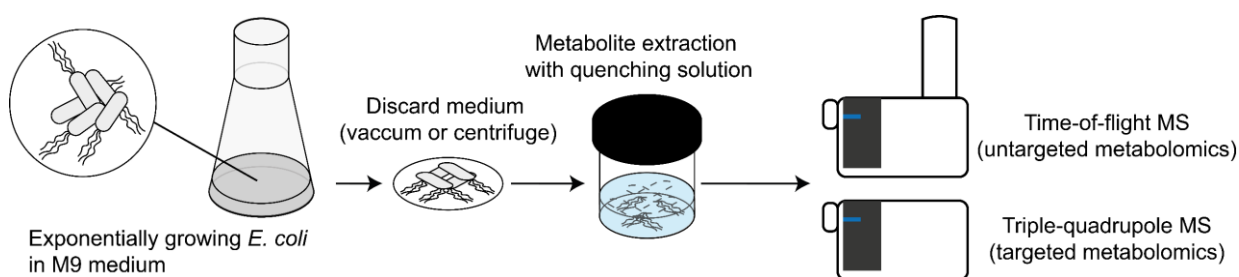

Figure 5: Brief recapitulation of experimental workflow for metabolomics.

This thesis takes advantage of both methods for its investigations, with focus on targeted metabolomics. Technical details on the methods used can be found in associated publications[146,147] and in the material and methods sections of Chapter 2.

FI-TOF and HPLC-TQ also have biological limitations. In *E. coli*, metabolite levels cannot be inferred from single cells but entire populations. This can be problematic since it has been suggested that single cells display heterogeneity in a bacterial population[152,153]. Furthermore, metabolites were measured in bacterial populations growing in liquid culture, and resistance was here often tested using agar dilution. Differences between planktonic and biofilm growth are unclear[154,155] and may blur extrapolation and conclusions.

Bottom-up proteomics

Proteomics is the study of the protein content of a cell. Understanding which proteins are expressed in a bacterium, and to which abundance, can provide useful information on metabolic regulations. Combined with metabolomics, proteomics furnish a refined picture of metabolism[96,156,157].

Proteomics relies on an ensemble of technologies including mass spectrometry[158] which will not be discussed in detail here. Proteomics in *E. coli* requires protein extraction from a bacterial population. This thesis provides data from bottom-up proteomics experiments (Chapter 3). In the case of bottom-up proteomics, the protein extract is digested by enzymes which generates multiple peptides of which the amino acid composition is measured in the mass spectrometer[159]. Here, a quadrupole-orbitrap mass spectrometer was used[160]. Using algorithms, peptides can be identified by analysing the amino-acid sequences detected on the mass spectrometers, relying on a process known as "deconvolution"[161]. The number of times a peptide is detected corresponds to its abundance in the extract, although this is not always trivial[162]. In this thesis, proteomics faces the same limitations as metabolomics.

Genome engineering using CREATE

CRISPR-enabled trackable genome engineering (CREATE) is a method that enables the implementation of mutations on the genome of *E. coli* by using the CRISPR-Cas9 machinery and lambda-phage mediated recombination. This technique is important for this dissertation and will be described in detail here.

The CREATE system used in this thesis[163] is a modified version of the original method[164] but employs the same editing principles.

Clustered regularly interspaced short palindromic repeats (CRISPR) - Cas9 relies on the association between the nuclease Cas9 (from *Streptococcus pneumoniae*) and a single-guide RNA (sgRNA). The sgRNA carries a 20 base pairs (bp) DNA sequence (termed "protospacer") complementary to a gene of interest[165]. Upon complexation with the sgRNA, Cas9 searches the genome until finding its genomic target[166]. The recognition of the target DNA sequence is conditioned by the presence of a protospacer adjacent motif (PAM), a sequence of three nucleotides (5'-NGG-3' for Cas9)[167]. When the target is found, Cas9 generates a double-stranded break (DSB) three bases upstream of the PAM[168]. This DSB is generally lethal for *E. coli*[169].

However, the DSB can be repaired by homologous recombination with a double stranded DNA (dsDNA) sharing homologies with the severed genomic region, thereby re-establishing genome continuity[170]. This homologous dsDNA is called "repair template" and can be plasmid-borne. The repair template does not need to share perfect homology with the DSB region and recombination can be successful even when nucleotides sequences vary to a certain extent[164]. Therefore, if the repair template carries mutations, they will be implemented on the repaired genome upon recombination. This is the main principle behind CREATE: a DSB is induced by Cas9, and a repair template carrying a mutation to implement on the genome is provided for the cell to repair its genome with homologous recombination. To prevent new protospacer recognition and subsequent DSB by Cas9, the repair template has to carry a silent PAM mutation. Cells which successfully repair their genomes are selected and survive (**Fig. 6**).

Cells can also perform homologous recombination without a prior presence of a DSB. Either ways, Cas9 cannot further break the edited genome. In CREATE, DNA recombination relies on heterologous proteins (called exo, bet and gam) from the λ phage[171] which are efficient and provide high recombination rates[10].
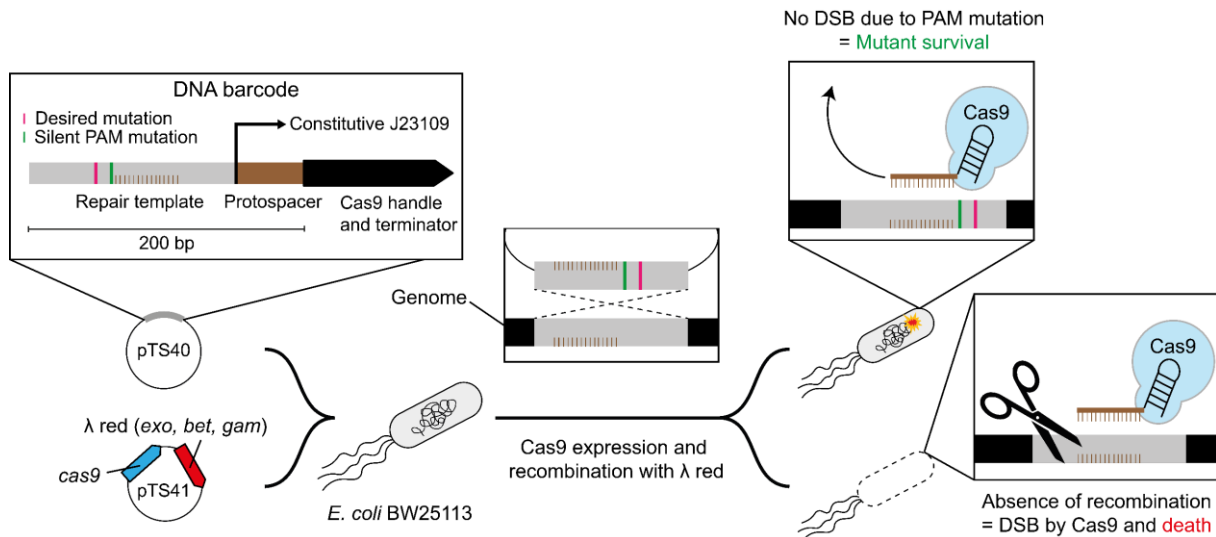
Figure 6: Principles of CREATE as used in this thesis

One essential aspect of CREATE is its trackability. Indeed, both the sgRNA and repair template nucleotide sequences are proximally located on the same plasmid. The repair template-sgRNA association is called a "DNA barcode". Sequencing of the DNA barcode allows the identification of the mutation in the strain carrying it. The CREATE system used in this thesis relies on a pair of plasmids (**Fig. 6**). The plasmid pTS41 carries the different genes necessary for lambda phage mediated recombination (exo, bet and gam) and the Cas9 coding sequence, both regulated by inducible promoters. The second plasmid, pTS40, carries the DNA barcode which varies according to the mutation to be implemented. The repair template and the sgRNA are separated by only 4 base pairs. The DNA barcode is only 200 base pairs long, which permits its sequencing and the identification of the mutation of the strain.

Due to its nature, CREATE suffers from limitations. The number of mutation sites is limited by the presence of NGG PAMs, although *E. coli* BW25113 genome has a guanine-cytosine content of 51%[12]. Furthermore, *E. coli* can employ a variety of evolutionary strategies to escape Cas9-mediated DSB, notably by deleting or mutating the genes carried by the plasmids pTS41 and pTS40. Therefore, DNA barcode sequencing does not guarantee that genome editing was successful. Finally, CREATE depends on two uncurable plasmids, which can impose a burden on the host[172]. Usage of kanamycin and chloramphenicol was also necessary to maintain the plasmids. Since the two resistance markers (KanR and CamR) on pTS41 and pTS40 do not confer resistance to the other antibiotic tested (see various chapters), this was evaluated as acceptable and further explored in Chapter 3.

The main reasons motivating the use of CREATE for this project were its ease of utilisation, its efficiency, and its trackability. This was of exceptional importance for the successful cloning and usage of the CRISPR pooled library (Chapter 2), as well as the multiple mutants used in this dissertation (all chapters).

CRISPR interference

CRISPR interference (CRISPRi-dCas9) differs from CRISPR-Cas9 by the use of a Cas9 enzyme (deactivated Cas9 – dCas9) of which the nuclease activity has been supressed by mutations D10A and H841A[173]. Since dCas9 cannot induce DSB, it binds to the DNA and remains on target, inducing a steric block of the RNA polymerase which alleviates transcription. This system is useful to study genes which cannot get knocked-out of genomes due to their essentiality. Furthermore, it also allows the study of metabolism dynamics in response to perturbation[96]. Indeed, dCas9 can be expressed using an inducible promoter, which permits the transcriptional repression of its target on demand.
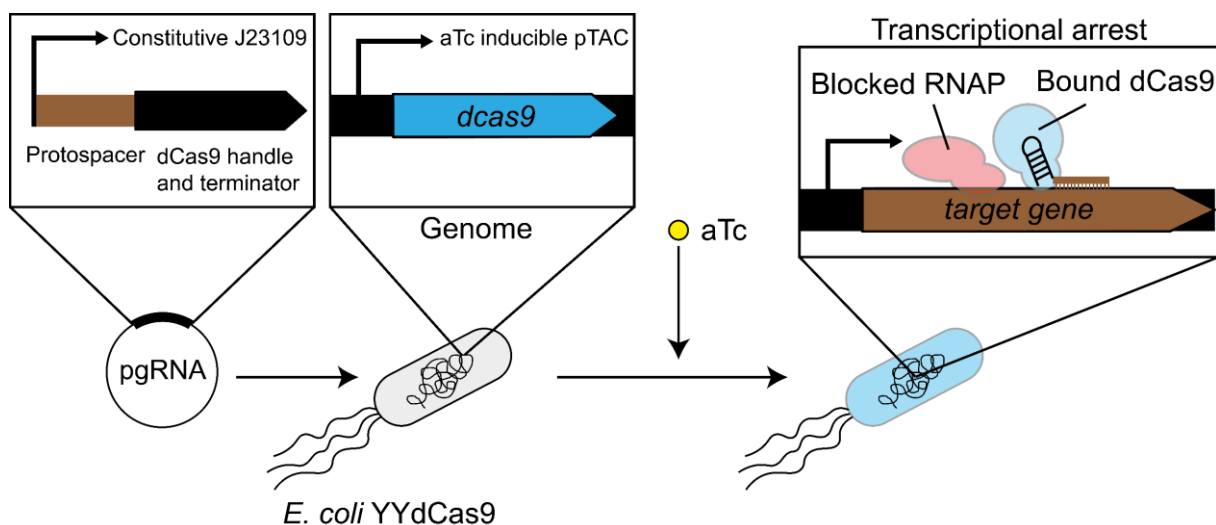

Figure 7: Principles of CRISPRi as used in this study.

CRISPRi is limited by "off targeting": dCas9 may bind unwanted regions of the genome even if they share limited homologies with its protospacer[174]. This can lead to unwanted transcriptional arrest of non-targeted genes and blur study results. However, CRISPRi is a valuable system which is easy to use.

In this thesis, CRISPRi relies on an *E. coli* BW25993 strain (close to *E. coli* BW25113), named *E. coli* YYdCas9[175] (**Fig. 7**) with a genome-integrated dCas9 gene under the control of an inducible promoter. The sgRNA is carried on the plasmid pgRNA and constitutively expressed[173]. This system has been shown to be tightly regulated[96], which is crucial to avoid unwanted effect from dCas9 overproduction[176]. CRISPRi is used in Chapter 2 of this thesis for hypothesis confirmation.

Pooled libraries

A strain library is a collection of multiple bacterial strains. In general, the collection consists of variations of a chassis strain depending on the biological phenomenon to be investigated[11,163,177]. A library can either be arrayed or pooled[178]. In arrayed libraries, each strain is stored and studied individually. In pooled libraries, all strains are cultivated and studied together as a mixed population. Pooled libraries are particularly useful to explore hypothesis with a much higher throughput than by using individual strains. However, depending on the experiments performed, strains may behave differently in community than if cultivated individually, likely due to cross-feeding[179–181]. Hence, pooled libraries are suited for large screens but not for individual strain characterisation.

Chassis variation can be constrained to genetic constructs carried by a plasmid. To efficiently generate such a pool of strains, each with a different plasmid, plasmids are also cloned using a pooled approach (**Fig. 8**). During the cloning, the variable genetic constructs (oligonucleotides) are pooled together and ligated into a common backbone. The ligation step generates the plasmid pool, which is then transformed either directly to the chassis strain[96], or an intermediate strain (as for the CREATE library described in Chapter 1). The pooled library is then generated by harvesting all transformants together. The transformation and recovery steps are of high importance. Transformation efficiency dictates the number of transformants which influences final library composition[182].
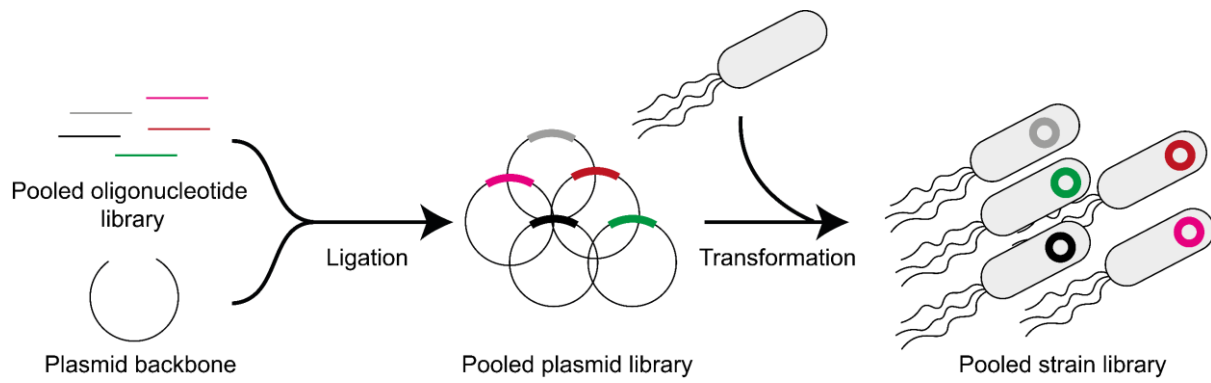
Figure 8: The cloning of a pooled strain library. Depending on the methodology, sub-cloning may be required.

This thesis relies on a pooled library developed using CREATE. Its design strategy is described in Chapter 1 and its use shown in Chapter 2.

Bibliography

1. Tenaillon, O., Skurnik, D., Picard, B. & Denamur, E. The population genetics of commensal *Escherichia coli*. *Nat Rev Microbiol* **8**, 207–217 (2010).

2. Eckburg, P. B. *et al.* Diversity of the human intestinal microbial flora. *Science* **308**, 1635–1638 (2005).

3. Blount, Z. D. The unexhausted potential of *E. coli*. *Elife* **4**, e05826 (2015).

4. Chen, X. *et al.* Metabolic engineering of *Escherichia coli*: a sustainable industrial platform for bio-based chemical production. *Biotechnol Adv* **31**, 1200–1223 (2013).

5. Zhou, Z. *et al.* The EnteroBase user's guide, with case studies on *Salmonella* transmissions, *Yersinia pestis* phylogeny, and *Escherichia* core genomic diversity. *Genome Res* **30**, 138–152 (2020).

6. Denamur, E., Clermont, O., Bonacorsi, S. & Gordon, D. The population genetics of pathogenic *Escherichia coli*. *Nat Rev Microbiol* **19**, 37–54 (2021).

7. Kaper, J. B., Nataro, J. P. & Mobley, H. L. Pathogenic *Escherichia coli*. *Nat Rev Microbiol* **2**, 123–140 (2004).

8. Mann, R., Mediati, D. G., Duggin, I. G., Harry, E. J. & Bottomley, A. L. Metabolic Adaptations of Uropathogenic *E. coli* in the Urinary Tract. *Front. Cell. Infect. Microbiol.* **7**, 241 (2017).

9. Wijetunge, D. S. S. *et al.* Characterizing the pathotype of neonatal meningitis causing *Escherichia coli* (NMEC). *BMC Microbiol* **15**, 211 (2015).

10. Datsenko, K. A. & Wanner, B. L. One-step inactivation of chromosomal genes in *Escherichia coli* K-12 using PCR products. *Proc Natl Acad Sci U S A* **97**, 6640–6645 (2000).

11. Baba, T. *et al.* Construction of *Escherichia coli* K-12 in-frame, single-gene knockout mutants: the Keio collection. *Mol Syst Biol* **2**, (2006).

12. Grenier, F., Matteau, D., Baby, V. & Rodrigue, S. Complete Genome Sequence of *Escherichia coli* BW25113. *Genome Announc* **2**, e01038-14 (2014).

13. Sims, G. E. & Kim, S.-H. Whole-genome phylogeny of *Escherichia coli*/*Shigella* group by feature frequency profiles (FFPs). *Proc Natl Acad Sci U S A* **108**, 8329–8334 (2011).

14. Touchon, M. *et al.* Organised genome dynamics in the *Escherichia coli* species results in highly diverse adaptive paths. *PLoS Genet* **5**, e1000344 (2009).

15. Wald-Dickler, N., Holtom, P. & Spellberg, B. Busting the Myth of 'Static vs Cidal': A Systemic Literature Review. *Clin Infect Dis* **66**, 1470–1474 (2018).

16. Nemeth, J., Oesch, G. & Kuster, S. P. Bacteriostatic versus bactericidal antibiotics for patients with serious bacterial infections: systematic review and meta-analysis. *J Antimicrob Chemother* **70**, 382–395 (2015).

17. Pishchany, G. & Kolter, R. On the possible ecological roles of antimicrobials. *Mol Microbiol* **113**, 580–587 (2020).

18. Larsson, D. G. J. & Flach, C.-F. Antibiotic resistance in the environment. *Nat Rev Microbiol* **20**, 257–269 (2022).

19. Williams, K. J. The introduction of 'chemotherapy' using arsphenamine - the first magic bullet. *J R Soc Med* **102**, 343–348 (2009).

20. Hutchings, M. I., Truman, A. W. & Wilkinson, B. Antibiotics: past, present and future. *Curr Opin Microbiol* **51**, 72–80 (2019).

21. Browne, A. J. *et al.* Global antibiotic consumption and usage in humans, 2000-18: a spatial modelling study. *Lancet Planet Health* **5**, e893–e904 (2021).

22. Bush, K. & Bradford, P. A. β-Lactams and β-Lactamase Inhibitors: An Overview. *Cold Spring Harb Perspect Med* **6**, a025247 (2016).

23.   Gaynes, R. The Discovery of Penicillin—New Insights After More Than 75 Years of Clinical Use. *Emerg. Infect. Dis.* **23**, 849–853 (2017).

24.   Lima, L. M., Silva, B. N. M. da, Barbosa, G. & Barreiro, E. J. β-lactam antibiotics: An overview from a medicinal chemistry perspective. *Eur J Med Chem* **208**, 112829 (2020).

25.   Cochrane, S. A. & Lohans, C. T. Breaking down the cell wall: Strategies for antibiotic discovery targeting bacterial transpeptidases. *Eur J Med Chem* **194**, 112262 (2020).

26.   Egan, A. J. F., Errington, J. & Vollmer, W. Regulation of peptidoglycan synthesis and remodelling. *Nat Rev Microbiol* **18**, 446–460 (2020).

27.   Prajapati, J. D., Kleinekathöfer, U. & Winterhalter, M. How to Enter a Bacterium: Bacterial Porins and the Permeation of Antibiotics. *Chem. Rev.* **121**, 5158–5192 (2021).

28.   Tomasz, A. The mechanism of the irreversible antimicrobial effects of penicillins: how the beta-lactam antibiotics kill and lyse bacteria. *Annu Rev Microbiol* **33**, 113–137 (1979).

29.   Wong, F. *et al.* Understanding Beta-Lactam-Induced Lysis at the Single-Cell Level. *Front Microbiol* **12**, 712007 (2021).

30.   Chung, H. S. *et al.* Rapid β-lactam-induced lysis requires successful assembly of the cell division machinery. *Proc. Natl. Acad. Sci. U.S.A.* **106**, 21872–21877 (2009).

31.   Kawai, Y. *et al.* On the mechanisms of lysis triggered by perturbations of bacterial cell wall biosynthesis. *Nat Commun* **14**, 4123 (2023).

32.   Fontana, R., Cornaglia, G., Ligozzi, M. & Mazzariol, A. The final goal: penicillin-binding proteins and the target of cephalosporins. *Clin Microbiol Infect* **6 Suppl 3**, 34–40 (2000).

33.   Spratt, B. G. Properties of the penicillin-binding proteins of *Escherichia coli* K12,. *Eur J Biochem* **72**, 341–352 (1977).

34.   Hashizume, T., Ishino, F., Nakagawa, J., Tamaki, S. & Matsuhashi, M. Studies on the mechanism of action of imipenem (N-formimidoylthienamycin) in vitro: binding to the penicillin-binding proteins (PBPs) in *Escherichia coli* and *Pseudomonas aeruginosa*, and inhibition of enzyme activities due to the PBPs in *E. coli*. *J Antibiot (Tokyo)* **37**, 394–400 (1984).

35.   Straume, D., Piechowiak, K. W., Kjos, M. & Håvarstein, L. S. Class A PBPs: It is time to rethink traditional paradigms. *Mol Microbiol* **116**, 41–52 (2021).

36.   Evans, M. E. & Pollack, M. Effect of antibiotic class and concentration on the release of lipopolysaccharide from *Escherichia coli*. *J Infect Dis* **167**, 1336–1343 (1993).

37.   Spratt, B. G. Distinct penicillin binding proteins involved in the division, elongation, and shape of *Escherichia coli* K12. *Proc. Natl. Acad. Sci. U.S.A.* **72**, 2999–3003 (1975).

38.   Yao, Z., Kahne, D. & Kishony, R. Distinct single-cell morphological dynamics under beta-lactam antibiotics. *Mol Cell* **48**, 705–712 (2012).

39.   Hisada, A. *et al.* Detection of antimicrobial impact on gram-negative bacterial cell envelope based on single-cell imaging by scanning electron microscopy. *Sci Rep* **13**, 11258 (2023).

40.   Cho, H., Uehara, T. & Bernhardt, T. G. Beta-Lactam Antibiotics Induce a Lethal Malfunctioning of the Bacterial Cell Wall Synthesis Machinery. *Cell* **159**, 1300–1311 (2014).

41.   Kingston, W. Streptomycin, Schatz v. Waksman, and the balance of credit for discovery. *J Hist Med Allied Sci* **59**, 441–462 (2004).

42.   Matt, T., Akbergenov, R., Shcherbakov, D. & Böttger, E. C. The Ribosomal A-site: Decoding, Drug Target, and Disease. *Israel Journal of Chemistry* **50**, 60–70 (2010).

43.   Davis, B. D., Chen, L. L. & Tai, P. C. Misread protein creates membrane channels: an essential step in the bactericidal action of aminoglycosides. *Proc. Natl. Acad. Sci. U.S.A.* **83**, 6164–6168 (1986).

44.   Wohlgemuth, I. *et al.* Translation error clusters induced by aminoglycoside antibiotics. *Nat Commun* **12**, 1830 (2021).

45.   Krause, K. M., Serio, A. W., Kane, T. R. & Connolly, L. E. Aminoglycosides: An Overview. *Cold Spring Harb Perspect Med* **6**, a027029 (2016).

46.   Taber, H. W., Mueller, J. P., Miller, P. F. & Arrow, A. S. Bacterial uptake of aminoglycoside antibiotics. *Microbiol Rev* **51**, 439–457 (1987).

47.   Lang, M., Carvalho, A., Baharoglu, Z. & Mazel, D. Aminoglycoside uptake, stress, and potentiation in Gram-negative bacteria: new therapies with old molecules. *Microbiol Mol Biol Rev* **87**, e0003622 (2023).

48.   Webster, C. M. & Shepherd, M. A mini-review: environmental and metabolic factors affecting aminoglycoside efficacy. *World J Microbiol Biotechnol* **39**, 7 (2022).

49.   World Health Organization. *Critically Important Antimicrobials for Human Medicine*. (World Health Organization, Geneva, 2019).

50.   Antimicrobial Resistance Division (AMR). *Model List of Essential Medicines*. (World Health Organization, 2023).

51.   Montaner, M., Lopez-Argüello, S., Oliver, A. & Moya, B. PBP Target Profiling by β-Lactam and β-Lactamase Inhibitors in Intact *Pseudomonas aeruginosa*: Effects of the Intrinsic and Acquired Resistance Determinants on the Periplasmic Drug Availability. *Microbiol Spectr* **11**, e03038-22 (2023).

52.   Sainsbury, S. *et al.* Crystal Structures of Penicillin-Binding Protein 3 from *Pseudomonas aeruginosa*: Comparison of Native and Antibiotic-Bound Forms. *Journal of Molecular Biology* **405**, 173–184 (2011).

53.   Kocaoglu, O. & Carlson, E. E. Profiling of β-Lactam Selectivity for Penicillin-Binding Proteins in *Escherichia coli* Strain DC2. *Antimicrob Agents Chemother* **59**, 2785–2790 (2015).

54.   Yoshizawa, S. Structural origins of gentamicin antibiotic action. *The EMBO Journal* **17**, 6437–6448 (1998).

55.   Vučićević-Prčetić, K., Cservenák, R. & Radulović, N. Development and validation of liquid chromatography tandem mass spectrometry methods for the determination of gentamicin, lincomycin, and spectinomycin in the presence of their impurities in pharmaceutical formulations. *Journal of Pharmaceutical and Biomedical Analysis* **56**, 736–742 (2011).

56.   Vicens, Q. & Westhof, E. Crystal Structure of a Complex between the Aminoglycoside Tobramycin and an Oligonucleotide Containing the Ribosomal Decoding A Site. *Chemistry & Biology* **9**, 747–755 (2002).

57.   Brauner, A., Fridman, O., Gefen, O. & Balaban, N. Q. Distinguishing between resistance, tolerance and persistence to antibiotic treatment. *Nat Rev Microbiol* **14**, 320–330 (2016).

58.   Darby, E. M. *et al.* Molecular mechanisms of antibiotic resistance revisited. *Nat Rev Microbiol* **21**, 280–295 (2023).

59.   Blair, J. M. A., Webber, M. A., Baylay, A. J., Ogbolu, D. O. & Piddock, L. J. V. Molecular mechanisms of antibiotic resistance. *Nat Rev Microbiol* **13**, 42–51 (2015).

60.   Tooke, C. L. *et al.* β-Lactamases and β-Lactamase Inhibitors in the 21st Century. *Journal of Molecular Biology* **431**, 3472–3500 (2019).

61.   Fritsche, T. R., Castanheira, M., Miller, G. H., Jones, R. N. & Armstrong, E. S. Detection of Methyltransferases Conferring High-Level Resistance to Aminoglycosides in Enterobacteriaceae from Europe, North America, and Latin America. *Antimicrob Agents Chemother* **52**, 1843–1845 (2008).

62.   Du, D. *et al.* Multidrug efflux pumps: structure, function and regulation. *Nat Rev Microbiol* **16**, 523–539 (2018).

63.   Randall, C. P., Mariner, K. R., Chopra, I. & O'Neill, A. J. The Target of Daptomycin Is Absent from *Escherichia coli* and Other Gram-Negative Pathogens. *Antimicrob Agents Chemother* **57**, 637–639 (2013).

64.   Blázquez, J., Rodríguez-Beltrán, J. & Matic, I. Antibiotic-Induced Genetic Variation: How It Arises and How It Can Be Prevented. *Annu. Rev. Microbiol.* **72**, 209–230 (2018).

65.   Ovchinnikov, Y. A. *et al.* Primary Structure of Escherichia coli RNA Polymerase Nucleotide Substitution in the fl Subunit Gene of the Rifampicin Resistant rpoB255 Mutant.

66.   Goldstein, B. P. Resistance to rifampicin: a review. *J Antibiot* **67**, 625–630 (2014).

67.   Dabernat, H. *et al.* Diversity of beta-lactam resistance-conferring amino acid substitutions in penicillin-binding protein 3 of *Haemophilus influenzae*. *Antimicrob Agents Chemother* **46**, 2208–2218 (2002).

68.   Garneau-Tsodikova, S. & Labby, K. J. Mechanisms of Resistance to Aminoglycoside Antibiotics: Overview and Perspectives. *Medchemcomm* **7**, 11–27 (2016).

69.   Schindler, B. D. *et al.* Functional Consequences of Substitution Mutations in MepR, a Repressor of the *Staphylococcus aureus mepA* Multidrug Efflux Pump Gene. *J Bacteriol* **195**, 3651–3662 (2013).

70.   Murray, C. J. *et al.* Global burden of bacterial antimicrobial resistance in 2019: a systematic analysis. *The Lancet* **399**, 629–655 (2022).

71.   De Oliveira, D. M. P. *et al.* Antimicrobial Resistance in ESKAPE Pathogens. *Clin Microbiol Rev* **33**, e00181-19 (2020).

72.   Ventola, C. L. The antibiotic resistance crisis: part 1: causes and threats. *P T* **40**, 277–283 (2015).

73.   Cassini, A. *et al.* Attributable deaths and disability-adjusted life-years caused by infections with antibiotic-resistant bacteria in the EU and the European Economic Area in 2015: a population-level modelling analysis. *The Lancet Infectious Diseases* **19**, 56–66 (2019).

74.   Serra-Burriel, M. *et al.* Impact of multi-drug resistant bacteria on economic and clinical outcomes of healthcare-associated infections in adults: Systematic review and meta-analysis. *PLoS ONE* **15**, e0227139 (2020).

75.   Antimicrobial Resistance Division (AMR), World Health Organization (WHO). *Global Antimicrobial Resistance and Use Surveillance System (GLASS) Report.* (2022).

76.   Belanger, C. R. & Hancock, R. E. W. Testing physiologically relevant conditions in minimal inhibitory concentration assays. *Nat Protoc* **16**, 3761–3774 (2021).

77.   Wiegand, I., Hilpert, K. & Hancock, R. E. W. Agar and broth dilution methods to determine the minimal inhibitory concentration (MIC) of antimicrobial substances. *Nat Protoc* **3**, 163–175 (2008).

78.   Handwerger, S. & Tomasz, A. Antibiotic tolerance among clinical isolates of bacteria. *Annu Rev Pharmacol Toxicol* **25**, 349–380 (1985).

79.   Lee, A. J. *et al.* Robust, linear correlations between growth rates and β-lactam-mediated lysis rates. *Proc Natl Acad Sci U S A* **115**, 4069–4074 (2018).

80.   Tong, M. *et al.* Gene Dispensability in *Escherichia coli* Grown in Thirty Different Carbon Environments. *mBio* **11**, e02259-20 (2020).

81.   Fridman, O., Goldberg, A., Ronin, I., Shoresh, N. & Balaban, N. Q. Optimization of lag time underlies antibiotic tolerance in evolved bacterial populations. *Nature* **513**, 418–421 (2014).

82.   Chubukov, V., Gerosa, L., Kochanowski, K. & Sauer, U. Coordination of microbial metabolism. *Nat Rev Microbiol* **12**, 327–340 (2014).

83.   Keseler, I. M. *et al.* The EcoCyc Database in 2021. *Front Microbiol* **12**, 711077 (2021).

84.   Schilling, C. H., Schuster, S., Palsson, B. O. & Heinrich, R. Metabolic pathway analysis: basic concepts and scientific applications in the post-genomic era. *Biotechnol Prog* **15**, 296–303 (1999).

85.   Kanehisa, M. & Goto, S. KEGG: Kyoto encyclopedia of genes and genomes. *Nucleic Acids Res* **28**, 27–30 (2000).

86.   Link, H., Fuhrer, T., Gerosa, L., Zamboni, N. & Sauer, U. Real-time metabolome profiling of the metabolic switch between starvation and growth. *Nat Methods* **12**, 1091–1097 (2015).

87.   Christodoulou, D. *et al.* Reserve Flux Capacity in the Pentose Phosphate Pathway Enables *Escherichia coli*'s Rapid Response to Oxidative Stress. *Cell Systems* **6**, 569-578.e7 (2018).

88.   Gerosa, L. & Sauer, U. Regulation and control of metabolic fluxes in microbes. *Curr Opin Biotechnol* **22**, 566–575 (2011).

89.   Lempp, M. *et al.* Systematic identification of metabolites controlling gene expression in *E. coli*. *Nat Commun* **10**, 4463 (2019).

90.   Sander, T. *et al.* Allosteric Feedback Inhibition Enables Robust Amino Acid Biosynthesis in *E. coli* by Enforcing Enzyme Overabundance. *Cell Syst* **8**, 66-75.e8 (2019).

91.   Rajagopal, B. S., DePonte, J., Tuchman, M. & Malamy, M. H. Use of Inducible Feedback-Resistant *N*-Acetylglutamate Synthetase (*argA*) Genes for Enhanced Arginine Biosynthesis by Genetically Engineered *Escherichia coli* K-12 Strains. *Appl Environ Microbiol* **64**, 1805–1811 (1998).

92.   Cho, B.-K., Federowicz, S., Park, Y.-S., Zengler, K. & Palsson, B. Ø. Deciphering the transcriptional regulatory logic of amino acid metabolism. *Nat Chem Biol* **8**, 65–71 (2012).

93.   Jin, L. *et al.* Asymmetric allosteric activation of the symmetric ArgR hexamer. *J Mol Biol* **346**, 43–56 (2005).

94.   Sander, T., Wang, C. Y., Glatter, T. & Link, H. CRISPRi-Based Downregulation of Transcriptional Feedback Improves Growth and Metabolism of Arginine Overproducing *E. coli*. *ACS Synth. Biol.* **8**, 1983–1990 (2019).

95.   Donati, S., Sander, T. & Link, H. Crosstalk between transcription and metabolism: how much enzyme is enough for a cell? *WIREs Mechanisms of Disease* **10**, e1396 (2018).

96.   Donati, S. *et al.* Multi-omics Analysis of CRISPRi-Knockdowns Identifies Mechanisms that Buffer Decreases of Enzymes in *E. coli* Metabolism. *Cell Systems* **12**, 56-67.e6 (2021).

97.   Beuter, D. *et al.* Selective Enrichment of Slow-Growing Bacteria in a Metabolism-Wide CRISPRi Library with a TIMER Protein. *ACS Synth. Biol.* **7**, 2775–2782 (2018).

98.   Goodall, E. C. A. *et al.* The Essential Genome of *Escherichia coli* K-12. **9**, (2018).

99.   Gerdes, S. Y. *et al.* Experimental Determination and System Level Analysis of Essential Genes in *Escherichia coli* MG1655. *J Bacteriol* **185**, 5673–5684 (2003).

100.   Noor, E. *et al.* The Protein Cost of Metabolic Fluxes: Prediction from Enzymatic Rate Laws and Cost Minimization. *PLoS Comput Biol* **12**, e1005167 (2016).

101.   Wessely, F. *et al.* Optimal regulatory strategies for metabolic pathways in *Escherichia coli* depending on protein costs. *Mol Syst Biol* **7**, 515 (2011).

102.   Tao, H., Bausch, C., Richmond, C., Blattner, F. R. & Conway, T. Functional genomics: expression analysis of *Escherichia coli* growing on minimal and rich media. *J Bacteriol* **181**, 6425–6440 (1999).

103.   Wei, Y. *et al.* High-density microarray-mediated gene expression profiling of *Escherichia coli*. *J Bacteriol* **183**, 545–556 (2001).

104.   Burton, K. Transport of adenine, hypoxanthine and uracil into *Escherichia coli*. *Biochem J* **168**, 195–204 (1977).

105.   Xi, H., Schneider, B. L. & Reitzer, L. Purine catabolism in *Escherichia coli* and function of xanthine dehydrogenase in purine salvage. *J Bacteriol* **182**, 5332–5341 (2000).

106. Cho, B.-K. *et al.* The PurR regulon in *Escherichia coli* K-12 MG1655. *Nucleic Acids Res* **39**, 6456–6464 (2011).

107. Zhang, Y., Morar, M. & Ealick, S. E. Structural biology of the purine biosynthetic pathway. *Cell Mol Life Sci* **65**, 3699–3724 (2008).

108. Wang, B., Grant, R. A. & Laub, M. T. ppGpp Coordinates Nucleotide and Amino-Acid Synthesis in E. coli During Starvation. *Mol Cell* **80**, 29-42.e10 (2020).

109. Botsford, J. L. & Harman, J. G. Cyclic AMP in prokaryotes. *Microbiol Rev* **56**, 100–122 (1992).

110. Rébora, K., Laloo, B. & Daignan-Fornier, B. Revisiting Purine-Histidine Cross-Pathway Regulation in *Saccharomyces cerevisiae*. *Genetics* **170**, 61–70 (2005).

111. Winkler, M. E. & Ramos-Montañez, S. Biosynthesis of Histidine. *EcoSal Plus* **3**, (2009).

112. Malykh, E. A. *et al.* Specific features of L-histidine production by *Escherichia coli* concerned with feedback control of AICAR formation and inorganic phosphate/metal transport. *Microb Cell Fact* **17**, 42 (2018).

113. King, Z. A. *et al.* BiGG Models: A platform for integrating, standardizing and sharing genome-scale models. *Nucleic Acids Res* **44**, D515–D522 (2016).

114. Basan, M. *et al.* Overflow metabolism in *Escherichia coli* results from efficient proteome allocation. *Nature* **528**, 99–104 (2015).

115. Szenk, M., Dill, K. A. & De Graff, A. M. R. Why Do Fast-Growing Bacteria Enter Overflow Metabolism? Testing the Membrane Real Estate Hypothesis. *Cell Systems* **5**, 95–104 (2017).

116. Benarroch, J. M. & Asally, M. The Microbiologist's Guide to Membrane Potential Dynamics. *Trends Microbiol* **28**, 304–314 (2020).

117. Borisov, V. B. *et al.* Aerobic respiratory chain of *Escherichia coli* is not allowed to work in fully uncoupled mode. *Proc Natl Acad Sci U S A* **108**, 17320–17324 (2011).

118. Unden, G. & Bongaerts, J. Alternative respiratory pathways of *Escherichia coli*: energetics and transcriptional regulation in response to electron acceptors. *Biochim Biophys Acta* **1320**, 217–234 (1997).

119. Unden, G. & Dünnwald, P. The Aerobic and Anaerobic Respiratory Chain of *Escherichia coli* and *Salmonella enterica* : Enzymes and Energetics. *EcoSal Plus* **3**, 10.1128/ecosalplus.3.2.2 (2008).

120. Frank, A. & Groll, M. The Methylerythritol Phosphate Pathway to Isoprenoids. *Chem. Rev.* **117**, 5675–5703 (2017).

121. Franza, T. & Gaudu, P. Quinones: more than electron shuttles. *Research in Microbiology* **173**, 103953 (2022).

122. Puustinen, A. & Wikström, M. The heme groups of cytochrome o from *Escherichia coli*. *Proc Natl Acad Sci U S A* **88**, 6122–6126 (1991).

123. Bryant, D. A., Hunter, C. N. & Warren, M. J. Biosynthesis of the modified tetrapyrroles—the pigments of life. *Journal of Biological Chemistry* **295**, 6888–6925 (2020).

124. Gennis, R. B. The cytochromes of *Escherichia coli*. *FEMS Microbiology Letters* **46**, 387–399 (1987).

125. Haines, T. H. & Dencher, N. A. Cardiolipin: a proton trap for oxidative phosphorylation. *FEBS Lett* **528**, 35–39 (2002).

126. Stokes, J. M., Lopatkin, A. J., Lobritz, M. A. & Collins, J. J. Bacterial Metabolism and Antibiotic Efficacy. *Cell Metabolism* **30**, 251–259 (2019).

127. Belenky, P. *et al.* Bactericidal Antibiotics Induce Toxic Metabolic Perturbations that Lead to Cellular Damage. *Cell Reports* **13**, 968–980 (2015).

128.   Dwyer, D. J. *et al.* Antibiotics induce redox-related physiological alterations as part of their lethality. *Proc Natl Acad Sci U S A* **111**, E2100-2109 (2014).

129.   Liu, Y. & Imlay, J. A. Cell death from antibiotics without the involvement of reactive oxygen species. *Science* **339**, 1210–1213 (2013).

130.   Keren, I., Wu, Y., Inocencio, J., Mulcahy, L. R. & Lewis, K. Killing by Bactericidal Antibiotics Does Not Depend on Reactive Oxygen Species. *Science* **339**, 1213–1216 (2013).

131.   Zhao, X., Hong, Y. & Drlica, K. Moving forward with reactive oxygen species involvement in antimicrobial lethality. *Journal of Antimicrobial Chemotherapy* **70**, 639–642 (2015).

132.   Dwyer, D. J., Collins, J. J. & Walker, G. C. Unraveling the Physiological Complexities of Antibiotic Lethality. *Annu. Rev. Pharmacol. Toxicol.* **55**, 313–332 (2015).

133.   Lopatkin, A. J. *et al.* Bacterial metabolic state more accurately predicts antibiotic lethality than growth rate. *Nat Microbiol* **4**, 2109–2117 (2019).

134.   Lobritz, M. A. *et al.* Antibiotic efficacy is linked to bacterial cellular respiration. *Proc. Natl. Acad. Sci. U.S.A.* **112**, 8173–8180 (2015).

135.   Yang, J. H. *et al.* A White-Box Machine Learning Approach for Revealing Antibiotic Mechanisms of Action. *Cell* **177**, 1649-1661.e9 (2019).

136.   Lopatkin, A. J. & Yang, J. H. Digital Insights Into Nucleotide Metabolism and Antibiotic Treatment Failure. *Front. Digit. Health* **3**, 583468 (2021).

137.   Lopatkin, A. J. *et al.* Clinically relevant mutations in core metabolic genes confer antibiotic resistance. *Science* **371**, eaba0862 (2021).

138.   Muir, M. E., Hanwell, D. R. & Wallace, B. J. Characterization of a respiratory mutant of *Escherichia coli* with reduced uptake of aminoglycoside antibiotics. *Biochim Biophys Acta* **638**, 234–241 (1981).

139.   Bryan, L. E. & Van Den Elzen, H. M. Effects of membrane-energy mutations and cations on streptomycin and gentamicin accumulation by bacteria: a model for entry of streptomycin and gentamicin in susceptible and resistant bacteria. *Antimicrob Agents Chemother* **12**, 163–177 (1977).

140.   Zhao, X. *et al.* Glutamine promotes antibiotic uptake to kill multidrug-resistant uropathogenic bacteria. *Sci. Transl. Med.* **13**, eabj0716 (2021).

141.   Su, Y. *et al.* Pyruvate cycle increases aminoglycoside efficacy and provides respiratory energy in bacteria. *Proc. Natl. Acad. Sci. U.S.A.* **115**, (2018).

142.   Alseekh, S. *et al.* Mass spectrometry-based metabolomics: a guide for annotation, quantification and best reporting practices. *Nat Methods* **18**, 747–756 (2021).

143.   Lay, J. O., Liyanage, R., Borgmann, S. & Wilkins, C. L. Problems with the "omics". *TrAC Trends in Analytical Chemistry* **25**, 1046–1056 (2006).

144.   Link, H., Kochanowski, K. & Sauer, U. Systematic identification of allosteric protein-metabolite interactions that control enzyme activity in vivo. *Nat Biotechnol* **31**, 357–361 (2013).

145.   Dai, X. & Shen, L. Advances and Trends in Omics Technology Development. *Front. Med.* **9**, 911861 (2022).

146.   Guder, J. C., Schramm, T., Sander, T. & Link, H. Time-Optimized Isotope Ratio LC–MS/MS for High-Throughput Quantification of Primary Metabolites. *Anal. Chem.* **89**, 1624–1631 (2017).

147.   Farke, N., Schramm, T., Verhülsdonk, A., Rapp, J. & Link, H. Systematic analysis of in-source modifications of primary metabolites during flow-injection time-of-flight mass spectrometry. *Anal Biochem* **664**, 115036 (2023).

148.   Glish, G. L. & Vachet, R. W. The basics of mass spectrometry in the twenty-first century. *Nat Rev Drug Discov* **2**, 140–150 (2003).

149.   Roberts, L. D., Souza, A. L., Gerszten, R. E. & Clish, C. B. Targeted metabolomics. *Curr Protoc Mol Biol* **Chapter 30**, Unit 30.2.1-24 (2012).

150.   Alonso, A., Marsal, S. & Juliã, A. Analytical Methods in Untargeted Metabolomics: State of the Art in 2015. *Front. Bioeng. Biotechnol.* **3**, (2015).

151.   Schrimpe-Rutledge, A. C., Codreanu, S. G., Sherrod, S. D. & McLean, J. A. Untargeted Metabolomics Strategies—Challenges and Emerging Directions. *J. Am. Soc. Mass Spectrom.* **27**, 1897–1905 (2016).

152.   Evans, T. D. & Zhang, F. Bacterial metabolic heterogeneity: origins and applications in engineering and infectious disease. *Current Opinion in Biotechnology* **64**, 183–189 (2020).

153.   Martins, B. M. & Locke, J. C. Microbial individuality: how single-cell heterogeneity enables population level strategies. *Current Opinion in Microbiology* **24**, 104–112 (2015).

154.   Fortuin, S., Nel, A. J. M., Blackburn, J. M. & Soares, N. C. Comparison between the proteome of *Escherichia coli* single colony and during liquid culture. *Journal of Proteomics* **228**, 103929 (2020).

155.   Díaz-Pascual, F. *et al.* Spatial alanine metabolism determines local growth dynamics of Escherichia coli colonies. *eLife* **10**, e70794 (2021).

156.   Wang, C.-Y. *et al.* Metabolome and proteome analyses reveal transcriptional misregulation in glycolysis of engineered *E. coli*. *Nat Commun* **12**, 4929 (2021).

157.   You, C. *et al.* Coordination of bacterial proteome with metabolism by cyclic AMP signalling. *Nature* **500**, 301–306 (2013).

158.   Han, M.-J. & Lee, S. Y. The *Escherichia coli* proteome: past, present, and future prospects. *Microbiol Mol Biol Rev* **70**, 362–439 (2006).

159.   Dupree, E. J. *et al.* A Critical Review of Bottom-Up Proteomics: The Good, the Bad, and the Future of this Field. *Proteomes* **8**, 14 (2020).

160.   Bekker-Jensen, D. B. *et al.* A Compact Quadrupole-Orbitrap Mass Spectrometer with FAIMS Interface Improves Proteome Coverage in Short LC Gradients. *Molecular & Cellular Proteomics* **19**, 716–729 (2020).

161.   Mann, M., Hendrickson, R. C. & Pandey, A. Analysis of Proteins and Proteomes by Mass Spectrometry. *Annu. Rev. Biochem.* **70**, 437–473 (2001).

162.   Mori, M. *et al.* From coarse to fine: the absolute *Escherichia coli* proteome under diverse growth conditions. *Molecular Systems Biology* **17**, e9536 (2021).

163.   Schramm, T. *et al.* Mapping temperature-sensitive mutations at a genome scale to engineer growth switches in *Escherichia coli*. *Mol Syst Biol* **19**, e11596 (2023).

164.   Garst, A. D. *et al.* Genome-wide mapping of mutations at single-nucleotide resolution for protein, metabolic and genome engineering. *Nat Biotechnol* **35**, 48–55 (2017).

165.   Jinek, M. *et al.* A Programmable Dual-RNA–Guided DNA Endonuclease in Adaptive Bacterial Immunity. *Science* **337**, 816–821 (2012).

166.   Cofsky, J. C., Soczek, K. M., Knott, G. J., Nogales, E. & Doudna, J. A. CRISPR-Cas9 bends and twists DNA to read its sequence. *Nat Struct Mol Biol* **29**, 395–402 (2022).

167.   Gleditzsch, D. *et al.* PAM identification by CRISPR-Cas effector complexes: diversified mechanisms and structures. *RNA Biol* **16**, 504–517 (2019).

168.   Wu, X., Kriz, A. J. & Sharp, P. A. Target specificity of the CRISPR-Cas9 system. *Quant Biol* **2**, 59–70 (2014).

169.   Cui, L. & Bikard, D. Consequences of Cas9 cleavage in the chromosome of *Escherichia coli*. *Nucleic Acids Res* **44**, 4243–4251 (2016).

170.   Kim, H. & Kim, J.-S. A guide to genome engineering with programmable nucleases. *Nat Rev Genet* **15**, 321–334 (2014).

171.   Murphy, K. C. Use of bacteriophage lambda recombination functions to promote gene replacement in *Escherichia coli*. *J Bacteriol* **180**, 2063–2071 (1998).

172.   Silva, F., Queiroz, J. A. & Domingues, F. C. Evaluating metabolic stress and plasmid stability in plasmid DNA production by Escherichia coli. *Biotechnology Advances* **30**, 691–708 (2012).

173.   Qi, L. S. *et al.* Repurposing CRISPR as an RNA-Guided Platform for Sequence-Specific Control of Gene Expression. *Cell* **152**, 1173–1183 (2013).

174.   Boyle, E. A. *et al.* High-throughput biochemical profiling reveals sequence determinants of dCas9 off-target binding and unbinding. *Proc Natl Acad Sci U S A* **114**, 5461–5466 (2017).

175.   Lawson, M. J. *et al.* In situ genotyping of a pooled strain library after characterizing complex phenotypes. *Mol Syst Biol* **13**, 947 (2017).

176.   Cui, L. *et al.* A CRISPRi screen in *E. coli* reveals sequence-specific toxicity of dCas9. *Nat Commun* **9**, 1912 (2018).

177.   Wang, H. H. *et al.* Programming cells by multiplex genome engineering and accelerated evolution. *Nature* **460**, 894–898 (2009).

178.   Rousset, F. *et al.* Genome-wide CRISPR-dCas9 screens in *E. coli* identify essential genes and phage host factors. *PLoS Genet* **14**, e1007749 (2018).

179.   Kost, C., Patil, K. R., Friedman, J., Garcia, S. L. & Ralser, M. Metabolic exchanges are ubiquitous in natural microbial communities. *Nat Microbiol* **8**, 2244–2252 (2023).

180.   Yu, J. S. L. *et al.* Microbial communities form rich extracellular metabolomes that foster metabolic interactions and promote drug tolerance. *Nat Microbiol* **7**, 542–555 (2022).

181.   Morin, M., Pierce, E. C. & Dutton, R. J. Changes in the genetic requirements for microbial interactions with increasing community complexity. *Elife* **7**, e37072 (2018).

182.   Firth, A. E. & Patrick, W. M. Statistics of protein library construction. *Bioinformatics* **21**, 3314–3315 (2005).

Chapter 1: Design and challenge of an *Escherichia coli* strain library with metabolic mutations

This chapter relates to the following paper:

Thorben Schramm, Paul Lubrano, Vanessa Pahl, Amelie Stadelmann, Andreas Verhülsdonk, Hannes Link. Mapping temperature-sensitive mutations at a genome-scale to engineer growth-switches in *E. coli*[1]

Contribution: This project was entirely designed by Dr. Thorben Schramm and Prof. Dr. Hannes Link. The author of this thesis contributed in the revision work hereby presented and wrote the chapter text, made the figures, and performed experiments with the CysS mutants as well as the mock mutants.

Chapter relevance: This chapter describes the design of the strain library used in Chapter 2.

Introduction

Context of the study

Industrial biotechnology relies on enzymes or micro-organisms to convert a feedstock (wood biomass, sugar) into a product of economic interest (vitamins, biofuel)[2]. Processes employing microbes such as *Escherichia coli* generally rely on batch or continuous cultivation in bioreactor[3]. Microbes are often engineered to maximise conversion of feedstock to the product of interest. This competes with other cellular processes and may lead to substantial growth burden and loss of production[4]. One way of abolishing such constraint is to rely on dual-stage processes. In these processes, cells are first grown until they reach a defined biomass[5]. Growth is then artificially stopped and cells kept metabolically active to maximise product yield.

Dual-stage bioprocesses remain rare owing to the technical difficulty in stopping microbial growth as well as maintaining a long-term stable production phase. Nevertheless, various methods have been elaborated. Amongst these, a study from our group has demonstrated the use of a thermosensitive ArgG mutant in *E. coli*[6]. Temperature change from 30°C to 41°C led to inactivation of the enzyme which is essential for *E. coli* to produce arginine in minimal medium. This led to a metabolic bottleneck and growth arrest. The ArgG substrate, citrulline, accumulated to high levels and is a molecule of commercial interest.

Temperature-sensitive enzymes have multiple advantages for dual-stage bioprocesses. The simplicity of implementing genomic mutations over complex genetic systems, often carried by plasmids, is a considerable advantage in industrial setup where genetic instability (also called "degeneration") is highly prevalent[7,8]. Deactivated temperature-sensitive proteins may be reactivated, allowing potential process flexibility[9]. Temperature is also a physical parameter easily tuneable in bioreactors.

Before the publication of the study from which this chapter originates, only 184 temperature-sensitive mutations were known for *E. coli*, many of which being redundant[10]. This low diversity of available temperature-sensitive mutations hindered the development of related dual-stage processes and there was a need to discover new ones. However, finding an adequate temperature-sensitive mutation for ArgG required extensive efforts, including error-prone polymerase chain reaction (PCR) and individual variant testing. Therefore, the development of a high-throughput assay was

needed to generate and characterise simultaneously multiple temperature-sensitive mutants for many industrial applications. This is what drove the development of the mutant library with temperature-sensitive mutations which played a crucial role for this thesis. Generating thousands of potential temperature-sensitive mutants and testing them all together presented tremendous advantages over individual variant testing. Hence, the initial purpose for the library used in Chapter 2 was not antibiotic research, but industrial processes.

Design and cloning of a temperature-sensitive mutant library

Generating a temperature-sensitive mutant library is not trivial. First, mutations should be implemented in genes which are essential, so that the deactivation of their encoded enzyme lead to growth arrest. Therefore, genes selected for the library design were all essential genes of *E. coli* in minimal medium supplemented with glucose[11,12].

An informatic approach was used to design a set of temperature-sensitive mutations for each essential gene. This was done using the algorithm TSpred[13]. TSpred identifies buried sites in protein structures by using hydrophobicity and hydrophobic moment as properties. It is assumed that destabilisation of buried sites with a mutation might increase protein thermal instability[14]. The use of TSpred was necessary to limit the number of mutations per genes, each offering a considerable design space. As an example, mutating each of the 447 amino-acids residues of ArgG to any of 20 other amino-acids would lead to the generation of 8940 variants, many of which will be unlikely to carry any temperature-sensitive mutation. To further downscale the number of mutations, only aspartate, alanine, tryptophan, proline and asparagine were selected for potential substitutions. A final list of 16 038 potential temperature-sensitive mutations was generated. Whether these mutations were temperature-sensitive or not remained unknown and could only be tested experimentally. Some mutations may have no effects on their recipient proteins (ineffective mutations), while others may be destabilising their recipient proteins without the requirement for high temperatures (constant mutations).

The mutations were cloned in *E. coli* genome using CREATE in a pooled approach and a pooled library of 15 120 strains was generated (see Thesis framework and **Fig. 1**). This pooled library was called "CRISPR library".
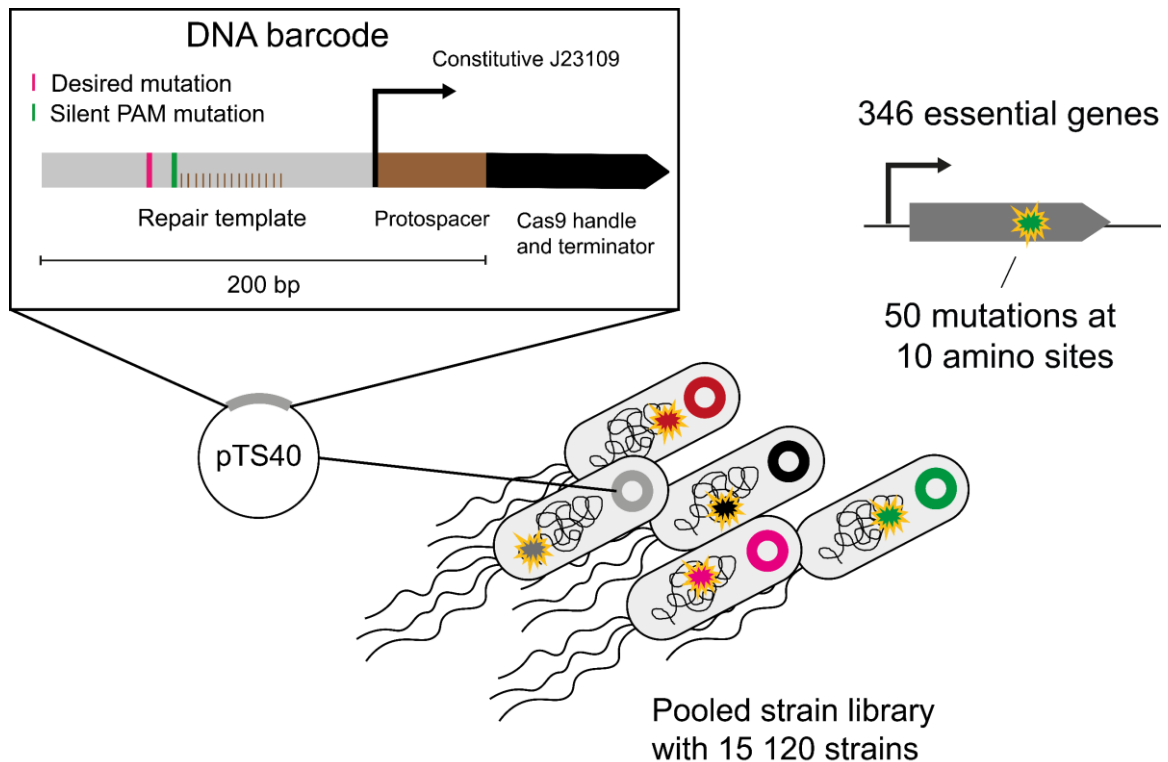
Figure 1: Design of the mutant CRISPR library used in this study. 15 120 strains were successfully cloned out of the originally 16 038 designed mutations.

Competition assay

To discriminate temperature-sensitive mutants from mutants with ineffective or constant mutations, the library was submitted to a competitive assay (**Fig. 2**).

Since the CREATE method was used for genome editing of the mutations, each strain of the library carried a DNA barcode (on pTS40, see Thesis Framework), of which the sequencing would inform on the identity of the mutation in that strain. In a pooled assay, strains are cultivated together. Extracting plasmids from a pooled library results in a mixed DNA barcode population, of which the distribution should theoretically match strain abundance[15]. Population distribution can be measured using next generation sequencing (NGS). The abundance of each DNA barcode (and its associated mutant) from the extracted population can be assessed by its read counts normalised by the total read counts of DNA barcodes obtained from the entire population.

The CRISPR library was cultivated at 30°C in minimal medium supplemented with glucose for 15 h to allow the depletion of strains unable to grow in this condition (for example, strains which had a lethal mutation at 30°C). Then, the culture was split into

two sub-cultures, one incubated at 30°C and the other at 42°C. Samples were taken every 2 hours for 12 hours after the split. Plasmids were extracted and DNA barcodes were sequenced. Ideally, mutants with temperature-sensitive mutations would deplete from the library at 42°C because of growth-arrest, and remain abundant at 30°C.
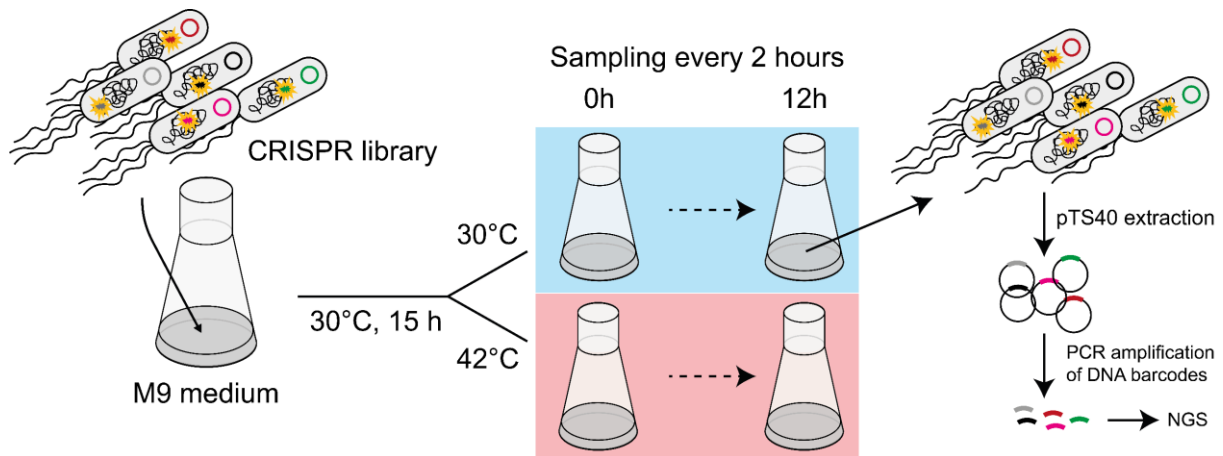

Figure 2: Description of the competition assay used to discriminate temperature-sensitive mutants from the CRISPR library. The library was first cultivated in M9 medium for 15 h at 30°C to allow depletion of slow or non-growing strains. The culture was then split into two sub-cultures at either 30° or 42°C. Samples were taken every two hours. Plasmid populations were extracted, and DNA barcodes were amplified using PCR and sequenced using NGS.

In total, 1 269 barcodes corresponded to the temperature-sensitive criterion, which accounted for 8.4% of the library. A total of 6 236 barcodes were not detected in the library at (t=0), showing protein inactivation from 30°C (constant mutation). Many barcodes had low abundance at both temperatures, indicating they encoded constant mutations which were reducing fitness but not strongly enough to be lethal for their associated strain. These strains may suffer from a non-lethal metabolic bottleneck. Interestingly, it is this category of strains which is the most relevant for Chapter 2.

These results were highly encouraging. However, there remained to confirm the temperature-sensitivity of the mutants, as cultivation and sequencing in pooled assays have numerous bias. Furthermore, there was uncertainty on whether some observed growth phenotypes might also be caused by the genome editing itself. Indeed, genome editing might result in pleiotropic effects independent from the mutation added to the genome, which might cause unforeseen consequences falsely interpreted as a relevant phenotype. This could also considerably blur the screen results.

The author of this thesis performed work to elucidate both questions and assess whether results from this pooled screen could be extrapolated to individual strains with confidence.

Results and discussion

Confirmation of temperature-sensitive mutations in *CysS*

To evaluate the efficiency and reliability of the screening strategy, potential temperature-sensitive mutations were individually reimplemented into the wild-type strain *E. coli* BW25113. With 17 putative temperature-sensitive mutations, the gene *cysS*, encoding for the cysteine-tRNA ligase, was an adequate candidate. This protein catalyses the addition of the amino-acid cysteine to its cognate tRNAs which is crucial for protein synthesis[16]. Hence, the *cysS* gene is essential for growth of *E. coli* in LB medium[12].

Fourteen of the 17 strains were successfully cloned and subjected to growth experiments in plate readers. Temperatures of 30, 34, 38, 40, 42 and 44°C were chosen to provide a good resolution over the sensitivity of the mutated proteins. The strain *E. coli* BW25113 carrying pTS41 and a pTS40 without a DNA barcode was used as control (same "non-edited control" as in Chapter 2 and 3).

At 30°C, the growth rates of most strains belonged in the same range (0.4-0.7 h^{-1}), except for CysS^{M294P} which grew poorly at all temperatures tested and did not grow from 38°C (**Fig. 3**, Table 1). This showed that most mutants and controls were able to grow robustly at this temperature. CysS^{M294P} is likely a strain with a "constant mutation" which is active already at 30°C. That this strain was identified as temperature-sensitive might be the result of bias from pooled cultivation or NGS as previously mentioned.
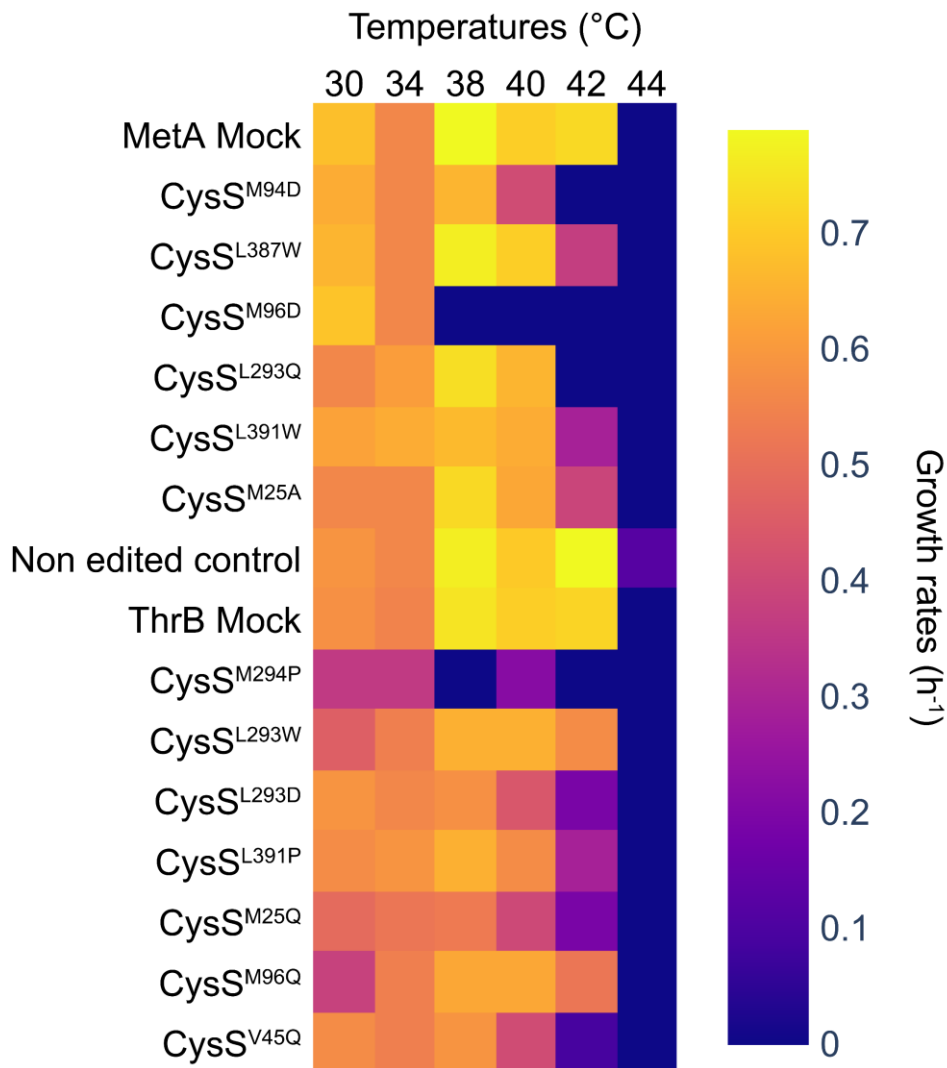
Figure 3: Heatmap representing the growth rates of the cloned *cysS* mutants, the mock controls as well as the non-edited control strain. Data is given in h⁻¹ and represent the mean growth rate of three replicates.

Differences are particularly pronounced at 42°C, where most mutants growth rates drop drastically by half of their 30°C values. Exceptions are CysS^{L293W} and CysS^{M96Q}, which have growth rate increases from 30°C to 42°C (respectively by 12.5% and 13.6%) although having lower growth rates than the non-edited control from 38°C. These two strains might not be temperature sensitive and carry mutations which modestly destabilise CysS at all tested temperatures and cause depletion at 42°C because of a slower growth rate.

Six of the 14 *cysS* mutants do not grow at 42°C (**Fig. 4**). Amongst these, CysS^{V45Q}, CysS^{M25Q} and CysS^{L293D}, have one replicate displaying exponential growth from 15h of cultivation at 42°C. This hints for genetic instability and potential escape mutations.

In conclusion, 11 of the 14 *cysS* mutants display a strong temperature-sensitive phenotype. Seven mutants display growth arrest at 42°C. The genetic instability observed in three of the growth-arrested strains tends to show limitations of these mutations for industrial applications. The screening method could identify growth impairment at 42°C, but not distinguish slower growth from growth arrest, neither pinpoint genetic instability, highlighting the need to test each identified mutant separately. Nevertheless, 78% of the tested strains were confirmed to have the correct phenotype, which was a good indication on the screen quality.
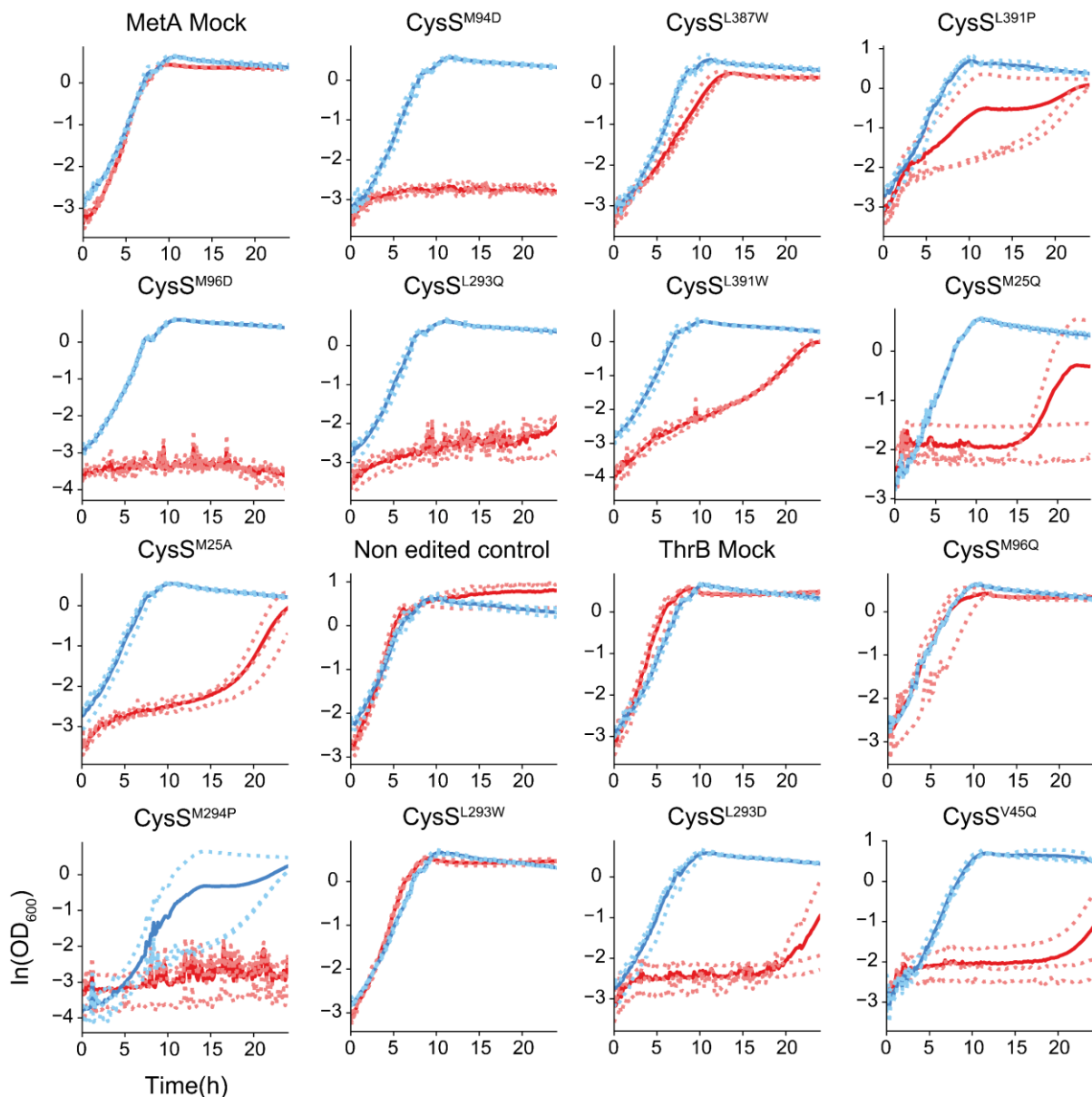

Figure 4: Growth curves of cloned *cysS* mutants, the mock controls as well as the non-edited control strain. Growth at 30°C (blue) or 42°C (red) is shown for each strain. Full lines represent the mean data across three replicates, also shown independently as dashed lines. Same data as used in Figure 3.

Mock mutations modestly impact growth rates

In addition to mutations in *cysS*, two "mock" controls were designed to ensure that CREATE genome editing *per se* could not cause any phenotypical changes in the strains because of a pleiotropic effect. Here, the homoserine *O*-succinyl transferase gene *metA* and the homoserine kinase gene *thrB* were chosen. Mock controls have only the silent PAM mutation necessary to escape Cas9 counterselection, and no substitution mutation. Mutations were cloned as aforementioned. The two strains MetA Mock and ThrB Mock were cultivated in plate readers at the same temperature range as previously stated.

The MetA Mock control showed lower growth rates than the non-edited control strain at 42°C (28% decrease). However, both ThrB Mock and MetA Mock had very similar growth rates to the non-edited control strain at all other tested temperatures. Could the slower growth rate of MetA mock at 42°C be due to experimental variation or indeed caused by the mock mutations? Synonymous mutations may have undesirable effects, although they are silent[17]. Indeed, it has been shown on multiple instances that synonymous mutations may impact gene expression[18,19], for example through mRNA folding destabilisation[20]. Hence, genome editing with CREATE may have more downsides than previously stated.

In conclusion, the CRISPR screen allowed for the successful identification of temperature-sensitive mutants amongst the cloned strains. Conservatively, it could be claimed that 11 of the 14 *cysS* mutants cloned have temperature-sensitive phenotypes. There would remain CysS^{L293W} and CysS^{M96Q} with almost no growth defect at 42°C, and CysS^{M294P}, which already has a severe fitness defect at 30°C. The screen suffers modestly from its lack of distinction between slow growth and growth arrest at 42°C, and is unable to identify strains with genetic instabilities. Furthermore, the inconclusive results regarding the mock controls also indicates that slow growth could be due to the edit itself. Overall, this dataset demonstrates the high potential for the CRISPR screen methodology in order to identify temperature-sensitive mutants while highlighting multiple limitations that remain to be addressed to improve this experimental strategy.

Bibliography :

1.   Schramm, T. *et al.* Mapping temperature-sensitive mutations at a genome scale to engineer growth switches in *Escherichia coli*. *Mol Syst Biol* **19**, e11596 (2023).

2.   Nielsen, J., Tillegreen, C. B. & Petranovic, D. Innovation trends in industrial biotechnology. *Trends in Biotechnology* **40**, 1160–1172 (2022).

3.   Croughan, M. S., Konstantinov, K. B. & Cooney, C. The future of industrial bioprocessing: Batch or continuous?: The Future of Industrial Bioprocessing. *Biotechnol. Bioeng.* **112**, 648–651 (2015).

4.   Lalwani, M. A., Zhao, E. M. & Avalos, J. L. Current and future modalities of dynamic control in metabolic engineering. *Current Opinion in Biotechnology* **52**, 56–65 (2018).

5.   Burg, J. M. *et al.* Large-scale bioprocess competitiveness: the potential of dynamic metabolic control in two-stage fermentations. *Current Opinion in Chemical Engineering* **14**, 121–136 (2016).

6.   Schramm, T. *et al.* High-throughput enrichment of temperature-sensitive argininosuccinate synthetase for two-stage citrulline production in *E. coli*. *Metabolic Engineering* **60**, 14–24 (2020).

7.   Peng, M. & Liang, Z. Degeneration of industrial bacteria caused by genetic instability. *World J Microbiol Biotechnol* **36**, 119 (2020).

8.   Park, Y., Espah Borujeni, A., Gorochowski, T. E., Shin, J. & Voigt, C. A. P recision design of stable genetic circuits carried in highly-insulated *E. coli* genomic landing pads. *Molecular Systems Biology* **16**, e9584 (2020).

9.   Chakshusmathi, G. *et al.* Design of temperature-sensitive mutants solely from amino acid sequence. *Proc. Natl. Acad. Sci. U.S.A.* **101**, 7925–7930 (2004).

10.   Berlyn, M. K. B. CGSC: The E.coli Genetic Stock Center Database. in *Bioinformatics: Databases and Systems* (ed. Letovsky, S.) 175–183 (Kluwer Academic Publishers, Boston, 2002). doi:10.1007/0-306-46903-0_16.

11.   Patrick, W. M., Quandt, E. M., Swartzlander, D. B. & Matsumura, I. Multicopy Suppression Underpins Metabolic Evolvability. *Molecular Biology and Evolution* **24**, 2716–2722 (2007).

12.   Goodall, E. C. A. *et al.* The Essential Genome of *Escherichia coli* K-12. **9**, (2018).

13.   Tan, K. P., Khare, S., Varadarajan, R. & Madhusudhan, M. S. TSpred: a web server for the rational design of temperature-sensitive mutants. *Nucleic Acids Research* **42**, W277–W284 (2014).

14.   Bajaj, K. *et al.* Structural Correlates of the Temperature Sensitive Phenotype Derived from Saturation Mutagenesis Studies of CcdB. *Biochemistry* **47**, 12964–12973 (2008).

15.   Donati, S. *et al.* Multi-omics Analysis of CRISPRi-Knockdowns Identifies Mechanisms that Buffer Decreases of Enzymes in E. coli Metabolism. *Cell Systems* **12**, 56-67.e6 (2021).

16.   Ibba, M. & Söll, D. Aminoacyl-tRNA Synthesis. *Annu. Rev. Biochem.* **69**, 617–650 (2000).

17.   Tenaillon, O. & Matic, I. The Impact of Neutral Mutations on Genome Evolvability. *Current Biology* **30**, R527–R534 (2020).

18.   Cortazzo, P. *et al.* Silent mutations affect in vivo protein folding in *Escherichia coli*. *Biochemical and Biophysical Research Communications* **293**, 537–541 (2002).

19.   Yang, D.-D., Rusch, L. M., Widney, K. A., Morgenthaler, A. B. & Copley, S. D. Synonymous edits in the *Escherichia coli* genome have substantial and condition-dependent effects on fitness. *Proc. Natl. Acad. Sci. U.S.A.* **121**, e2316834121 (2024).

20.   Deana, A., Ehrlich, R. & Reiss, C. Silent mutations in the *Escherichia coli* ompA leader peptide region strongly affect transcription and translation in vivo. *Nucleic Acids Res* **26**, 4778–4782 (1998).

Material and methods

Strains and medium

E. coli BW25113 was used for all performed experiments. *E. coli* TOP10 (Thermo Fischer) was used for cloning of the pTS40 plasmids. Cultivation was performed in either LB (Sigma #L3522) or M9 medium. M9 medium was composed by (per litre): 7.52 g Na_2HPO_4 2 H_2O, 5 g KH_2PO_4, 1.5 g $(NH_4)2SO_4$, 0.5 g NaCl. The following components were sterilized separately and then added (per litre of final medium): 1 mL 0.1 M $CaCl_2$, 1 mL 1 M $MgSO_4$, 0.6 mL 0.1 M $FeCl_3$, 2 mL 1.4 mM thiamine-HCl and 10 mL trace salts solution. The trace salts solution contained (per litre): 180 mg $ZnSO_4$ 7 H_2O, 120 mg $CuCl_2$ 2 H_2O, 120 mg $MnSO_4$ H_2O, 180 mg $CoCl_2$ 6 H_2O. Unless specified otherwise, chloramphenicol (30 µg/mL) and/or kanamycin (50 µg/mL) were added to the mediums when strains carried pTS41 and/or pTS40 respectively. M9 medium was always supplemented with 5 g/L of glucose.

Strain cloning

Refer to Chapter 2.

Strain cultivation

All strains were first transferred to a 96-well plate (called "stock plate"), with 3 wells occupied by each strain in 150 µL of LB with 25% glycerol. The stock plate was stored at -80°C. For precultures, strains were transferred from the stock plate to a deep-well plate (DWP) with 500 µl of LB medium/well using a 96-well replicator. Cultivation was performed for 6 h at 30°C and 220 rotation per minutes (RPM). Then, cells were transferred (dilution factor 1:500) to another DWP with wells filled with 500 µL of M9 medium and incubated overnight at 30°C and 220 RPM. Cells were then transferred to flat-bottomed 96-well plates containing 150 µL of M9 medium (dilution factor of 1:100). The plates were sealed with a lid and parafilm and incubated with shaking at

chosen temperatures for 24 h in plate readers Epoch 2 (Biotek) and Infinite 200 Pro (Tecan). OD_{600} was recorded every 10 minutes.

Data analysis

Data were first converted from plate reader OD_{600} to normalised OD_{600} values using previously determined conversion factors. Growth rates were determined as explained in Chapter 2. Figures were made using Python 3 and Adobe Illustrator. Any reference to the CRISPR screen comes from the original publication[1].

Supplements

	30°C	34°C	38°C	40°C	42°C	44°C
MetA Mock	0.68 ± 0.0	0.56 ± 0.0	0.79 ± 0.04	0.71 ± 0.01	0.73 ± 0.11	0.0 ± 0.0
CysS^{M94D}	0.64 ± 0.04	0.56 ± 0.01	0.66 ± 0.02	0.41 ± 0.01	0.0 ± 0.0	0.0 ± 0.0
CysS^{L387W}	0.66 ± 0.08	0.56 ± 0.02	0.77 ± 0.03	0.71 ± 0.01	0.37 ± 0.01	0.0 ± 0.0
CysS^{M96D}	0.69 ± 0.01	0.56 ± 0.01	0.0 ± 0.0	0.0 ± 0.0	0.0 ± 0.0	0.0 ± 0.0
CysS^{L293Q}	0.56 ± 0.08	0.61 ± 0.04	0.74 ± 0.15	0.66 ± 0.02	0.0 ± 0.0	0.0 ± 0.0
CysS^{L391W}	0.62 ± 0.06	0.64 ± 0.04	0.67 ± 0.14	0.64 ± 0.05	0.29 ± 0.03	0.0 ± 0.0
CysS^{M25A}	0.56 ± 0.07	0.56 ± 0.02	0.73 ± 0.07	0.63 ± 0.02	0.39 ± 0.06	0.0 ± 0.0
Non-edited control	0.59 ± 0.08	0.56 ± 0.01	0.77 ± 0.1	0.7 ± 0.01	0.79 ± 0.03	0.12 ± 0.21
ThrB Mock	0.58 ± 0.05	0.55 ± 0.01	0.75 ± 0.04	0.71 ± 0.02	0.72 ± 0.08	0.0 ± 0.0
CysS^{M294P}	0.36 ± 0.08	0.36 ± 0.04	0.0 ± 0.0	0.22 ± 0.39	0.0 ± 0.0	0.0 ± 0.0
CysS^{L293W}	0.46 ± 0.12	0.54 ± 0.03	0.65 ± 0.01	0.65 ± 0.02	0.57 ± 0.14	0.0 ± 0.0
CysS^{L293D}	0.59 ± 0.03	0.56 ± 0.02	0.58 ± 0.09	0.44 ± 0.0	0.19 ± 0.34	0.0 ± 0.0
CysS^{L391P}	0.57 ± 0.08	0.59 ± 0.04	0.65 ± 0.05	0.57 ± 0.01	0.29 ± 0.03	0.0 ± 0.0
CysS^{M25Q}	0.49 ± 0.03	0.52 ± 0.03	0.53 ± 0.01	0.4 ± 0.34	0.19 ± 0.33	0.0 ± 0.0
CysS^{M96Q}	0.38 ± 0.13	0.54 ± 0.03	0.63 ± 0.16	0.63 ± 0.02	0.52 ± 0.05	0.0 ± 0.0
CysS^{V45Q}	0.57 ± 0.05	0.54 ± 0.01	0.59 ± 0.02	0.41 ± 0.01	0.09 ± 0.16	0.0 ± 0.0

Table 1: Growth rates values (h^{-1}) as shown in Figure 3, with standard deviation (n = 3).

Chapter 2: Metabolic mutations induce antibiotic resistance by pathway-specific bottlenecks

Contribution: This chapter is an included Scientific Manuscript. Contribution of each author is discussed in a declaration of contributions as required.

Chapter relevance: This chapter shows the main body of work done during this thesis. It is the most important chapter of the thesis.

Additional note: During the time of the thesis redaction (April-May 2024), the manuscript was in revision. Hence, the version shown here is not necessarily the final version that ought to be published.

Metabolic mutations induce antibiotic resistance by pathway-specific bottlenecks

Paul Lubrano[1,2], Fabian Smollich[1], Thorben Schramm[1]†, Elisabeth Lorenz[1], Alejandra Alvarado[1,2], Seraina Carmen Eigenmann[5], Amelie Stadelmann[1], Sevvalli Thavapalan[1,2], Nils Waffenschmidt[1], Timo Glatter[3], Nadine Hoffmann[2,4], Silke Peter[2,4], Knut Drescher[5], Hannes Link[1,2]*

[1]Interfaculty Institute of Microbiology and Infection Medicine, University of Tübingen, Auf der Morgenstelle 24, 72076 Tübingen, Germany
[2]Cluster of Excellence "Controlling Microbes to Fight Infections", University of Tübingen, 72076 Tübingen, Germany
[3]Max Planck Institute for Terrestrial Microbiology, Karl-von-Frisch-Straße 10, 35043 Marburg, Germany
[4]Institute of Medical Microbiology and Hygiene, University of Tübingen, Elfriede-Aulhorn-Str. 6, 72076 Tübingen
[5]Biozentrum, University of Basel, Spitalstrasse 41, 4056 Basel, Switzerland
†Present address: Institute of Molecular Systems Biology, ETH Zurich, Otto-Stern-Weg 3, [8093] Zürich, Switzerland

* Corresponding author: hannes.link@uni-tuebingen.de

Abstract

Metabolic variation across pathogenic bacterial strains can impact their susceptibility to antibiotics and promote evolution of antimicrobial resistance (AMR). However, little is known about how metabolic mutations influence metabolism and which pathways contribute to AMR. Here, we measured antibiotic resistance of 15,120 *Escherichia coli* mutants, each with a single amino acid change in one of 346 essential proteins. Most of the mutant strains that showed resistance to either of the two tested antibiotics carried mutations in metabolic genes. The effect of metabolic mutations on resistance was antibiotic- and pathway-specific: resistance mutations against the β-lactam antibiotic carbenicillin converged on purine nucleotide biosynthesis, those against the aminoglycoside gentamicin converged on the respiratory chain. Additionally, metabolic mutations conferred tolerance to carbenicillin by reducing growth rates, which promoted the evolution of higher resistance levels. These results, along with evidence that metabolic bottlenecks are common among clinical *E. coli* isolates, highlight the relevance of metabolic mutations for AMR.

Introduction

Antimicrobial resistance (AMR) is a major threat to global health, and the associated death toll is alarmingly increasing[1]. Among the major contributors to AMR are pathogenic strains of *Escherichia coli*, which have been associated with more than 800,000 deaths in 2019[2]. AMR is either a consequence of mobilized resistance genes (e.g. drug-modifying enzymes), or of mutations that change drug-transport or binding to the drug-target[3,4]. Apart from such canonical resistance mechanisms, mutations in genes that are not directly related to the drug or the drug-target can also confer antibiotic resistance or promote its evolution. However, these non-canonical resistance mutations are difficult to identify due to their indirect effects on antibiotic action, which is often mediated by changes in bacterial physiology and metabolism[5-7]. For example, mutations in arginine biosynthesis genes of Mycobacterium smegmatis upregulated an aminoglycoside-modifying enzyme[8], and a hypomorphic variant of an enzyme in CO_2 metabolism promoted fluoroquinolone resistance in *Neisseria gonorrhoeae*[9]. Laboratory evolution studies have provided further evidence for the role of metabolism in antibiotic resistance, suggesting that mutations in metabolic genes have clinical relevance[10], and that they influence the evolutionary pathway towards resistance[11].

Despite first approaches to map antibiotic resistance of single genes with single-nucleotide resolution[12,13], it remains difficult to delineate cellular functions and metabolic pathways that are most relevant for AMR. Metabolic pathways that are increasingly associated with antibiotic action are purine nucleotide metabolism[14] and respiration[15,16]. For example, ATP levels have been associated with antibiotic tolerance in *E. coli*[17,18], as well as with persister formation in *Staphylococcus aureus*[19] and *E. coli*[20,21]. While these studies demonstrated the role of metabolism in antibiotic lethality, mutations in metabolic genes that confer antibiotic resistance are rarely identified. This is because most studies tend to focus on single isolates and individual mutations[8,9], with few systematic analyses that explore the full spectrum of resistance mutations across metabolic genes[10].

Here, we used a high-throughput approach to analyze antibiotic resistance across 15,120 *E. coli* mutants each with a single amino acid change in one of 346 essential proteins. Most mutations that conferred resistance to the β-lactam antibiotic carbenicillin occurred in genes that are involved in purine nucleotide and amino acid biosynthesis. Resistance mutations against gentamicin occurred in metabolic

pathways related to the respiratory chain. These results show that metabolic mutations confer antibiotic resistance with specificity to certain pathways rather than a general association with reduced growth rates or a general metabolic state. The same metabolic mutations that conferred resistance to carbenicillin conferred also tolerance. However, this effect was due to reduced growth rates of metabolic mutants, which is consistent with previous studies[22]. Finally, we analyzed growth and metabolism of clinical *E. coli* isolates and identified metabolic bottlenecks similar to those observed in our CRISPR mutants.

Mapping mutations in essential genes that confer antibiotic resistance

We hypothesized that hypomorphic (or partial loss-of-function) mutations in essential genes confer antibiotic resistance because they decrease cellular growth and metabolic activities. To test this hypothesis, we measured antibiotic resistance of an *E. coli* CRISPR library that consisted of 15,120 strains, each with a single amino acid change in one of 346 essential proteins[23]. These mutations were designed such that the amino acid substitution destabilizes the protein. Therefore, the mutations are likely to reduce the activity of the gene product. Each strain of the library carries a plasmid with a repair template and a sgRNA for gene editing. The repair template-sgRNA combination is a strain-specific "barcode" and its sequencing informs about the mutation that is present in a given strain. As a control we used a non-edited *E. coli* laboratory strain (BW25113) carrying the barcode plasmid with no repair template and a sgRNA without protospacer.

First, we grew the CRISPR library and the control strain on agar plates with minimal glucose medium and carbenicillin as a representative of peptidoglycan targeting β-lactams. The carbenicillin concentrations ranged between 3.125 and 9.3 µg/mL, which is 2X and 6X of the minimal inhibitory concentration (MIC) of the control strain. The MIC of the control strain was 1.5 µg/mL, which is 0.4-fold of the ampicillin-sulbactam EUCAST breakpoint. At 2X MIC, we observed a marked difference in colony forming units (CFUs) between the control strain and the CRISPR library (**Fig. S1**), thus indicating that the CRISPR library contains carbenicillin resistant mutants. However, at higher carbenicillin concentrations there was no difference in CFUs between the

control strain and the CRISPR library, thus indicating that most mutations in our library confer low-level resistance.

Next, we screened the CRISPR library against carbenicillin at 2X MIC of the control strain (**Fig. 1a**). Additionally, we screened the CRISPR library against gentamicin (2X MIC of the control strain), a representative of aminoglycosides, that targets the 30S subunit of the bacterial ribosome. As a reference, we cultivated the library on agar plates without carbenicillin or gentamicin (reference-plate, **Fig. 1a**). Each experiment was performed twice on different days to test reproducibility. After 48 hours of incubation at 2X MIC, markedly more colonies formed on antibiotic-plates inoculated with the CRISPR library compared to antibiotic-plates inoculated with the control strain (**Fig. S2**). To identify resistant mutants in the CRISPR library, we harvested the colonies from agar plates and determined read counts of strain-specific barcodes by deep sequencing, which was reproducible between the two replicates (**Fig. S3**). Fold-changes for each mutant were calculated as the ratio of barcode read fractions on antibiotic-plates relative to reference-plates (**Fig. 1b**). Mutants with fold-changes > 20 in both replicates were considered putatively resistant, resulting in 149 resistance mutations for carbenicillin, and 83 resistance mutations for gentamicin (**Table S1**).

For carbenicillin, 123 of the 149 identified resistance mutations were located in genes that had multiple resistance mutations. For example, 27 genes had more than one resistance mutation, and the most frequently mutated genes were *purM* and *purD* in the purine nucleotide biosynthesis pathway (**Fig. 1c**). The repeated occurrence of resistance mutations in the same gene was a first indication that these are *bona fide* resistance mutations. In the case of gentamicin, 72 of the 83 identified resistance mutations were located in genes that had multiple resistance mutations, and 18 genes had more than one resistance mutation (**Fig. 1c**). Most mutations occurred in *ptsI*, a component of the phosphoenolpyruvate:carbohydrate phosphotransferase system (PTS) that transports and phosphorylates glucose in *E. coli*.

In summary, our CRISPR library included *E. coli* mutants with single amino acid changes that confer resistance to carbenicillin and gentamicin. Importantly, resistance mutations occurred mostly in metabolic genes (95% on carbenicillin and 84% on gentamicin), although 31% of all mutations detected in our screen were not metabolic (**Fig. 1b**). This indicates that cellular metabolism plays an important role in antibiotic

resistance, even if this effect was limited to low-level resistance in our mutants (**Fig. S1**). Next, we examined the pathway-specificity of resistance mutations.
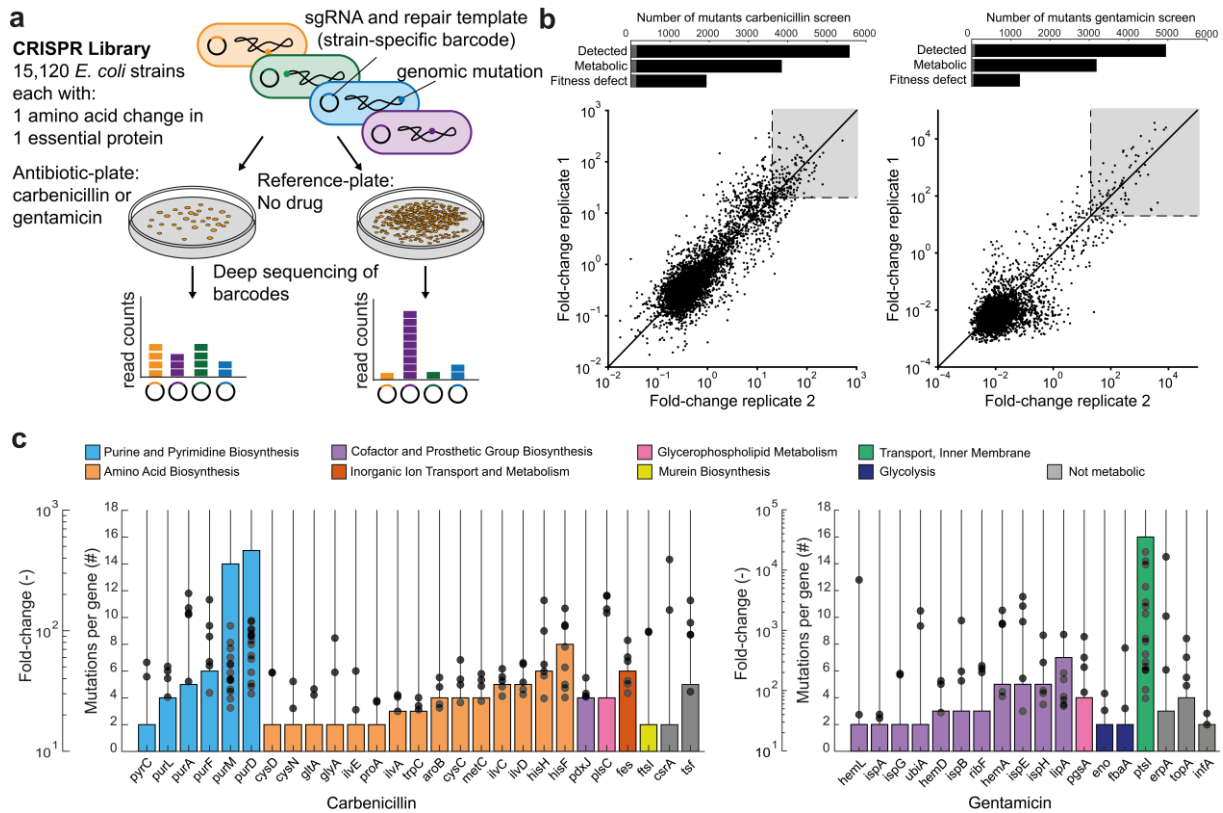

Figure 1: Mapping antibiotic resistance mutations with 15,120 *E. coli* mutants. a, Schematic of the CRISPR screen. The CRISPR library included 15,120 *E. coli* strains, each with a single amino acid change in one of 346 essential proteins. Each mutant has a sgRNA and a repair template on a plasmid. The CRISPR library was cultivated on agar plates with and without the antibiotic (n = 2 replicates at different days). Antibiotics were added at 2X of the minimal inhibitory concentration (MIC). Strain-specific barcodes (sgRNA and repair template) were sequenced after 48 h of incubation to determine the composition of the library. **b**, Fold-change of single mutants in the CRISPR library on carbenicillin and gentamicin. Fold-changes were calculated as barcode read-fractions on antibiotic-plates relative to barcode read-fractions on the reference-plates. Strains with a fold-change >20 in both replicates are considered putatively resistant against the respective antibiotic (grey regions). Bar plots show the number of mutants that: were detected in the screen (Detected), occurred in metabolic genes (Metabolic) , and had a fitness defected based on our previous screen with the library[23] (Fitness defect). Grey bars are mutants with fold-change >20. **c**, Genes with a putative resistance mutation against gentamicin (right) or carbenicillin (left). Bars show the number of different resistance mutations per gene. Dots show the mean fold-change of each mutation. Genes are grouped by functional categories in the genome-scale metabolic model of *E. coli* *i*ML1515[24]. Amino acid metabolism categories are shown as one functional category.

Resistance by metabolic mutations is caused by pathway-specific effects and not by fitness defects

Our CRISPR screen identified resistance mutations that mostly affected metabolic genes and we mapped them to the functional categories of the *E. coli* metabolic model *i*ML1515[24] (**Fig. 1c** and **Table S1**). For gentamicin, most mutations occurred in cofactor and prosthetic group biosynthesis pathways that produce components of the respiratory chain, such as genes in biosynthesis of heme (e.g. *hemA*) and ubiquinone (*ubiA*). Aminoglycosides bind ionically to the outer membrane and utilize the respiratory chain for cytosolic entry in *E. coli*[25]. Previous studies showed that mutations in the respiratory chain related genes *ubiF* and *hemA* lead to low-level aminoglycoside resistance due to decreased drug uptake[26,27]. Mutations in *pgsA* have been associated with tobramycin resistance[28] and might also alter the respiratory chain since cardiolipin acts as a proton trap[29]. The CRISPR screen identified seven genes with gentamicin resistance mutations that were not metabolic (**Table S1**), including DNA topoisomerase *topA* (4 mutations).

For carbenicillin, 44 resistance mutations affected metabolic enzymes in *de novo* biosynthesis of purine nucleotides. For example, 5 mutations occurred in *purA* (adenylosuccinate synthetase) and 4 of them had high fold-changes (>100). Another 54 mutations affected genes in amino acid biosynthesis, with 14 mutations in the histidine biosynthesis enzyme imidazole glycerol phosphate synthase (encoded by *hisF* and *hisH*). Although the heterodimer HisFH is an enzyme of the histidine biosynthesis pathway, it also produces the purine intermediate 5-amino-1-(5-phospho-D-ribosyl)imidazole-4-carboxamide (aicar). Thus, we assumed that mutations in *hisF* and *hisH* perturbed both the histidine and the purine pathway. Two resistance mutations occurred in the peptidoglycan DD-transpeptidase-encoding gene *ftsI*, which is a direct target of β-lactams[30], and the mutations may reduce carbenicillin binding. The carbenicillin screen identified only three genes that were not annotated to the *E. coli* metabolic model: the arginine—tRNA ligase *argS* (1 mutation), the elongation factor *tsf* (5 mutations) and the carbon storage regulator *csrA* (2 mutations). Since deletion of the transcription factor *csrA* has been shown to decrease expression of the porin OmpF in *E. coli*[31], the two *csrA* mutations observed in our screen might affect carbenicillin transport. However, to our knowledge, *csrA* has not yet been associated with □-lactam resistance.

Thus, our CRISPR screen identified potential resistance mutations predominantly in metabolic genes. A large fraction of these genes was in purine and amino acid biosynthesis for carbenicillin, and in the respiratory chain for gentamicin, indicating that resistance to these antibiotics results from specific metabolic perturbations rather than a universal metabolic state or general growth defects, which have previously been linked to antibiotic lethality[17,22]. Further, comparing the resistance phenotype of each mutant with their fitness phenotypes indicated that a growth defect alone does not confer resistance, because most mutants with a fitness defect did not show resistance in the screen against either antibiotic (**Fig. 1b** and **Table S1**). This implies that the observed resistance is pathway-specific and not merely a consequence of reduced growth.

Metabolic mutations induce bottlenecks in their associated pathways

To validate putative resistance mutations from the CRIPSR screen, we re-constructed three carbenicillin resistant mutants: PurM^{F105A} in the upper purine pathway, PurA^{L75D} in the ATP branch, and HisF^{V126P} at the branchpoint between the histidine and the purine pathway (**Fig. 2a**). All three mutants were resistant to carbenicillin, with at least 2-fold higher MICs than the non-edited control strain (**Fig. 2b**). The purine mutants were also resistant against aztreonam but not to meropenem (**Fig. S4**), suggesting that the resistance mechanism is linked to the structure of the respective □-lactam, because it influences drug transport[32] or penicillin binding protein specificity[33]. Additionally, we confirmed that the mutants PtsI^{I330P}, HemA^{L276Q}, RibD^{L364W}, PgsA^{V44P} and IspE^{V146W} (**Fig. 2c**) are resistant against gentamicin (**Fig. 2d**), as well as tobramycin, another aminoglycoside (**Fig. S4**).
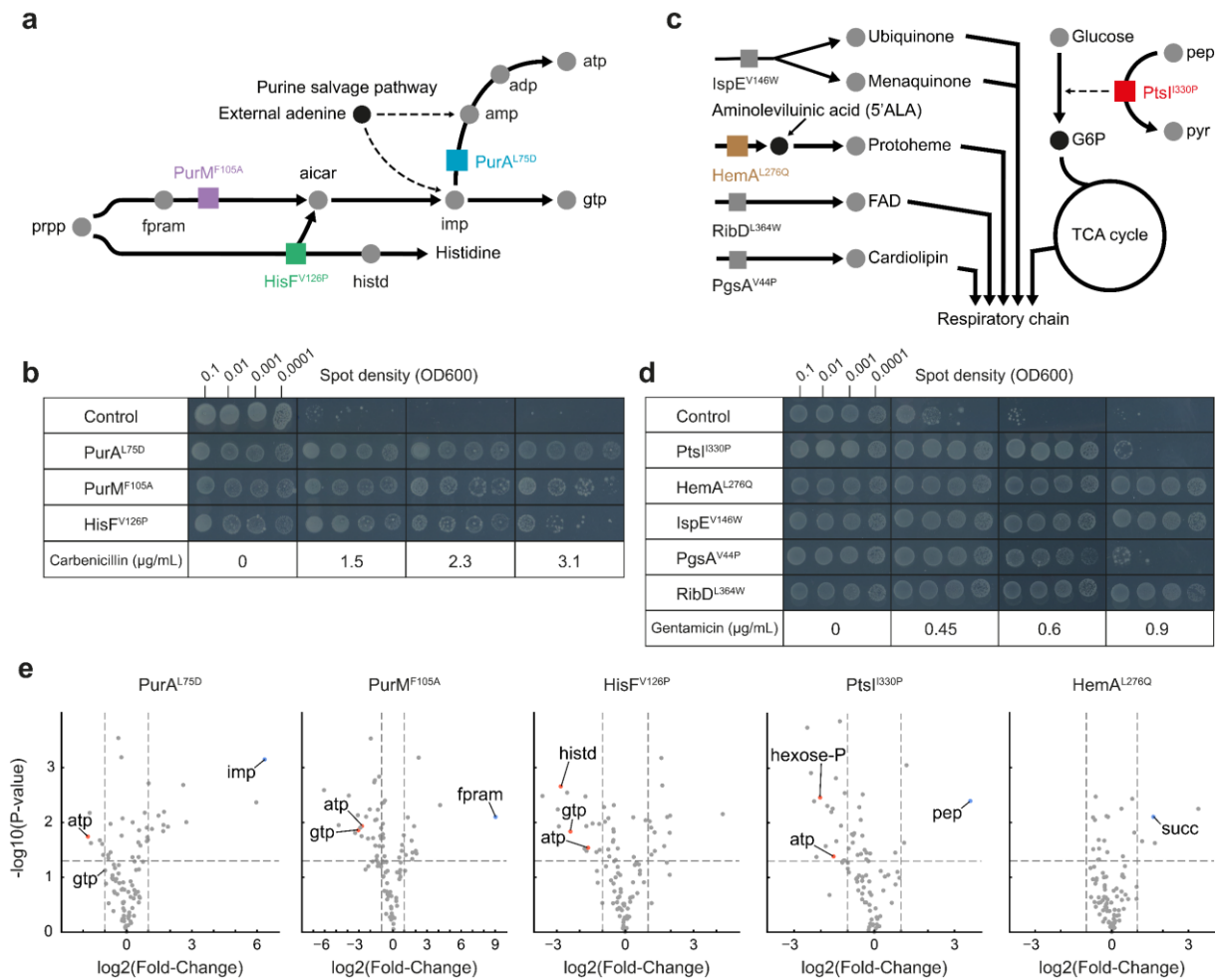
Figure 2: Metabolic mutations lead to biosynthetic bottlenecks that induce antibiotic resistance. a, Schematic of the biosynthesis pathways of purine nucleotides and histidine. Colored boxes indicate the enzymes with carbenicillin resistance mutations: HisF^{V126P}, PurM^{F105A} and PurA^{L75D}. **b,** Agar dilution assay with the control strain and three re-constructed mutants (HisF^{V126P}, PurM^{F105A} and PurA^{L75D}). Each strain was spotted on agar plates with minimal glucose medium containing increasing concentrations of carbenicillin (control strain MIC = 1.5 □g/mL). Multiple inoculum densities were used to assess inoculum effects. Plates were incubated 48 h. Shown is one of n = 2 replicates. **c,** Schematic of multiple metabolic pathways that are associated to gentamicin resistance mutations: PtsI^{I330P}, HemA^{L276Q}, IspE^{V146W}, PgsA^{V44P}, RibD^{L364W}. All pathways converge towards the respiratory chain. Boxes represent mutated enzymes with resistance mutations. **d,** Agar dilution assay with the control strain and mutants that were identified in the gentamicin screen (PtsI^{I330P}, HemA^{L276Q}, IspE^{V146W}, PgsA^{V44P}, RibD^{L364W}). Each strain was plated on agar plates with minimal glucose medium containing increasing concentrations of gentamicin (control strain MIC = 0.45 µg/mL). Multiple inoculum densities were used to assess inoculum effects. Plates were incubated 48 h. Shown is one of n = 2 replicates. **e,** Volcano plots show metabolite levels of resistant mutants as fold-changes relative to the control strain (n = 3 distinct samples). Significant metabolite changes (p-value < 0.05, FC>1) that are discussed in the text are annotated.

To understand how metabolic mutations influence cellular metabolism, we quantified intracellular metabolites with targeted metabolomics. Therefore, we grew the mutants on minimal glucose medium without antibiotics and measured metabolites during exponential growth with liquid chromatography-tandem mass spectrometry (LC-MS/MS)[34]. In the carbenicillin resistant mutants PurA^{L75D} and PurM^{F105A}, stronger metabolic changes occurred in nucleotide biosynthesis with decreases between 2- and 5-fold in the purine nucleotide end-products ATP and GTP (**Fig. 2e**). GTP levels were less perturbed in the PurA^{L75D} strain, probably because PurA catalyzes the first step in the ATP branch of the purine pathway. The strongest metabolome changes in the PurA^{L75D} and PurM^{F105A} strain were increases of the substrate metabolites of PurA and PurM, inosine monophosphate (imp) and 2-(formamido)-N1-(5-phospho-β-D-ribosyl)acetamidine (fpram), respectively. These substrate increases indicate that PurA^{L75D} and PurM^{F105A} are hypomorphic mutations that decrease the catalytic capacity of the enzymes, which in turn limits *de novo* biosynthesis of purine nucleotides. The HisF^{V126P} strain had also low levels of purine nucleotides, as well as low histidinol (histd) levels, thus indicating a deficiency of the HisFH complex that leads to bottlenecks in both the lower histidine pathway and the purine pathway.

The metabolome of gentamicin mutants indicated that they also introduce bottlenecks in their associated pathways. For example, the strongest metabolite change in the PtsI^{I330P} strain was an increase of phosphoenolpyruvate (pep), a substrate metabolite of the PTS (**Fig 2e**). This indicated a metabolic bottleneck at the initial step of glycolysis, which is further supported by low levels of hexose phosphates (hexose-p) in the PtsI^{I330P} strain. Although an *E. coli* mutant lacking PtsI (Δ*ptsI*) has been linked to antibiotic tolerance[35], a role in antibiotic resistance has not been reported to our knowledge. In the HemA^{L276Q} and RibD^{L364W} mutants, we detected high levels of succinate (succ, **Fig 2e** and **Fig S5**). Succinate is the substrate metabolite of succinate dehydrogenase (Sdh), which requires heme b groups as well as FAD as co-factor. Therefore, it is likely that the HemA^{L276Q} and RibD^{L364W} mutants have metabolic bottlenecks that respectively limit the production of heme and FAD, which then leads to a secondary bottleneck at Sdh and blocks the respiratory chain.

Thus, metabolic mutations can lead to bottlenecks in their associated pathways and may induce antibiotic resistance. To obtain additional evidence that resistance was

due to the bottlenecks and not pleiotropic effects caused by genome editing, we used CRISPR interference (CRISPRi) to decrease the concentration of PurA. The CRISPRi-*purA* strain was indeed resistant to carbenicillin and its metabolome was similar to the PurA^{L75D} strain metabolome, with strong increases of the PurA substrate IMP (**Fig. S6**).

If a limited supply of specific metabolites induced antibiotic resistance in our mutants, we expected that external sources of these metabolites would reverse resistance. *E. coli* can convert external adenine into ATP and GTP by nucleotide salvage pathways that are independent from *de novo* biosynthesis[36] (**Fig 2a**). As expected, feeding adenine to the PurA^{L75D}, PurM^{F105A} and HisF^{V126P} strains reversed their carbenicillin resistance (**Fig. S7**). We also confirmed that adenine supplementation restored the purine nucleotide levels in the PurA^{L75D} strain to the levels of the control strain (**Fig. S8**). Similarly, the PtsI^{I330P} mutant was not resistant against gentamicin during growth on glucose-6-phosphate, a non-PTS sugar (**Fig. S9**), and supplementing a heme biosynthesis intermediate (5-aminolevulinic acid) reversed gentamicin resistance of the HemA^{L276Q} mutant (**Fig. S9**).

In summary, metabolome analyses demonstrated that metabolic mutations induce specific bottlenecks in their associated pathways, which contribute to antibiotic resistance. This resistance can be reversed by supplementing external sources of the limiting metabolites, confirming that the resistance mechanisms are linked to bottlenecks within specific metabolic pathways. Next, we investigated if resistance was only due to pathway-specific effects or if global growth effects also play a role in resistance.

Growth defects from metabolic mutations influence tolerance but not resistance

To investigate the influence of cellular growth on resistance, we assessed the growth rates of the three carbenicillin resistant mutants (PurM^{F105A}, PurA^{L75D} and HisF^{V126P}) and five gentamicin resistant mutants (PtsI^{I330P}, HemA^{L276Q}, RibD^{L364W}, PgsA^{V44P} and IspE^{V146W}) in minimal glucose medium (**Fig. 3a**). All mutants had significantly lower growth rates than the control strain (p-value < 0.05). Given the known associations between growth rates and antibiotic efficacy[22], we explored whether slow growth contributes to resistance of the mutants. To account for such an effect, we used a LeuB^{I134P} mutant, which had a low growth rate (**Fig. 3a**) and was not resistant to

carbenicillin (**Fig. S10**), thus indicating that slow growth alone does not confer resistance. This is further supported by cross-resistance of the gentamicin and carbenicillin resistant mutants: the slow-growing purine mutants (PurM^{F105A}, PurA^{L75D} and HisF^{V126P}) were not resistant against gentamicin (**Fig. S11**), and vice versa, the slow-growing PtsI^{I330P} mutant was not resistant to carbenicillin (**Fig. S11**).
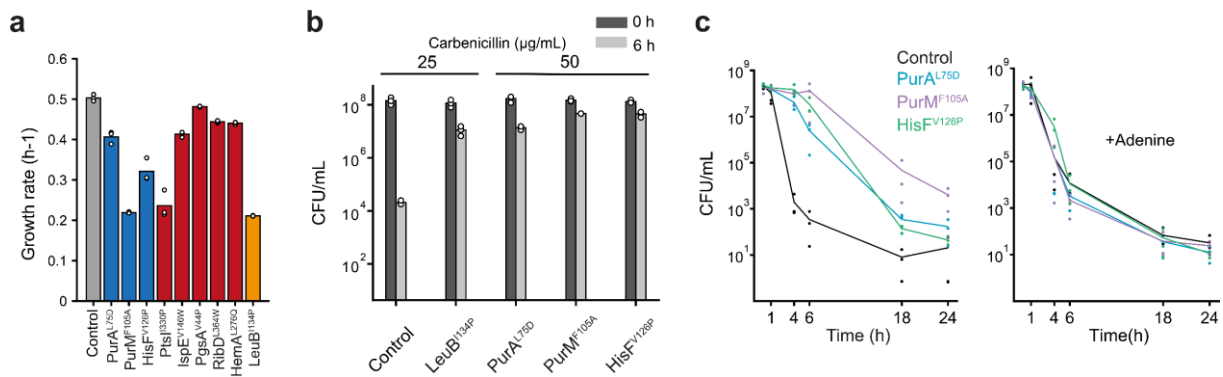

Figure 3: Slow growth but not metabolic bottlenecks confer β-lactam tolerance.
a, Growth rates of control strain and selected mutants in minimal medium with glucose. Blue: carbenicillin resistant mutants. Red: gentamicin resistant mutants. Orange: slow growth control strain LeuB^{I134P} (n = 3 distinct samples). **b,** Survival of carbenicillin treatment of the control strain, the LeuB^{I134P} mutant (slow growth control) and three purine mutants (PurA^{L75D}, PurM ^{F105A}, HisF^{V126P}). Cells were incubated for 6 h with carbenicillin at their respective 2X MIC (Control and LeuB^{I134P}: 25 µg/mL; purine mutants: 50 µg/mL) and colony forming units (CFU) were determined on minimal agar medium after 48 h of incubation. CFU/mL are shown for two time points, before carbenicillin addition 0 h (black), and after 6 h (grey), (n = 3 distinct samples). **c,** Time-kill assays with the control strain, and the HisF^{V126P}, PurM^{F105A} and PurA^{L75D} strains. Strains were incubated in minimal glucose medium and carbenicillin (50 µg/mL) for the time period indicated on the x-axis (n = 3 distinct samples). Left: time-kill assays without adenine supplementation, right: time-kill assays with supplementation of 1 mM adenine. 50 µg/mL carbenicillin is 4X MIC of all strains in the presence of adenine.

Apart from antibiotic resistance, antibiotic tolerance has been associated with slow growth, especially in the case of beta-lactams[22]. Therefore, we used the purine mutants to investigate whether their slow growth confers tolerance to carbenicillin or if the purine bottleneck has an additional survival benefit. After a 6-hour treatment with carbenicillin, the purine mutants showed significantly higher survival compared to the control strain (p-value < 0.05), even when we adjusted the carbenicillin concentration such that each strain was treated at their respective 2X MIC (**Fig. 3b** and **Fig. S12**). However, the higher tolerance to carbenicillin of the purine mutants is primarily due to their reduced growth rates, because the slow-growing mutant LeuB^{I134P} showed a

similar tolerance level, with an average survival rate of 11%, comparable to those of the purine mutants (PurA^{L75D}: 8%; PurM^{F105A}: 32%; HisF^{V126P}: 33%). Nevertheless, reversal of the tolerance phenotype in purine mutants by supplementing adenine demonstrates the metabolism dependency of the tolerance phenotype (**Fig. 3c**).

In summary, metabolism has pathway-specific effects on carbenicillin and gentamicin resistance, which are unrelated to growth rates. Tolerance against carbenicillin, however, is primarily due to slow growth of the PurM^{F105A}, PurA^{L75D} and HisF^{V126P} mutants, as shown by the slow-growing control LeuB^{I134P} strain. This tolerance against carbenicillin is probably a driver for the evolution of higher resistance levels[37], as evidenced by the >10X MIC increases found in the PurA^{L75D} strain after prolonged exposure to carbenicillin (**Fig. S13**). Thus, metabolic mutations can influence antibiotic action by two effects: 2-4X MIC increases by pathway-specific mechanisms and tolerance due to slow-growth. Together, these effects can promote evolution of high-level resistance (**Fig. S13**).

Clinical *E. coli* have metabolic bottlenecks and a mutation in *purK* confers carbenicillin/sulbactam tolerance

To understand the clinical relevance of metabolic mutations, we examined 235 *E. coli* strains from different clinical isolates of the Tübingen University Hospital (**Table S2**). To identify metabolic mutations in these isolates, we used metabolome analysis of strains with a growth defect in minimal glucose medium (**Fig. 4a**). Out of 235 strains, 41 strains showed a growth defect (**Fig. S14 and Table S2**), and we measured their metabolome after a shift from rich medium to minimal glucose medium by flow-injection mass spectrometry (FI-MS)[38]. FI-MS detected 636 ions with distinct masses that matched 811 metabolites. In 38 out of 41 isolates, at least one metabolite showed strong increases (fold-change > 8, **Fig. 4b and Table S3**). Across these 38 isolates, 44 metabolites showed fold-changes >8 and they mapped to 14 functional categories of the *E. coli* metabolic model iML1515[24], which included amino acid biosynthesis and purine nucleotide biosynthesis (**Table S3**). Next, we focused on three isolates EC-61, EC-96, and EC-244, which had high levels of cystathionine, histidinol-phosphate, and 5-amino-1-(5-phospho-β-D-ribosyl)imidazole (air), respectively. Cystathionine is involved in methionine biosynthesis and is metabolized by MetC, which had 4 resistance mutations in the CRISPR screen against carbenicillin (**Fig. 1c**). Histidinol-

phosphate and air are intermediates in biosynthetic pathways of histidine and purine nucleotides, which were also targets for carbenicillin resistance mutations. We assumed that increases of these biosynthetic intermediates indicate bottlenecks in their respective biosynthesis pathways. To test this, we grew the three isolates in minimal glucose medium which we supplemented either with methionine, histidine, or adenine. Indeed, supplementing these metabolites markedly improved growth of the respective isolate (**Fig 4c**), demonstrating that pathway-specific metabolic bottlenecks occur in clinical *E. coli*.
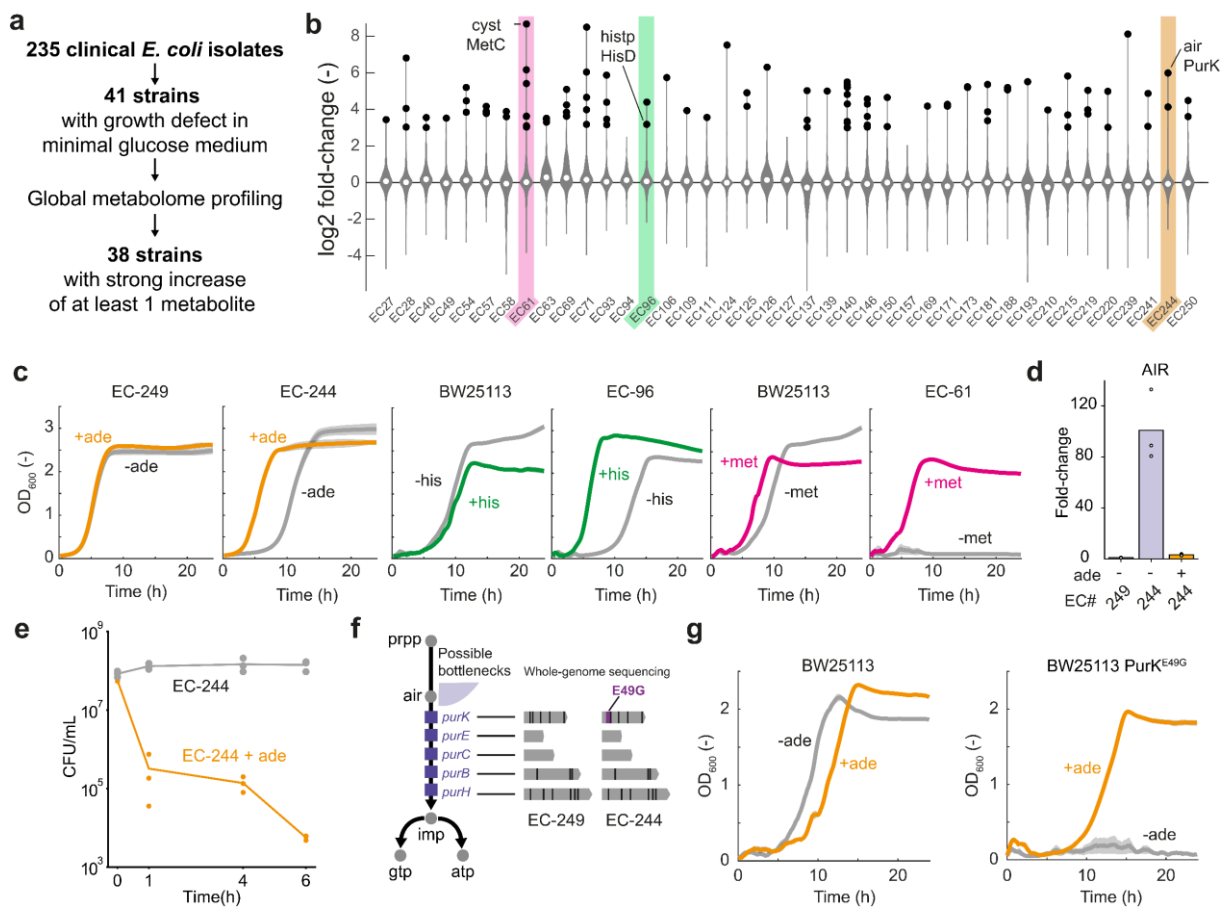

Fig. 4: Metabolome profiling identifies metabolic bottlenecks in clinical *E. coli* isolates and a purine bottleneck caused by PurK[E49G]. a, 235 *E. coli* isolates were obtained from different clinical specimens and cultivated in minimal glucose medium. 41 strains with growth defects were selected for metabolome profiling with flow-injection time-of-flight mass spectrometry (n = 2 distinct samples). **b,** Metabolome profile of 41 clinical isolates (mean of n = 2 distinct samples). Violin plot shows the distribution of 636 m/z features that were annotated to metabolites. M/z features with fold change > 3 are shown in black. Three isolates (EC-61, EC-96 and EC-244) are annotated due to their accumulation of m/z features that were annotated to cystathionine (cyst), histidinol-phosphate (histp) and 5-amino-1-(5-phospho-β-D-ribosyl)imidazole (air). **c,** Growth of EC-244 and EC-249 with (orange) and without

(grey) supplementation of adenine. Shown are also growth curves of two clinical isolates EC-96 and EC-61 in minimal glucose medium supplemented with L-histidine (green) or L-methionine (magenta). Growth data of the *E. coli* wild-type BW25113 is shown as reference. Growth curves show means from n = 3 minimal glucose medium cultures grown in a plate reader. Grey areas show the standard deviation. **d,** Relative concentrations of air in EC-244 (with and without adenine) and EC-249 (without adenine). Data are normalized to EC-249 (without adenine) and are represented as mean of n = 3 distinct samples (black dots). **e,** Time-kill assays with EC-244 without adenine (grey) and with supplementation of adenine (orange). EC-244 was incubated with 100 µg/mL carbenicillin and 12.5 µg/mL sulbactam for the time period indicated on the x-axis (n = 3 distinct samples). **f,** Whole genome sequencing was performed with EC-244 and EC-249. Sequences of genes of the purine *de novo* pathway were aligned to the *E. coli* wild-type BW25113 reference genome. **g,** A mutation in *purK* (PurK^{E49G}) was identified in EC-244 and not in EC-249 and was inserted into the *E. coli* wild-type BW25113. Shown is the growth of the control strain and the PurK^{E49G} mutant in minimal glucose medium. Strains were grown either without adenine (grey), or with 1 mM of adenine (orange) (n = 3 distinct samples).

Next, we followed up on the purine bottleneck in EC-244, which was a urinary tract isolate. First, we used targeted metabolomics to measure the concentration of nucleotides and air in EC-244 and compared it to EC-249, which is another urinary tract isolate with normal growth. As expected, ATP, ADP and AMP levels were lower in EC-244 compared to EC-249 (**Fig. S15**), and the LC-MS/MS data confirmed the high air levels detected by FI-MS (**Fig. 4d**). Notably, adenine feeding restored ATP levels and air levels in EC-244 (**Fig. 4d and S15**). Thus, the high levels of air, together with low purine end-products, suggested that EC-244 has a metabolic bottleneck in the middle of the purine pathway (**Fig. 4f**). To locate the bottleneck, we sequenced the genomes of EC-244 and EC-249 and compared sequences of the suspected purine genes to those of the laboratory *E. coli* strain BW25113. In total, we found 122 mutations in the 5 purine genes and 14 of them resulted in amino acid changes (**Table S4**). However, only one amino acid change was unique to EC-244: PurK^{E49G}. PurK sequences of *E. coli* isolates in the NCBI pathogen database suggest that PurK^{E49G} is a low frequency mutation, because none of the isolates in the database had this mutation. In contrast, the other 4 PurK mutations were high-frequency mutations, because they occurred in >364 isolates in the NCBI pathogen database (**Fig. S16**). Therefore, we assumed that PurK^{E49G} is a hypomorphic allele that is responsible for the purine nucleotide synthesis bottleneck in EC-244. To test this hypothesis, we inserted the PurK^{E49G} mutation into the laboratory *E. coli* strain BW25113, which indeed

led to a purine auxotrophy (**Fig. 4g**), confirming its causative role in the purine nucleotide synthesis bottleneck of EC-244.

Based on the results with our CRISPR purine mutants, we expected that the purine limitation impaired the efficacy of β-lactam antibiotics in EC-244. However, EC-244 was highly resistant against carbenicillin, probably due to the expression of a β-lactamase (**Table S2**). Therefore, we examined the killing activity of carbenicillin in the presence of the β-lactamase inhibitor sulbactam in EC-244. Consistent with our expectation, carbenicillin/sulbactam exhibited no killing activity in EC244 during a 6-hours treatment, and supplementation of adenine restored killing activity of carbenicillin/sulbactam, such that only 0.01% of the adenine-fed cells survived the 6-hours treatment (**Fig. 4e**). Although *E. coli* can salvage nucleotides present in urine[39], the *de novo* purine pathway has been shown to be essential for survival and colonization in niches such as the gut[40], human blood[41], or inside host cells[42]. This suggests that the bottleneck caused by the PurK^{E49G} mutation might have an impact on antibiotic treatment of that strain.

Discussion

In our study, we tested the resistance of 15,120 *E. coli* mutants, each with an amino-acid change in an essential gene, against two antibiotics of the β-lactam and aminoglycoside classes. Most mutations that led to antibiotic resistance were located in metabolic genes (95% on carbenicillin and 84% on gentamicin), although 31% of the mutations detected in our CRISPR screen were not metabolic. We found that resistance from these metabolic mutations does not result from a global fitness defect, but local defects in specific pathways. For instance, 39% of the mutations that conferred resistance against carbenicillin were linked to genes involved in the purine nucleotide biosynthesis pathway. Similarly, 54% of the mutations conferring resistance to gentamicin were associated with the respiratory chain.

Our results show that bottlenecks in specific metabolic pathways induce low-level antibiotic resistance, (2-4X MIC). This finding is consistent with previous reports about metabolic mutations that occurred during evolution of a laboratory *E. coli* strain[10] and future studies must clarify if metabolic mutations are generally restricted to low-level resistance.

For gentamicin, the resistance mechanism likely involves the known dependency on oxidative metabolism for uptake of aminoglycosides[25]. In the case of carbenicillin, several mechanisms have been proposed to explain why purine nucleotide biosynthesis influences antibiotic efficiency, for example an antibiotic-induced adenine limitation that increases purine biosynthesis[18] or changes in ATP levels[17,19]. However, because the PtsI^{I330P} mutant had low ATP levels and was not resistant to carbenicillin, we assume that low ATP levels alone are not sufficient to confer resistance and that a bottleneck in *de novo* purine biosynthesis is required. Another hypothesis is that purine bottlenecks change carbenicillin transport, either because nucleotide metabolism interacts with membrane permeability (via the porin OmpF)[43], or because of the higher efflux activities of auxotrophs[44]. Our observation that purine bottlenecks lead to MIC increases, supports the transport hypothesis.

In conclusion, our results demonstrate that bacterial metabolism plays an important role for antibiotic resistance, which in turn implies that the nutritional environment at an infection site is equally important. We used minimal media to control the supply of metabolites and to systematically evaluate the response of *E. coli* to the availability of nutrients like adenine. This is not feasible with complex media like Mueller-Hinton broth, which contains variable components that may deplete unevenly during an experiment. Although our experimental conditions differ from *in vivo* environments, our findings contribute to a more detailed understanding of how metabolic mutations can simultaneously influence both antibiotic resistance and tolerance. Given that the effect of metabolic mutations is highly condition- and nutrient dependent, our results emphasize the need for new approaches to treat bacterial infections, either by considering metabolic strain level variation or by targeting the extracellular environment at an infection site to maximize efficacy of an antibiotic.

Bibliography

1.   Mattar, C., Edwards, S., Baraldi, E. & Hood, J. An overview of the global antimicrobial resistance research and development hub and the current landscape. *Curr Opin Microbiol* **57**, 56–61 (2020).

2.   Murray, C. J. *et al.* Global burden of bacterial antimicrobial resistance in 2019: a systematic analysis. *The Lancet* **399**, 629–655 (2022).

3.   Yelin, I. & Kishony, R. Antibiotic Resistance. *Cell* **172**, 1136-1136.e1 (2018).

4.   Darby, E. M. *et al.* Molecular mechanisms of antibiotic resistance revisited. *Nat Rev Microbiol* **21**, 280–295 (2023).

5.   Stokes, J. M., Lopatkin, A. J., Lobritz, M. A. & Collins, J. J. Bacterial Metabolism and Antibiotic Efficacy. *Cell Metab* **30**, 251–259 (2019).

6.   Brauner, A. & Balaban, N. Q. Quantitative biology of survival under antibiotic treatments. *Curr Opin Microbiol* **64**, 139–145 (2021).

7.   Bhargava, P. & Collins, J. J. Boosting bacterial metabolism to combat antibiotic resistance. *Cell Metab* **21**, 154–155 (2015).

8.   Schrader, S. M. *et al.* Multiform antimicrobial resistance from a metabolic mutation. *Sci Adv* **7**, eabh2037 (2021).

9.   Rubin, D. H. F. *et al.* CanB is a metabolic mediator of antibiotic resistance in *Neisseria gonorrhoeae*. *Nat Microbiol* **8**, 28–39 (2023).

10.   Lopatkin, A. J. *et al.* Clinically relevant mutations in core metabolic genes confer antibiotic resistance. *Science* **371**, eaba0862 (2021).

11.   Zampieri, M. *et al.* Metabolic constraints on the evolution of antibiotic resistance. *Mol Syst Biol* **13**, 917 (2017).

12.   Garst, A. D. *et al.* Genome-wide mapping of mutations at single-nucleotide resolution for protein, metabolic and genome engineering. *Nat Biotechnol* **35**, 48–55 (2017).

13.   Dewachter, L. *et al.* Deep mutational scanning of essential bacterial proteins can guide antibiotic development. *Nat Commun* **14**, 241 (2023).

14.   Lopatkin, A. J. & Yang, J. H. Digital Insights Into Nucleotide Metabolism and Antibiotic Treatment Failure. *Front. Digit. Health* **3**, 583468 (2021).

15.   Lobritz, M. A. *et al.* Antibiotic efficacy is linked to bacterial cellular respiration. *Proc. Natl. Acad. Sci. U.S.A.* **112**, 8173–8180 (2015).

16.   Van den Bergh, B. *et al.* Mutations in respiratory complex I promote antibiotic persistence through alterations in intracellular acidity and protein synthesis. *Nat Commun* **13**, 546 (2022).

17.   Lopatkin, A. J. *et al.* Bacterial metabolic state more accurately predicts antibiotic lethality than growth rate. *Nat Microbiol* **4**, 2109–2117 (2019).

18.   Yang, J. H. *et al.* A White-Box Machine Learning Approach for Revealing Antibiotic Mechanisms of Action. *Cell* **177**, 1649-1661.e9 (2019).

19.   Conlon, B. P. *et al.* Persister formation in *Staphylococcus aureus* is associated with ATP depletion. *Nat Microbiol* **1**, 16051 (2016).

20.   Wilmaerts, D. *et al.* The Persistence-Inducing Toxin HokB Forms Dynamic Pores That Cause ATP Leakage. *mBio* **9**, e00744-18 (2018).

21.   Shan, Y. *et al.* ATP-Dependent Persister Formation in *Escherichia coli*. *mBio* **8**, e02267-16 (2017).

22.   Lee, A. J. *et al.* Robust, linear correlations between growth rates and β-lactam-mediated lysis rates. *Proc Natl Acad Sci U S A* **115**, 4069–4074 (2018).

23.   Schramm, T. *et al.* Mapping temperature-sensitive mutations at a genome scale to engineer growth switches in *Escherichia coli*. *Mol Syst Biol* **19**, e11596 (2023).

24.   Monk, J. M. *et al.* iML1515, a knowledgebase that computes *Escherichia coli* traits. *Nat Biotechnol* **35**, 904–908 (2017).

25.   Taber, H. W., Mueller, J. P., Miller, P. F. & Arrow, A. S. Bacterial uptake of aminoglycoside antibiotics. *Microbiol Rev* **51**, 439–457 (1987).

26.   Muir, M. E., Hanwell, D. R. & Wallace, B. J. Characterization of a respiratory mutant of *Escherichia coli* with reduced uptake of aminoglycoside antibiotics. *Biochim Biophys Acta* **638**, 234–241 (1981).

27.   Bryan, L. E. & Van Den Elzen, H. M. Effects of membrane-energy mutations and cations on streptomycin and gentamicin accumulation by bacteria: a model for entry of streptomycin and gentamicin in susceptible and resistant bacteria. *Antimicrob Agents Chemother* **12**, 163–177 (1977).

28.   Pal, A. & Andersson, D. I. Bacteria can compensate the fitness costs of amplified resistance genes via a bypass mechanism. *Nat Commun* **15**, 2333 (2024).

29.   Haines, T. H. & Dencher, N. A. Cardiolipin: a proton trap for oxidative phosphorylation. *FEBS Lett* **528**, 35–39 (2002).

30.   Miller, C. *et al.* SOS response induction by beta-lactams and bacterial defense against antibiotic lethality. *Science* **305**, 1629–1631 (2004).

31.   Potts, A. H. *et al.* Global role of the bacterial post-transcriptional regulator CsrA revealed by integrated transcriptomics. *Nat Commun* **8**, 1596 (2017).

32.   Prajapati, J. D., Kleinekathöfer, U. & Winterhalter, M. How to Enter a Bacterium: Bacterial Porins and the Permeation of Antibiotics. *Chem. Rev.* **121**, 5158–5192 (2021).

33.   Spratt, B. G. Properties of the penicillin-binding proteins of *Escherichia coli* K12,. *Eur J Biochem* **72**, 341–352 (1977).

34.   Guder, J. C., Schramm, T., Sander, T. & Link, H. Time-Optimized Isotope Ratio LC–MS/MS for High-Throughput Quantification of Primary Metabolites. *Anal. Chem.* **89**, 1624–1631 (2017).

35.   Zeng, J. *et al.* A broadly applicable, stress-mediated bacterial death pathway regulated by the phosphotransferase system (PTS) and the cAMP-Crp cascade. *Proc Natl Acad Sci U S A* **119**, e2118566119 (2022).

36.   Xi, H., Schneider, B. L. & Reitzer, L. Purine catabolism in *Escherichia coli* and function of xanthine dehydrogenase in purine salvage. *J Bacteriol* **182**, 5332–5341 (2000).

37.   Liu, J., Gefen, O., Ronin, I., Bar-Meir, M. & Balaban, N. Q. Effect of tolerance on the evolution of antibiotic resistance under drug combinations. *Science* **367**, 200–204 (2020).

38.   Farke, N., Schramm, T., Verhülsdonk, A., Rapp, J. & Link, H. Systematic analysis of in-source modifications of primary metabolites during flow-injection time-of-flight mass spectrometry. *Anal Biochem* **664**, 115036 (2023).

39.   Andersen-Civil, A. I. S. *et al.* The impact of inactivation of the purine biosynthesis genes, purN and purT, on growth and virulence in uropathogenic *E. coli*. *Mol Biol Rep* **45**, 2707–2716 (2018).

40.   Vogel-Scheel, J., Alpert, C., Engst, W., Loh, G. & Blaut, M. Requirement of purine and pyrimidine synthesis for colonization of the mouse intestine by *Escherichia coli*. *Appl Environ Microbiol* **76**, 5181–5187 (2010).

41.   Samant, S. *et al.* Nucleotide biosynthesis is critical for growth of bacteria in human blood. *PLoS Pathog* **4**, e37 (2008).

42.   Shaffer, C. L. *et al.* Purine Biosynthesis Metabolically Constrains Intracellular Survival of Uropathogenic *Escherichia coli*. *Infect Immun* **85**, e00471-16 (2017).

43.   Zhao, X. *et al.* Glutamine promotes antibiotic uptake to kill multidrug-resistant uropathogenic bacteria. *Science Translational Medicine* **13**, eabj0716 (2021).

44.   Yu, J. S. L. *et al.* Microbial communities form rich extracellular metabolomes that foster metabolic interactions and promote drug tolerance. *Nat Microbiol* **7**, 542–555 (2022).

45.   Lawson, M. J. *et al.* In situ genotyping of a pooled strain library after characterizing complex phenotypes. *Mol Syst Biol* **13**, 947 (2017).

46.   Qi, L. S. *et al.* Repurposing CRISPR as an RNA-Guided Platform for Sequence-Specific Control of Gene Expression. *Cell* **152**, 1173–1183 (2013).

47.   Sayers, E. W. *et al.* Database resources of the national center for biotechnology information. *Nucleic Acids Res* **50**, D20–D26 (2022).

48.   Edgar, R. C. MUSCLE: multiple sequence alignment with high accuracy and high throughput. *Nucleic Acids Res* **32**, 1792–1797 (2004).

Authors contribution: Conceptualization: PL, HL; Methodology: PL, TS, HL; Investigation: all authors; Visualization: PL, HL; Funding acquisition: PL, HL; Project administration: HL; Supervision: HL; Writing – original draft: PL, HL.

Competing interests: Authors declare that they have no competing interests.

Data availability statement: The experimental data that support the findings of this study are available in Figshare with the identifier: 10.6084/m9.figshare.25712259. Illumina sequencing data are provided on the EMBL-EBI European Nucleotide Archive (ENA) online repository: ERP159795.

Material and methods

Strains

E. coli BW25113 was used to construct the CRISPR library and the strains PurA^{L75D}, PurM^{F105A}, HisF^{V126P} and PurK^{E49G}. *E. coli* YYdCas9[45] was used for CRISPRi. One Shot™ TOP10 *E. coli* (Thermo Fischer #C404010) was used for intermediate cloning. Clinical isolates were obtained from the Institute for medical microbiology and hygiene (Tübingen) and were identified using MALDI-TOF mass spectrometry.

Media

Cultivations were performed in LB medium (Sigma #L3522) or M9 minimal medium with glucose as sole carbon source (5 g/L). M9 medium was composed by (per liter): 7.52 g Na$_2$HPO$_4$ 2 H$_2$O, 5 g KH$_2$PO$_4$, 1.5 g (NH$_4$)$_2$sO$_4$, 0.5 g NaCl. The following components were sterilized separately and then added (per liter of final medium): 1 mL 0.1 M CaCl$_2$, 1 mL 1 M MgSO$_4$, 0.6 mL 0.1 M FeCl$_3$, 2 mL 1.4 mM thiamine-HCl and 10 mL trace salts solution. The trace salts solution contained (per liter): 180 mg ZnSO$_4$ 7 H$_2$O, 120 mg CuCl$_2$ 2 H$_2$O, 120 mg MnSO$_4$ H$_2$O, 180 mg CoCl$_2$ 6 H$_2$O. When needed, M9 agar plates were done by mixing (1:1) a 2X M9 solution with 3 g/L molten agar (Roth #5210.2). In either liquid or agar medium, kanamycin (50 µg/mL; Roth #T832.3) was added when strains harboured a pgRNA plasmid with a kanamycin resistance cassette and was supplemented with chloramphenicol (30 µg/mL; Merck #C0378-25G) when strains harboured pTS040 and pTS041. When needed, gentamicin (Roth #O233.2), carbenicillin (Roth #6344.3), aztreonam (Biosynth #AA18120), tobramycin (Biosynth #AT161114) or meropenem (BLD pharm #BD23263) were added to the M9 medium at various concentrations specified for each experiment. Adenine (Sigma #A8751-1G) was added to agar and liquid medium at a final concentration of 1 mM, and to agar and liquid medium at final concentration 100 µM for experiments with hospital bacterial isolates. 5-aminolevulinic acid (Merck # A7793) was added to agar and liquid medium at a final concentration of 10 mg/mL. L-histidine (Merck # H8000) and L-methionine (Merck # 64319) were added to liquid medium at 200 µM. When required, glucose-6-phosphate (Merck #G7879) was added to agar and liquid minimal mediums in replacement of glucose at a final concentration of 1 g/L. To induce dCas9 expression, the CRISPRi experiments were performed with

0.2 µM of anhydrotetracycline (aTc; Cayman Chemicals #10009542) in liquid medium and 1 µM aTc in agar medium.

Agar dilution assays to measure MICs

M9 agar plates with various concentrations of antibiotics and additives were prepared as described above. Precultures in 4 mL LB were inoculated from glycerol stocks for 8 h at 37°C and 220 rotations per minutes (RPM) shaking and transferred to M9 medium for overnight incubation at 37°C and 220 RPM. Before starting the assay, precultures were reinoculated and grown in fresh M9 medium to obtain exponentially growing cells. Then, cultures were diluted with fresh M9 medium to set OD_{600} = 0.1. A 96-well plate was prepared with three wells containing 135 µL of fresh M9 medium for each strain to be spotted. Each preculture was then 1:10 diluted by mixing 15 µL of the 0.1 OD_{600} preculture with 135 µL of fresh medium. This process was repeated two times to generate the 1:100 and 1:1000 dilutions. 7 µL of each dilution was then added to the agar plate with a multi-channel pipette to generate the spots. Spots were then left to dry under a flame and plates were incubated for 48 h at 37°C. After incubation, plates were imaged with an Epson V370 scanner.

Cultivation conditions for metabolome sampling

Precultures in 4 mL LB were inoculated from glycerol stocks for 8 h at 37°C 220 RPM shaking and transferred to M9 medium for overnight incubation at 37°C and 220 RPM. M9 pre-cultures in exponential phase were used to inoculate shake flasks containing 10 mL of M9 medium with a starting OD_{600} of 0.1. Strains were cultivated in triplicates until OD_{600} reached 0.25-0.6. For metabolomics, flasks were then rapidly transferred to a thermostatically controlled hood at 37°C and an equivalent of OD_{600} = 1 was sampled. For metabolome profiling of clinical isolates, 96-well deep-well plates were prepared with 1 mL of LB medium. The selected 41 strains with growth defects were added each to two wells from glycerol stocks. The plate was sealed with Breathe-Easy foils (Diverse Biotech #BEM-1) and incubated for 6 h at 37°C 220 RPM. The plate was then centrifuged at maximum speed and 37°C. Supernatant was discarded and pellets were each resuspended with 1 mL of M9 medium with glucose. The washing step was repeated. The plate was then incubated for 1 h 30 min at 37°C and 220 RPM. Sampling was then performed by pelleting the cells in deep-well plates as described below.

Metabolomics measurements

Cultivations were performed as described above. For targeted metabolomics, culture aliquots were vacuum-filtered on a 0.45 µm pore size filter (Merck Millipore #HVLP02500). Filters were

immediately transferred into a 40:40:20 (v-%) acetonitrile (Honeywell # 14261-1I)/methanol (VWR # 83638.320)/water extraction solution at -20°C. Filters were incubated in the extraction solution for at least 30 minutes. Subsequently, metabolite extracts were centrifuged for 15 minutes at 13,000 RPM at -9°C and the supernatants were stored at -80°C until analysis. Metabolite extracts were mixed with a ^{13}C-labeled internal standard in a 1:1 ratio. LC-MS/MS analysis was performed with an Agilent 6495 triple quadrupole mass spectrometer (Agilent Technologies) as described previously[34]. An Agilent 1290 Infinity II UHPLC system (Agilent Technologies) was used for liquid chromatography. Temperature of the column oven was 30°C, and the injection volume was 3 µL. LC solvents in channel A were either water with 10 mM ammonium formate and 0.1% formic acid (v/v) (for acidic conditions), or water with 10 mM ammonium carbonate and 0.2% ammonium hydroxide (for basic conditions). LC solvents in channel B were either acetonitrile with 0.1% formic acid (v/v) (for acidic conditions) or acetonitrile without additive (for basic conditions). LC columns were an Acquity BEH Amide (30 x 2.1 mm, 1.7 µm) for acidic conditions, and an iHILIC-Fusion(P) (50 x 2.1 mm, 5 µm) for basic conditions. The gradient for basic and acidic conditions was: 0 min 90% B; 1.3 min 40 % B; 1.5 min 40 % B; 1.7 min 90 % B; 2 min 90 % B. The ratio of ^{12}C and ^{13}C peak heights was used to quantify metabolites.

For flow-injection metabolomics, metabolite extracts were obtained by pelleting the cells in deep-well plates at maximum speed for 2 minutes at 37°C. Supernatant was then discarded and pellets were resuspended with 200 µL of 40:40:20 (v-%) acetonitrile/methanol/water extraction solution at -20°C. The plates were sealed and incubated overnight at -20°C. Pellets were then resuspended and centrifugated at maximum speed for 5 min at -9°C. 150 µL of supernatant from each well was transferred to a 96-well plate and stored at -80°C for measurements. Extracts were directly injected into an Agilent 6546 Series quadrupole time-of-flight mass spectrometer (Agilent Technologies, USA) as described previously[38]. The electrospray source was operated in negative and positive ionization mode. The mobile phase was 60:40 isopropanol:water buffered with 10 mM ammonium carbonate (NH4)2CO3 and 0.04 % (v/v) ammonium hydroxide for both ionization modes, and the flow rate was 0.15 mL/min. For online mass axis correction, 2-propanol (in the mobile phase) and HP-921 were used for negative mode and purine and HP-921 were used for positive mode. Mass spectra were recorded in profile mode from 50 to 1700 m/z with a frequency of 1.4 spectra/s for 0.5 min using 10 Ghz resolving power. Raw data files were converted into mzXML files and processed by custom MATLAB scripts. The 32 spectra with the highest signal in the total ion count were summed and baseline

adjusted with *msbackadj.m*. Peaks with a minimum peak height of 5000 units and a peak prominence of 5000 units were selected with *findpeaks.m*, and annotated with a 3 mDa tolerance by matching monoisotopic masses of all metabolites in the *i*ML1515 model[24], considering a single proton loss ($[M-H]^-$) in negative mode and single proton gain ($[M+H]^+$) in positive mode. Positive and negative mode annotation were merged and if a metabolite was annotated in both modes positive mode was selected. For each metabolite, the height of the annotated ion peak was taken for further analysis and normalized to the mean across the 41 isolates to obtain fold-changes values.

Generation of growth curves and determination of growth rates

Precultures in 4 mL LB were inoculated from glycerol stocks for 8 h at 37°C 220 RPM shaking and transferred to M9 medium for overnight incubation at 37°C and 220 RPM. M9 pre-cultures in exponential phase were used to inoculate 96-well plates at starting OD_{600} <0.05. Incubation was performed for 24 h at 37°C. Various plate readers were used (BioTek Epoch, BioTek Synergy, Tecan Infinite 200 Pro, Tecan Spark). Therefore, OD_{600} values were corrected based on former calibration experiments

For generation of adenine feeding growth data (for the BW25113 PurK^{E49G} and control strain), precultures in 4 mL LB were inoculated from glycerol stocks for 6 h at 37°C 220 RPM shaking. Then, 2 mL of each culture was centrifugated at maximum speed for 5 minutes. Supernatant was discarded and pellet was resuspended in 2 mL of M9 medium with glucose. Washing and resuspension was repeated. OD_{600} was then measured and normalised across the strains. A 96-well plate with M9 medium supplemented with or without 1 mM adenine was then inoculated with the washed cultures. OD_{600} was measured in a BioTek Synergy plate reader for 24 h at 37°C.

Growth rates were determined with the following method: coefficients of determination (R^2) were calculated over a 2 h time window. Only arrays with R^2> 0.99 were selected. Growth rates were determined by linear regression and maximal growth rates were selected. For clinical isolates Area Under Curve (AUC) determination, six 96-well deep-well plates were prepared with 500 µL of LB medium without antibiotics per well. Strains EC-1 to EC-256 were added each to a single well from glycerol stocks in duplicates. Plates were sealed with Breathe-Easy foils and incubated for 6 h at 37°C 220 RPM. Then, 50 µL of each well was used to inoculate any of six deep-well plates with 450 µL M9 medium with glucose and no antibiotics (1:10 dilution). This operation was repeated for a final 1:100 dilution of the LB inoculum in M9 medium. Six 96-well plates were prepared with each 135 µL of M9 medium with glucose and

no antibiotics. 15 μL in wells of the previously prepared deep-well plates were used to inoculate these 96-well plates. The plates were sealed with a lid and parafilm and incubated for 24 h at 37°C in BioTek Logphase 600 plate readers. The AUC was determined as the integral of ODs between 0 and 12 h via the trapezoidal method with unit spacing (*trapz.m* MATLAB function).

Screening of antibiotic resistance of the CRISPR library

Antibiotic resistance was screened in a pooled CRISPR library with 15,120 *E. coli* mutants that was constructed previously[26]. The CRISPR library and the control strain were each cultivated in 10 mL LB medium at 30°C until OD_{600} reached 0.5. An equivalent of $OD_{600} = 5$ was then centrifuged at 30°C and pellets were resuspended in 10 mL of fresh M9 medium. Centrifugation was repeated to remove traces of LB medium. Cells were resuspended in 10 mL of M9 medium and further incubated at 30°C for 1 h. OD_{600} was then set to 0.5 and 500 μL were used to inoculate 150x20 mm M9 agar plates. Plates were then incubated at 37°C for 48 h. After incubation, plates were imaged with an Epson V370 scanner. If necessary, colonies were counted. Then, colonies were harvested from each plate using 7.5 mL of LB medium. OD_{600} was measured and an equivalent of $OD_{600} = 10$ was pelleted in a microcentrifuge tube. Plasmids were then purified by miniprep (Thermo scientist, GeneJET Plasmid Miniprep Kit) for amplification of repair templates and sgRNA (barcodes). Hereafter, 3 ng of plasmid DNA was used for amplification (15 cycles) of the barcodes using two primers suited for further indexing PCRs:

forward primer:

5'-TCGTCGGCAGCGTCAGATGTGTATAAGAGACAGGTATCACGAGGCAGATCCTCTG-3'

reverse primer:

 5'-GTCTCGTGGGCTCGGAGATGTGTATAAGAGACAGACTCGGTGCCACTTTTTCAAGTT-3'

Amplicons were purified by AMPure XP PCR beads (Beckman Coulter, #A63881). Using standard Illumina indexing primers, amplicons were indexed in a second PCR and again purified by bead-clean up. Amplicons were pooled and sequenced on an Illumina NextSeq 500 (paired-end, NextSeq™ 500 Mid Output Kit v2.5, #20024908, 300 cycles).

Statistical testing

All p-values obtained in this manuscript were obtained by performing paired two-tailed t-tests using custom python scripts (bioinfokit package) and Microsoft Excel. Volcano plots were made using custom python scripts (bioinfokit package). Pearson correlation coefficients (PCC) and coefficients of determination (R^2) were calculated with custom python scripts (sci-kit learn and SciPy packages).

Illumina sequencing data analysis

Demultiplexed paired-end reads were aligned, merged (based on overlapping sequences), and trimmed to the region of interest using a custom Matlab script. The resulting processed reads were mapped against the designed sequences of the library. For each library member, the number of matching reads was counted. Only reads that shared a 100% identity with a designed sequence were considered for further analysis. Read counts of 0 were set to 1, to avoid division by 0. Read counts lower than 15 on both reference plates and antibiotic plates were not considered in the analysis. Read counts were normalized by dividing the read counts of each mutants by the total number of reads in a given sample. Fold-changes were calculated by dividing normalized read counts of each mutant on the antibiotic plates by normalized read counts on the reference plates obtained from the same experiment.

Construction of single CRISPR strains

The PurK^{E49G}, PurA^{L75D}, PurM^{F105A} and HisF^{V126P} strains were re-constructed with the same method as the CRISPR library. Plasmid pT0S41 was first transformed with electroporation into WT BW25113. Plasmids pTS040 were built by assembling the pTS040 backbone with oligonucleotides (Twist Bioscience) encoding sgRNA and homology arms associated with the desired mutations. Then, plasmids pTS040 were transformed with electroporation after 30 min induction with 7.5 g/L arabinose (lambda red expression). Strains were cultivated for 1 h in SOC medium with kanamycin and 1 µM aTc to induce Cas9 expression. Strains were then plated on LB agar with kanamycin, chloramphenicol and 1 µM aTc. Incubation was done at 37°C overnight. Subsequently, single colonies were picked for colony PCR to amplify the potentially mutated genes of interest. PCR amplicons were purified (Macherey-Nagel #740609) and used for sequencing (Eurofins genomics). Sequences were analysed with the Benchling software and the MAFFT algorithm. Strains with the correct mutations were

cultivated overnight in 4 mL LB with kanamycin and chloramphenicol to prepare glycerol stocks. Mutants PtsI[I330P], RibD[L364W], PgsA[V44P], IspE[V146W] and HemA[L276Q] were isolated directly from the CRISPR library after gentamicin challenge and mutations were confirmed by sequencing the genomic region as described above. The cloning and isolation of the LeuB[I134P] mutant has been described previously[23].

Construction of CRISPRi strains

Plasmids pgRNAK-*purA*#1 (protospacer: 5'-TTTACCTTCGTCACCCCATT-3') and pgRNAK-*mRFP* (protospacer: 5'-AACTTTCAGTTTAGCGGTCT-3') were constructed by exchanging the ampicillin resistance cassette of the plasmid pgRNA (Addgene #44251)[46] with a kanamycin resistance cassette. Plasmids were then transformed into the *E. coli* strain YYdCas9[37] using electroporation.

Time-kill assay

Precultures in 4 mL LB were inoculated from glycerol stocks for 8 h at 37°C and 220 RPM and transferred to M9 medium for overnight incubation at 37°C and 220 RPM. M9 pre-cultures were used to re-inoculate shake flasks containing 25 mL of M9 medium with kanamycin and chloramphenicol. When OD_{600} 0.25 was reached, 10 mL of medium were transferred to a new shake flask and carbenicillin was added at a final concentration 50 µg/mL or 25 µg/mL depending on the strain tested. Cells were incubated at 37°C and 220 RPM. At each time point, 1 mL of each culture was sampled into a microcentrifuge tube and cells were centrifuged at 3000 RPM for 10 min. Supernatant was discarded and cells were resuspended in 1 mL of fresh M9 medium without carbenicillin. This washing step was then repeated. Cells were then serial diluted in fresh M9 medium by a factor of 10 to obtain dilutions of 1:100, 1:1000, 1:10000 and 1:100000. 100 µL from each dilution were then plated on M9 agar and incubated 48 h at 37°C. Colonies were then counted to quantify colony forming units (CFUs) per mL.

For time-kill assays with hospital bacterial isolates, precultures of EC-244 were first performed in LB for 8 h at 37°C. Each preculture was then split into one M9 preculture with 100 µM adenine and one preculture without adenine, and grown overnight at 37°C. The next day, cultures in exponential phase were used to inoculate shake flasks with 25 mL of M9 medium with or without 100 µM adenine, with starting OD_{600} 0.25. Sulbactam (TCI #S0868) was added at a final concentration of 12.5 µg/mL and

carbenicillin was added at final concentration of 100 µg/mL. At indicated time points, 1 mL of culture were sampled from each flask and cells were washed with M9 medium supplemented with 5 g/L glucose and 100 µM adenine and plated on M9 agar supplemented with 100 µM adenine.

Whole genome sequencing of *E. coli* clinical isolates EC-244 and EC-249

DNA was extracted from of EC-244 and EC-249 using the DNeasy UltraClean Microbial Kit (Qiagen), followed by library preparation (Illumina DNA Prep, (M) Tagmentation, Illumina) and barcoding (IDT for Illumina DNA/RNA UD Indexes). Sequencing was performed using a MidOutput Cartridge (NextSeq 500/550 Mid Output Kit v2.5 (300 Cycles)) on an Illumina NextSeq 500 machine. Following the sequencing, an alignment of the resulting fastq files was performed using bowtie2. The genome of *E. coli* BW25113 was used as reference. Subsequently, the alignment was investigated using the Integrative Genomics Viewer (Version 2.16.0). A comparison of mutations within the *purK* gene was performed with genomes of clinical isolates from the NCBI Pathogens database[47]. A total of 9 369 genomes were collected, and PurK protein sequences were obtained for 4 352 genomes. Amino acid changes in these PurK protein sequences were identified by alignment with MUSCLE[48].
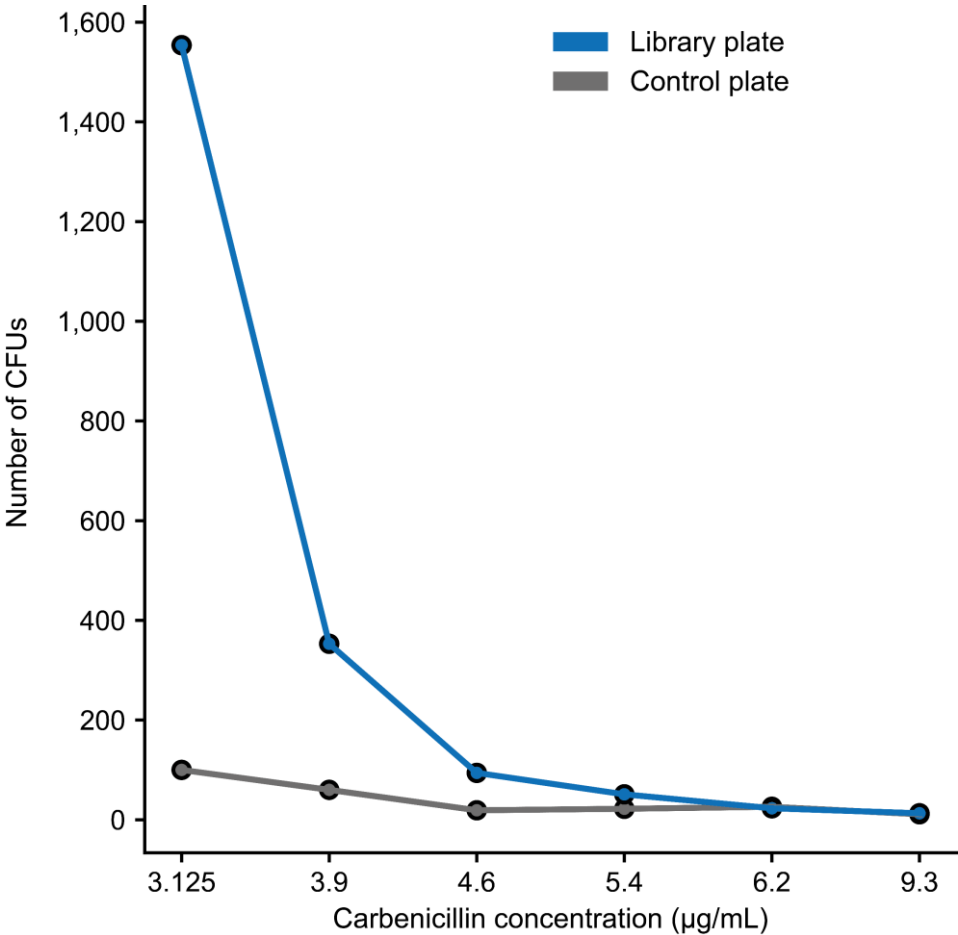
Supplements

Figure S1: The CRISPR library and control strain were plated on minimal agar medium with increasing concentration of carbenicillin. Colonies were counted after 48 h of incubation at 37°C.
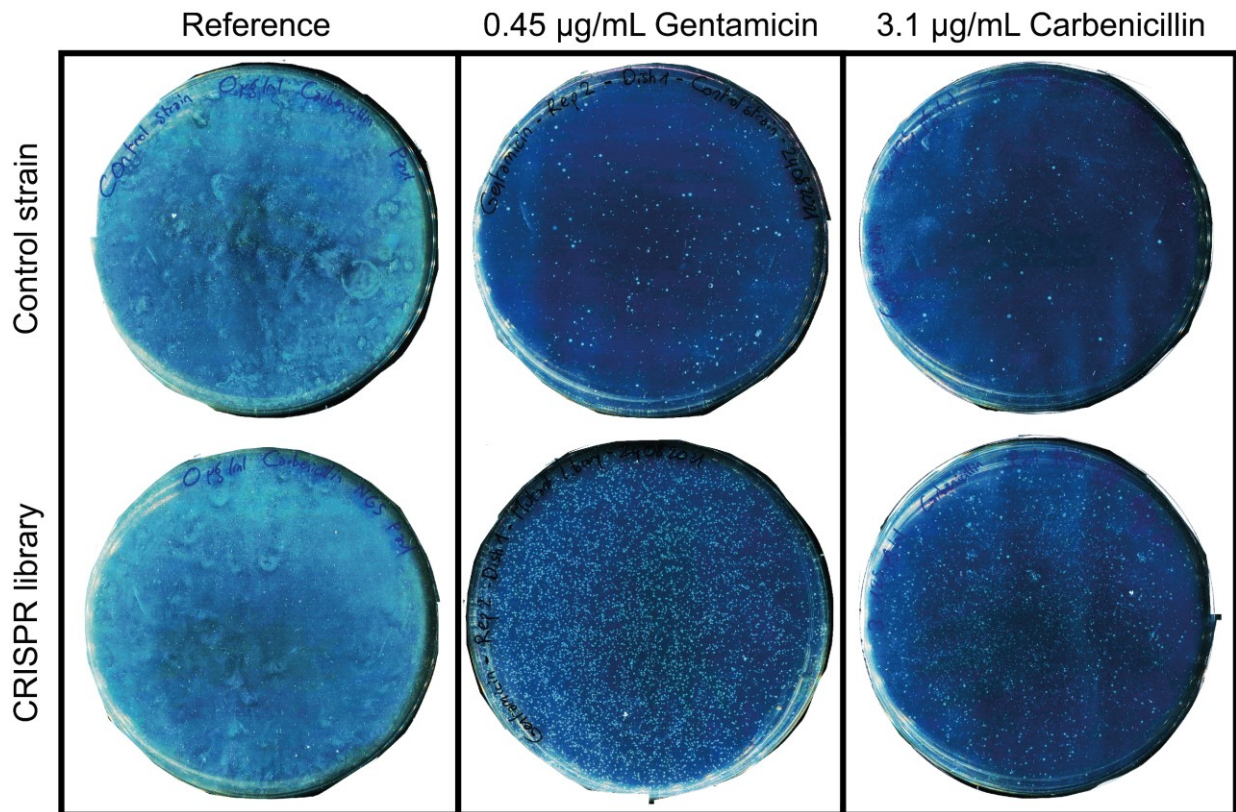
Figure S2: Images of M9 agar plates inoculated with the control strain (top) or the CRISPR library (bottom). Plates contained either gentamicin, carbenicillin, or no additional antibiotics (reference). Images were made with an Epson V370 scanner. Images were assembled using Adobe Illustrator. Brightness and contrast were adjusted with Microsoft PowerPoint.
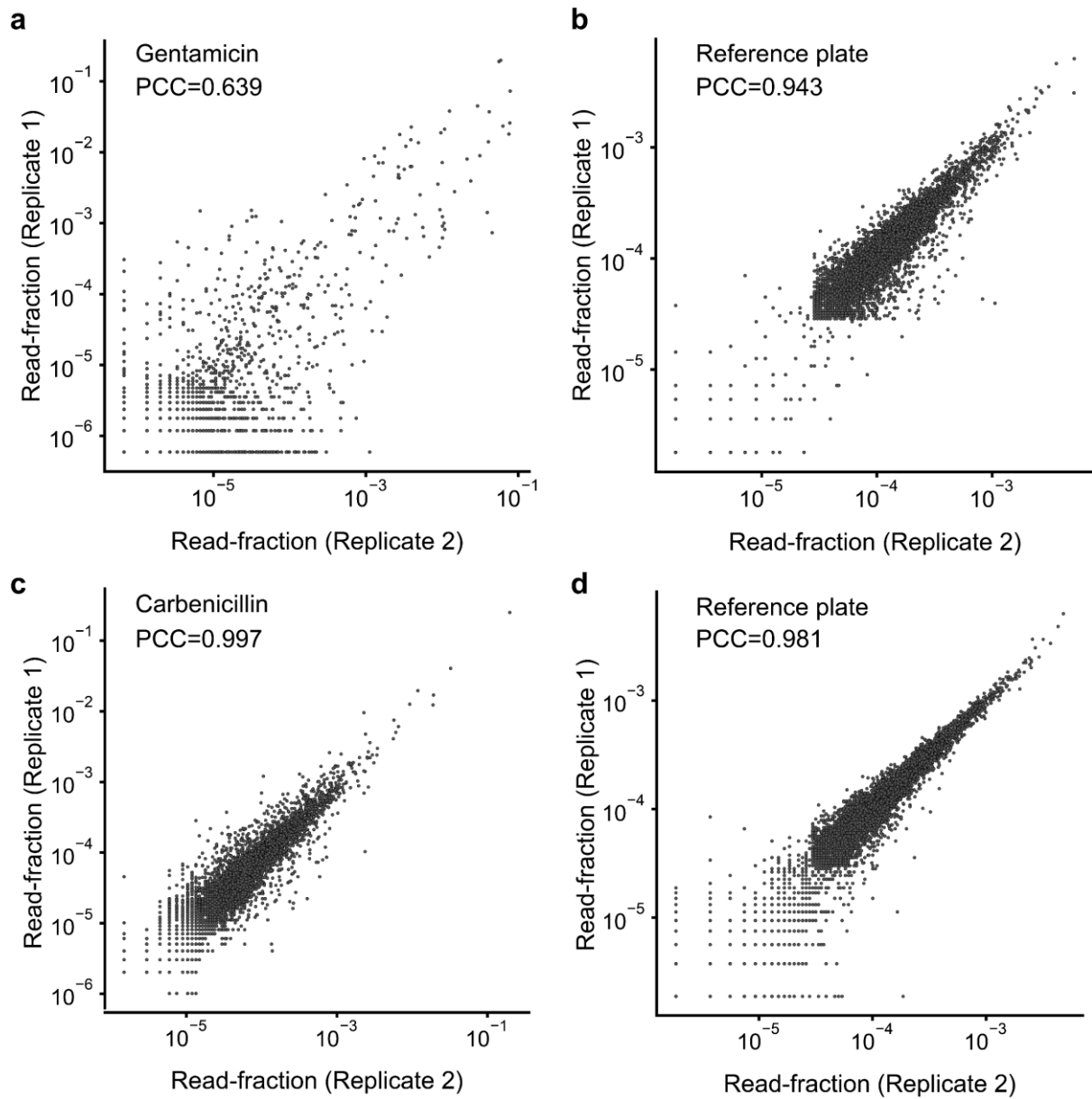
Figure S3: Scatter plots show read-fractions of barcodes of mutants in the CRISPR library. (a) and (b) are barcode read-fractions from the gentamicin screen. (c) and (d) are barcode read-fractions from the carbenicillin screen. The Pearson correlation coefficient (PCC) is shown for the two replicates.
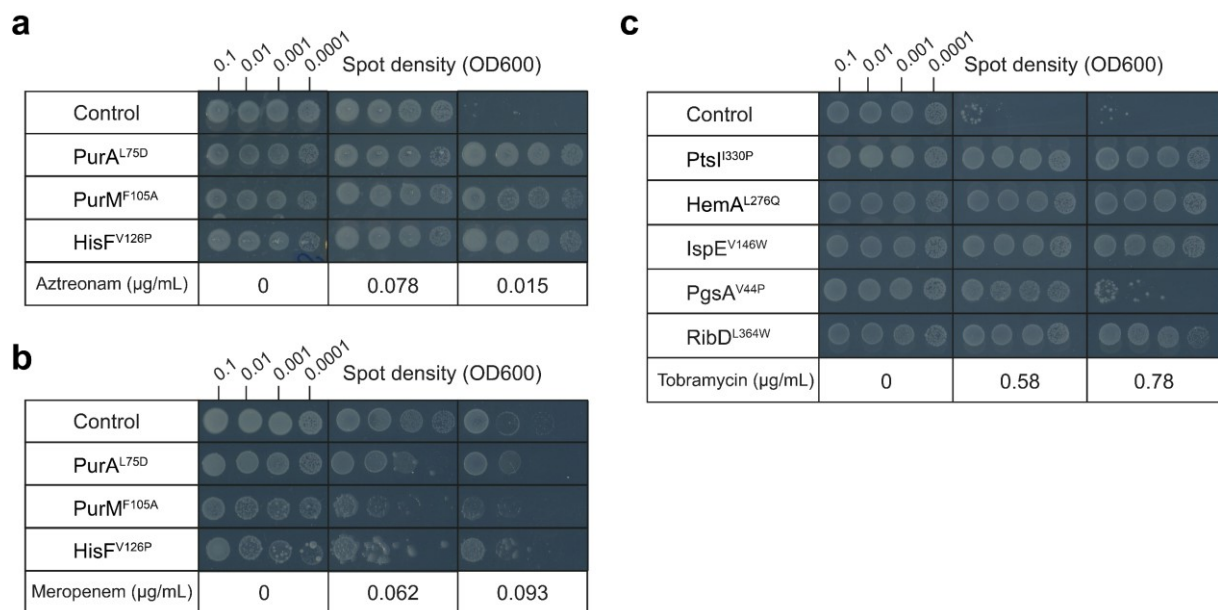
a

	0.1 0.01 0.001 0.0001 Spot density (OD600)		
Control			
PurA^{L75D}			
PurM^{F105A}			
HisF^{V126P}			
Aztreonam (µg/mL)	0	0.078	0.015

b

	0.1 0.01 0.001 0.0001 Spot density (OD600)		
Control			
PurA^{L75D}			
PurM^{F105A}			
HisF^{V126P}			
Meropenem (µg/mL)	0	0.062	0.093

c

	0.1 0.01 0.001 0.0001 Spot density (OD600)		
Control			
PtsI^{I330P}			
HemA^{L276Q}			
IspE^{V146W}			
PgsA^{V44P}			
RibD^{L364W}			
Tobramycin (µg/mL)	0	0.58	0.78

Figure S4: Agar dilution assays with the control strain and CRISPR mutants (RibD^{L364W}, PgsA^{V44P}, IspE^{V146W}, PtsI^{I330P}, HemA^{L276Q}, PurA^{L75D}, PurM^{F105A} and HisF^{V126P}). Strains were plated on minimal agar medium supplemented with the respective antibiotic of the β-lactam class aztreonam (a) or meropenem (b), or the aminoglycoside tobramycin (c). Multiple inoculum densities were used to assess inoculum effects. Plates were incubated 48 h. Shown are one of n = 2 replicates. Spot assays were performed on the same plate per concentration, and scans of plates with different concentrations were assembled into a single figure using Adobe Illustrator.
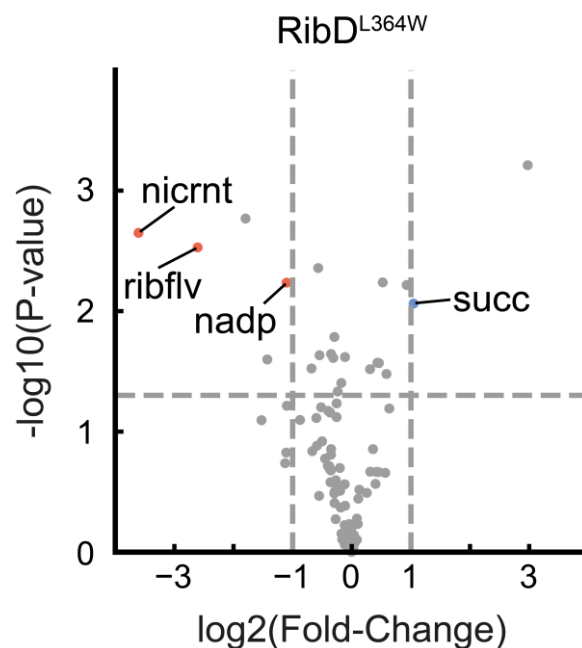

Figure S5: Volcano plot showing metabolite levels of the RibD^{L364W} mutant relative to the control strain (n = 3 distinct samples). Significant metabolites of interest are annotated (p-value < 0.05).

a

b

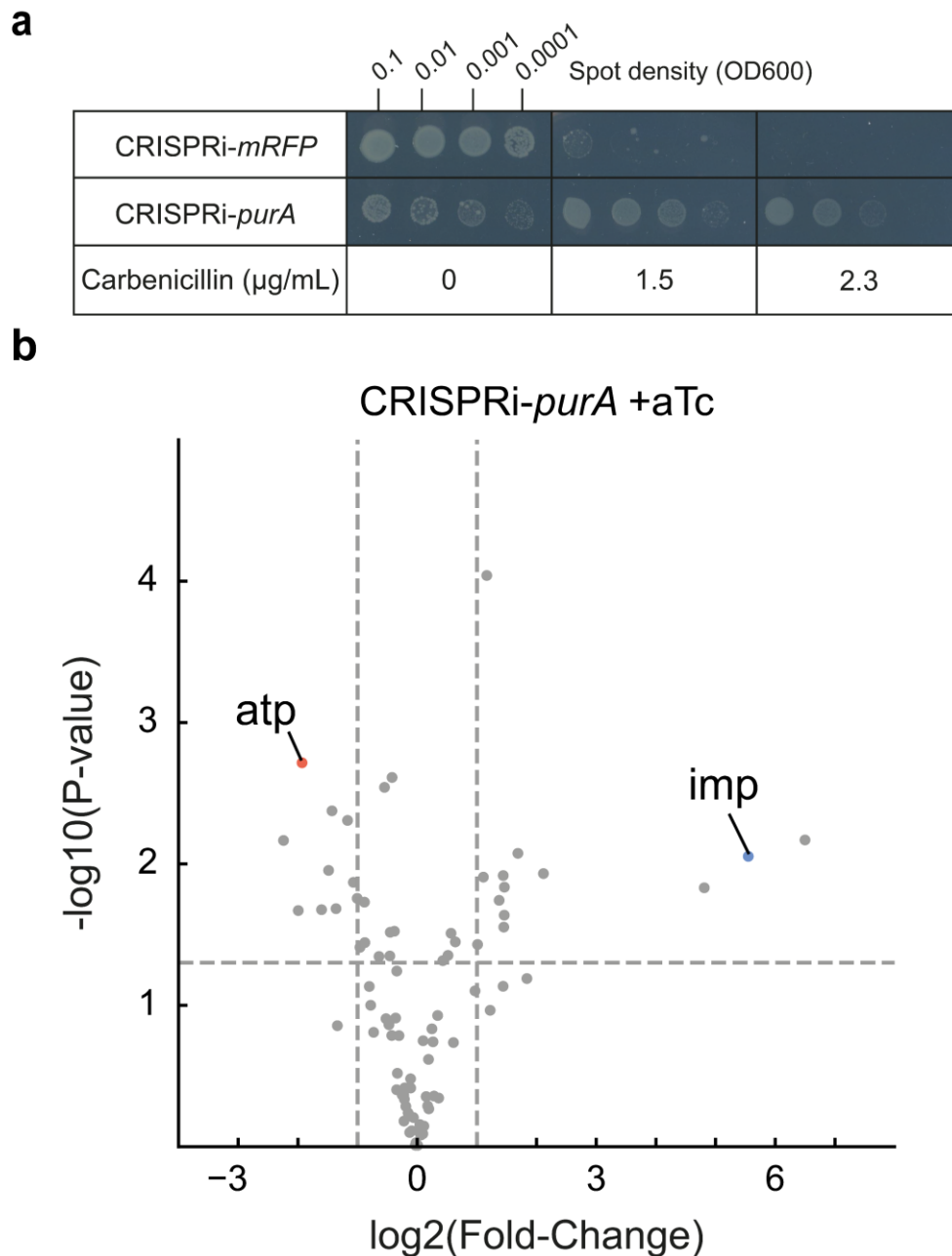**Figure S6: a,** Agar dilution assay with the CRISPRi-*purA* strain and the CRISPRi-*mRFP* strain (control). Each strain was plated on agar plates with minimal glucose medium containing increasing concentrations of carbenicillin (MIC = 1.5 µg/mL). 1 µM anhydrotetracycline (aTc) was added to induce the expression of dCas9. Multiple inoculum densities were used to assess inoculum effects. Plates were incubated 48 h. Shown is one of n = 2 replicates. Spot assays were performed on the same plate per concentration, and scans of plates with different concentrations were assembled into a single figure using Adobe Illustrator. **b,** Volcano plot showing metabolite levels of the aTc-induced CRISPRi-*purA* strain relative to the non-induced CRISPRi-*purA* strain (n = 3 distinct samples). Significant metabolites of interest are annotated (p-value < 0.05).

	0.1	0.01	0.001	0.0001	Spot density (OD600)		
Control							
PurA^{L75D}							
PurM^{F105A}							
HisF^{V126P}							
Carbenicillin (µg/mL)	0			1.5		2.3	3.1
Adenine (µM)	100						

Figure S7: Agar dilution assay with the control strain and three purine mutants (HisF^{V126P}, PurM^{F105A} and PurA^{L75D}). Each strain was spotted on agar plates with minimal glucose medium supplemented with 100 µM adenine and increasing concentrations of carbenicillin (MIC = 1.5 ☐g/mL). Plates were incubated 48 h. Shown is one of n = 2 replicates. Spot assays were performed on the same plate per concentration, and scans of plates with different concentrations were assembled into a single figure using Adobe Illustrator.
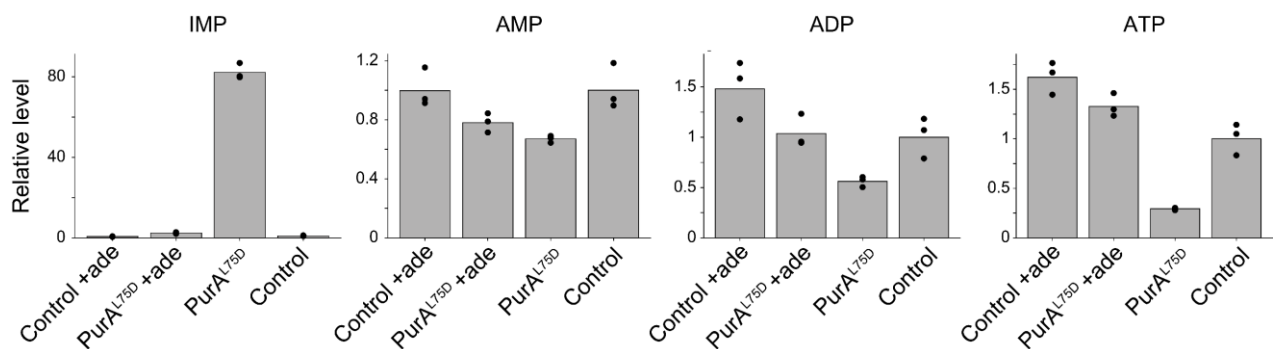

Figure S8: Relative levels of intracellular ATP, ADP, AMP and IMP in the Control and PurA^{L75D} strain in minimal glucose medium with or without supplementation of 1 mM adenine (ade). Data are normalized to the control strain without adenine. Bars are means of n = 3 distinct samples (black dots). Data for the control strain and the PurA^{L75D} mutant without adenine feeding is the same as shown in Fig. 2e.
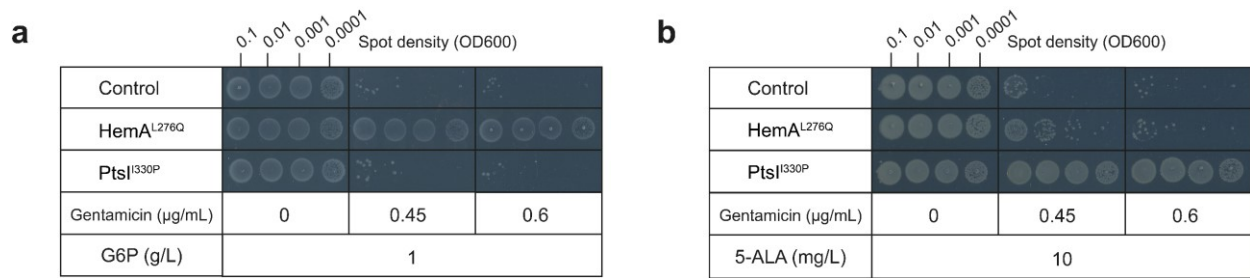
a

	0.1 0.01 0.001 0.0001 Spot density (OD600)		
Control			
HemA^{L276Q}			
PtsI^{I330P}			
Gentamicin (µg/mL)	0	0.45	0.6
G6P (g/L)	1		

b

	0.1 0.01 0.001 0.0001 Spot density (OD600)		
Control			
HemA^{L276Q}			
PtsI^{I330P}			
Gentamicin (µg/mL)	0	0.45	0.6
5-ALA (mg/L)	10		

Figure S9: a, Agar dilution assay with the control strain, the HemA^{L276Q} strain and the PtsI^{I330P} strain. Each strain was spotted on agar plates with minimal medium containing glucose-6-phosphate (G6P) instead of glucose as carbon source, and with increasing concentrations of gentamicin (MIC = 0.45 □g/mL). **b,** same as (a) but with glucose as carbon source and supplementation of 5-aminolevulinic acid (5-ALA). Plates were incubated 48 h. Spot assays were performed on the same plate per concentration, and scans of plates with different concentrations were assembled into a single figure using Adobe Illustrator.
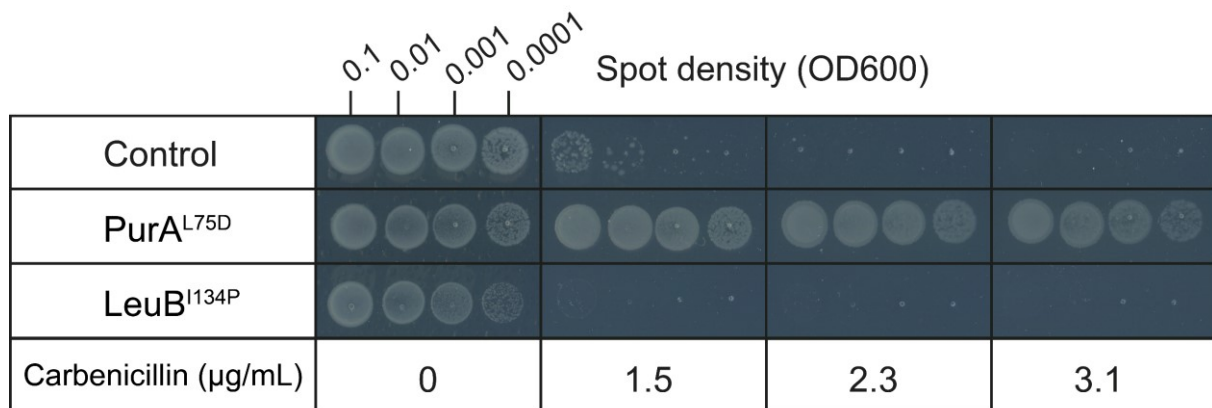
	0.1 0.01 0.001 0.0001 Spot density (OD600)			
Control				
PurA^{L75D}				
LeuB^{I134P}				
Carbenicillin (µg/mL)	0	1.5	2.3	3.1

Figure S10: Agar dilution assay with the control strain, the PurA^{L75D} strain and the slow-growth control LeuB^{I134P}. Plates were incubated 48 h. Spot assays were performed on the same plate per concentration, and scans of plates with different concentrations were assembled into a single figure using Adobe Illustrator. Shown is one of n = 2 replicates.
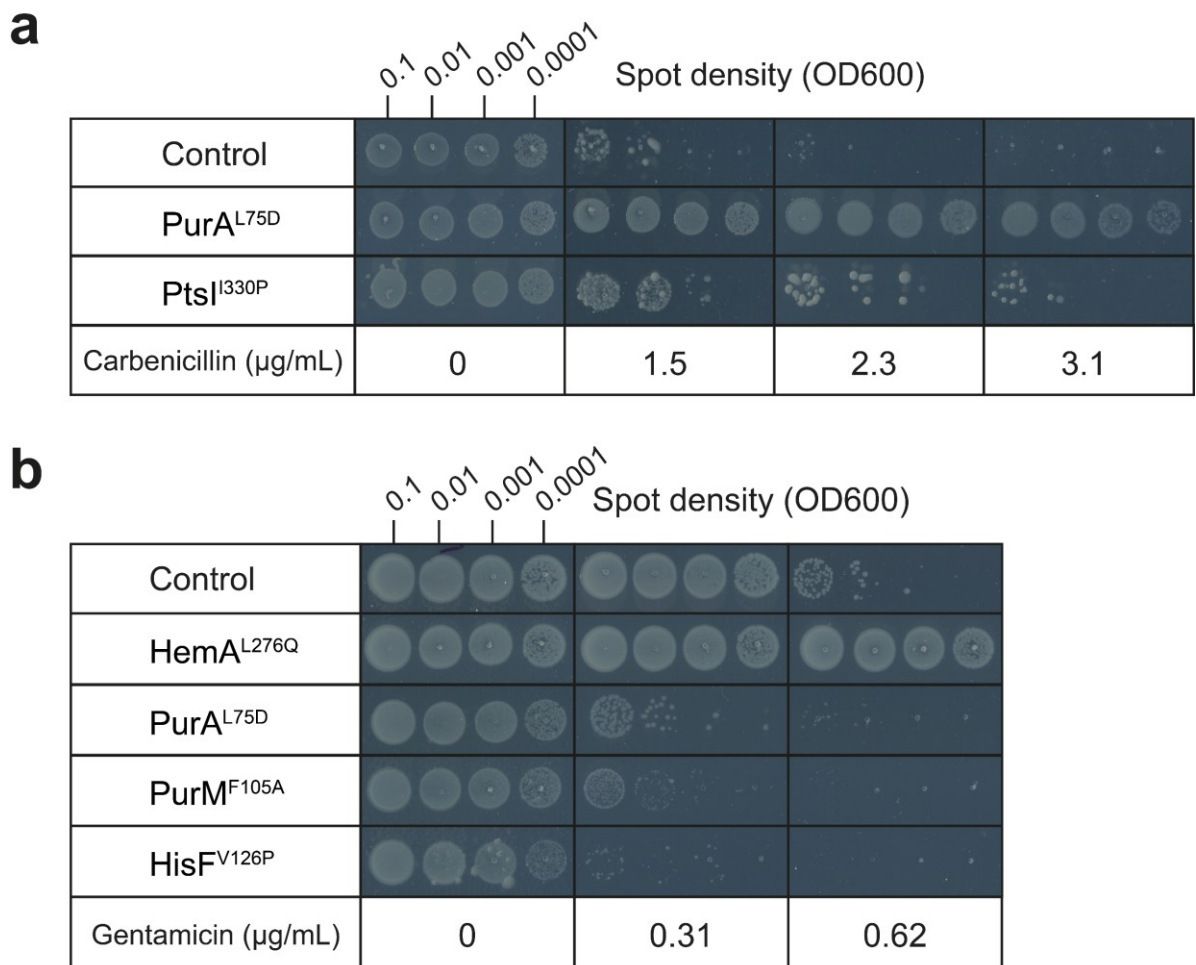
a

	Spot density (OD600)			
	0.1 0.01 0.001 0.0001			
Control				
PurA^{L75D}				
PtsI^{I330P}				
Carbenicillin (µg/mL)	0	1.5	2.3	3.1

b

	Spot density (OD600)		
	0.1 0.01 0.001 0.0001		
Control			
HemA^{L276Q}			
PurA^{L75D}			
PurM^{F105A}			
HisF^{V126P}			
Gentamicin (µg/mL)	0	0.31	0.62

Figure S11: Agar dilution assays with the control strain and the mutants PtsI^{I330P}, HemA^{L276Q}, PurA^{L75D}, PurM^{F105A} and HisF^{V126P}. Strains were plated on minimal agar medium supplemented either with carbenicillin (a) or with gentamicin (b). Spot assays were performed on the same plate per concentration, and scans of plates with different concentrations were assembled into a single figure using Adobe Illustrator.
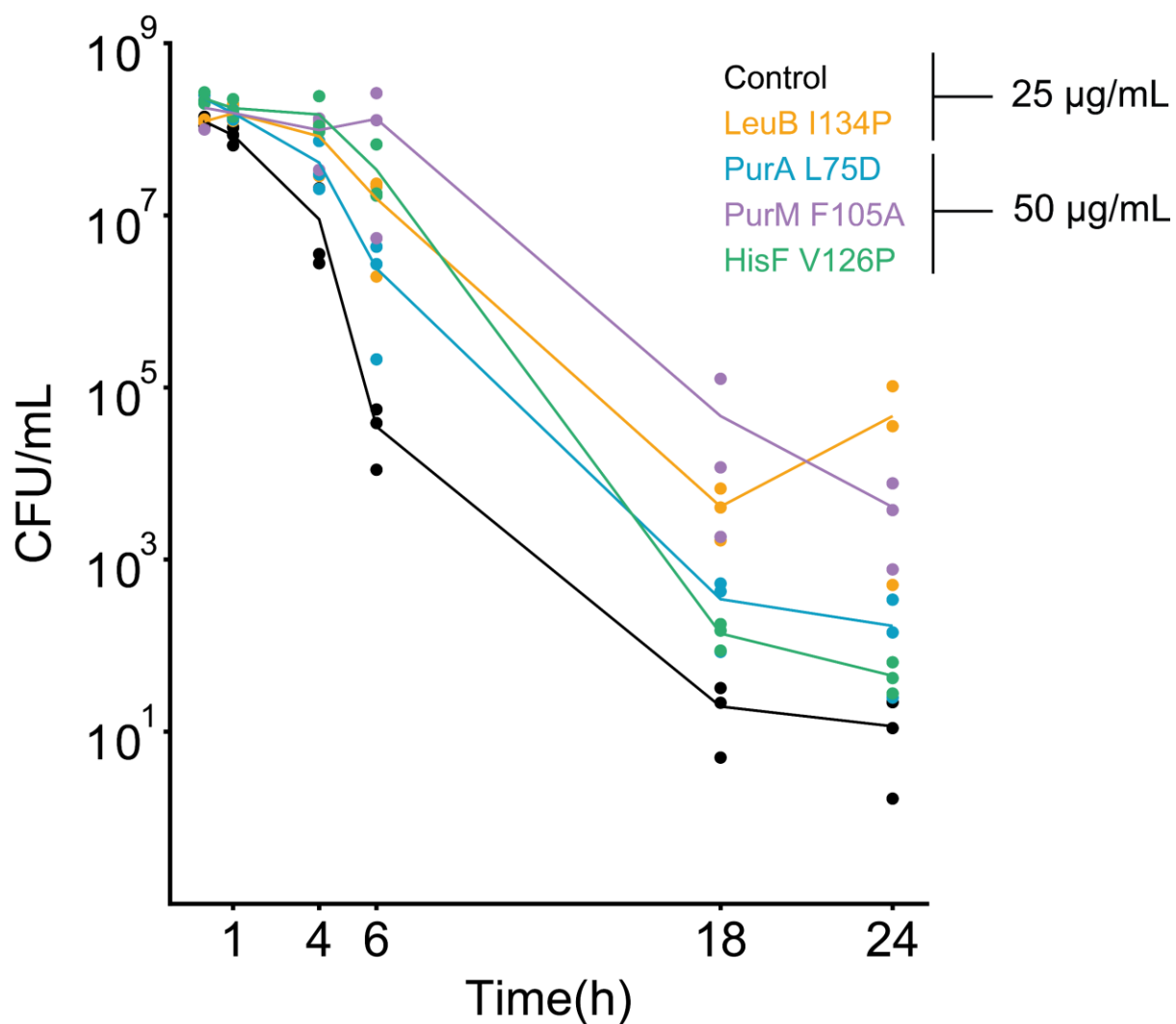
Figure S12: Time-kill assays with the control strain and the LeuB[I134P], HisF[V126P], PurM[F105A] and PurA[L75D] strains. Strains were incubated in minimal glucose medium and carbenicillin (25 and 50 µg/mL) for the time period indicated on the x-axis (n = 3 distinct samples). Data for the HisF[V126P], PurM[F105A] and PurA[L75D] mutants is the same as in Fig. 3c and shown as a reference.
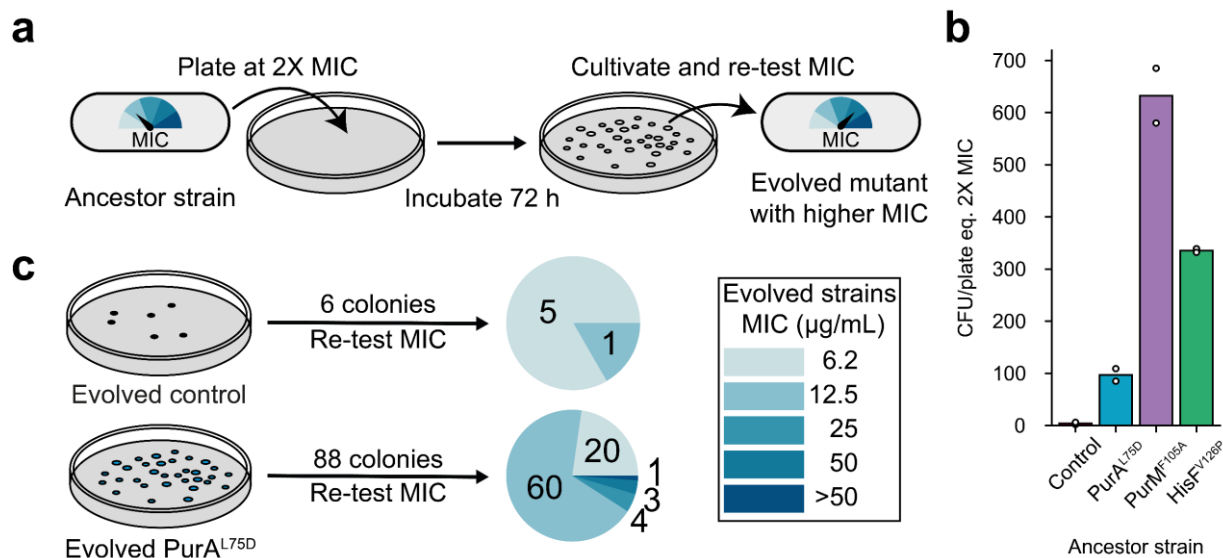
Figure S13: a, Schematic of the experimental workflow to evolve higher carbenicillin resistance. **b,** Number of spontaneous mutants that appeared after 3 days incubation of the control strains and the three mutants (HisF^{V126P}, PurM^{F105A} and PurA^{L75D}) at their respective 2X MIC (3.1 µg/mL for the control strain and 6.2 µg/mL for the purine mutants). Bars are means of n = 2 distinct samples (dots). **c,** Pie charts show carbenicillin MIC values of the evolved control strains and the evolved PurA^{L75D} strains. 88 colonies were picked from a plate inoculated with the PurA^{L75D} strain. All 6 colonies on the plate with the control strain were picked. Agar dilution assays on minimal glucose agar were performed to assess the MIC of these strains.
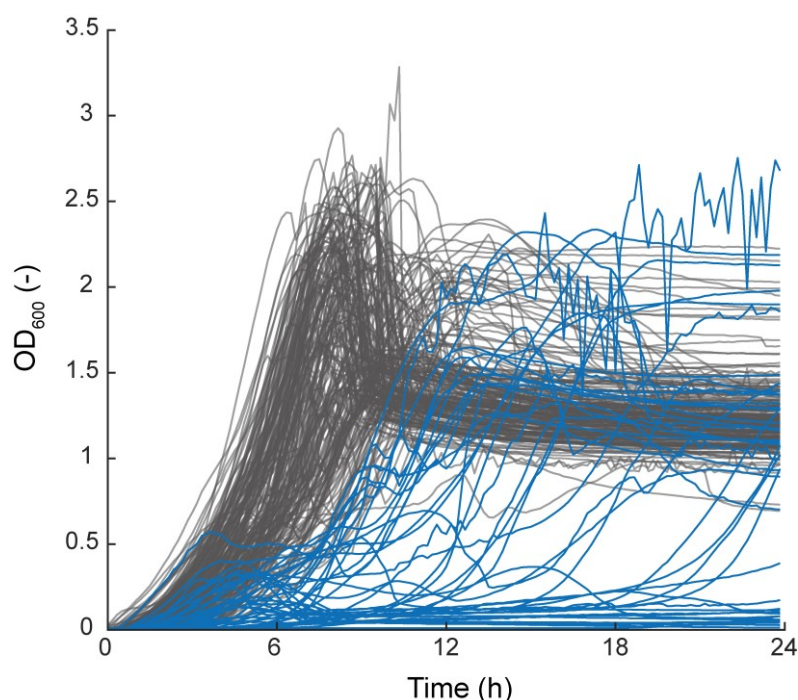

Figure S14: Growth of 235 clinical *E. coli* isolates on minimal glucose medium. Curves are the mean of n = 2 distinct samples. Blue lines show 41 strains with the lowest area under the curve (AUC). These strains were used for metabolome analysis.
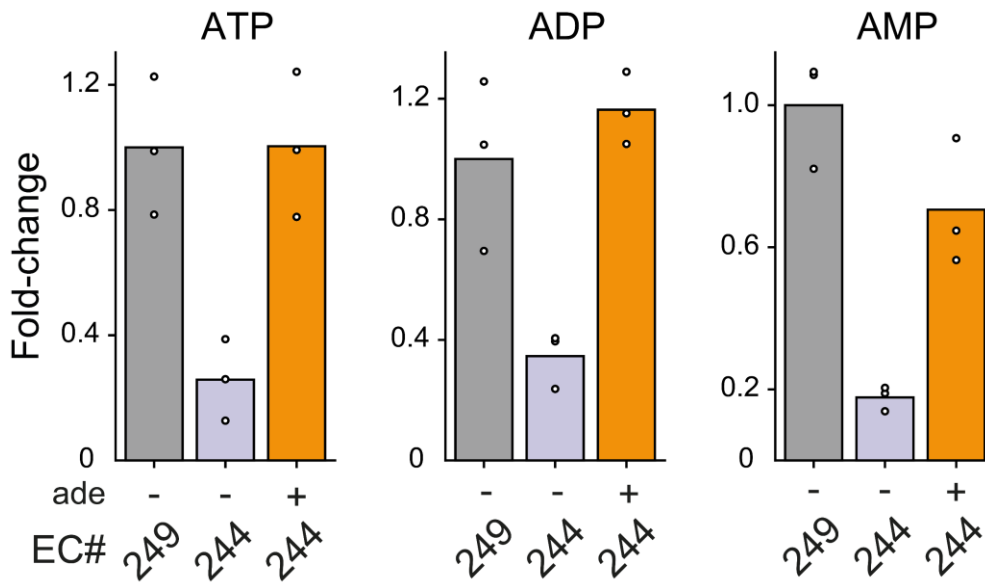
Figure S15: Relative levels of ATP, ADP and AMP in EC-244 (with and without adenine) and EC-249 (without adenine). Data are normalized to EC-249 (without adenine) and are represented as mean of n = 3 distinct samples (shown as black dots).
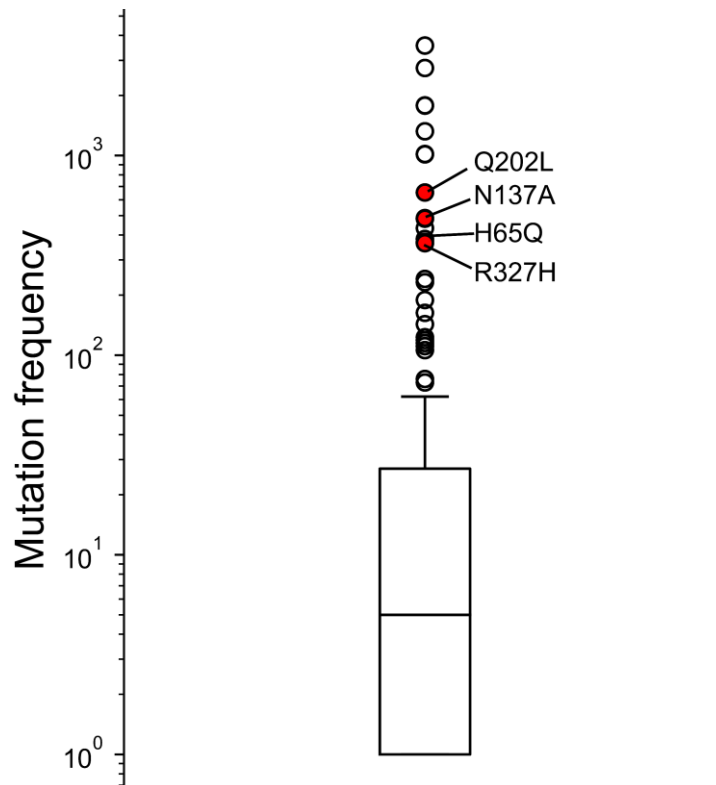

Figure S16: Distribution of the frequency of 146 amino-acid mutations in PurK found in the NCBI pathogen database (4352 *E. coli* strains). Mutations were found by alignment with the *purK* gene of *E. coli* BW25113. Each dot represents an amino-acid mutation, and its frequency in various isolates is indicated on the y-axis. Mutations detected in EC-244 and EC-249 are annotated, except for E49G which was not present in the dataset.

Chapter 3: Investigation on the relationship between carbenicillin and the *de novo* purine pathway

Contribution: All experiments presented in this chapter were designed by the author of this thesis as well as Prof. Hannes Link. Data analysis, writing, and figures were done by the author of this thesis. Nils Waffenschmidt cloned pTS40-p10X variants and performed experiments with them. He also performed dynamic metabolomics. Elisabeth Lorenz performed growth assays with 6-mercaptopurine. Fabian Smollich performed the qPCR experiment. Amelie Stadelmann performed agar dilution assays with the Δ*punC* strains. Proteomics data was obtained in collaboration with Dr. Timo Glatter. The author of this thesis performed the rest of the experiments.

Chapter relevance: This chapter shows numerous experiments that explored hypothesis which were not discussed in detail in Chapter 2 and provides interesting results to discuss the resistance phenotypes of the PurA^{L75D}, HisF^{V126P} and PurM^{F105A} mutants.

Introduction

Chapter 2 presented the core of this thesis investigation on the relationship between metabolism and antibiotic resistance. However, one key limitation of this publication was the lack of explanations regarding the mechanism linking the metabolic mutations and their resulting resistance phenotype. In other words, a causality was solidly established, but its logic remained elusive. This was mainly the case for the *de novo* purine and histidine pathways mutants. Indeed, it was relatively clear that mutations in enzymes related to the respiratory chain likely led to a decreased import of gentamicin and tobramycin in the bacterial cytosol. However, the reason why a perturbation of the *de novo* purine pathway would induce a resistance to a peptidoglycan-targeting antibiotic remains unclear. Furthermore, the carbenicillin-sensitive mutant PtsI^{I330P} mutant also had an impaired *de novo* purine pathway likely due to a decrease of glycolytic activity. Hence, the purine and histidine mutants were likely resistant due to a response to a local perturbation of the purine pathway and unrelated to a general response like in the PtsI^{I330P} mutant. In the conclusion of Chapter 2, it was assumed that the observed resistance was likely related to transport of carbenicillin to the periplasm.

How did we come up with such a conclusion? The current Chapter shows the experimental work achieved to explore multiple hypothesis explaining the resistance of the purine and histidine pathway mutants. This work played a significant role in orienting our final conclusion in Chapter 2. It includes proteomics, dynamic metabolomics, as well as generation of knock-out strains and testing of the reactive oxygen species (ROS) hypothesis.

This chapter also covers a supplementary set of experiments exploring the robustness of the link established between the *de novo* purine pathway and carbenicillin. Here, the *de novo* purine pathway will be perturbed using 6-mercaptopurine (6-MP), a drug generally used for Crohn's disease treatment which acts as an inhibitor of purine synthesis to stop cell proliferation.

Results and discussion

A deeper understanding of the proteomes and metabolomes of the PurA^{L75D}, HisF^{V126P} and PurM^{F105A} mutants

It was reasoned that a better understanding of the carbenicillin resistance phenotype of the three mutants PurA^{L75D}, PurM^{F105A} and HisF^{V126P} could be achieved by combining proteomics and metabolomics. The three mutants and the non-edited control strain were cultivated in M9 medium with glucose until they reached exponential phase. Proteomes were then sampled and measured using mass spectrometry.

The simultaneous analysis of the proteomes (**Fig. 1a**) and metabolomes (**Fig. 1b**) of the mutants highlights several differences and similarities. All three mutants have elevated levels of *de novo* histidine pathway enzymes, and commonly show significant level increase of the *de novo* purine pathway enzymes GuaA, GuaB and PurT. The HisF^{V126P} mutant displays elevated levels of other *de novo* purine pathway enzymes like PurA, PurC and PurE. The increased abundance of both *de novo* L-histidine and purine pathways enzymes in the mutants is likely a leverage to restore low purine end-products levels. This phenotype has been previously observed in other *de novo* amino-acid pathways in *E. coli*[1].

Enzymes involved in nucleotide salvage are also highly expressed in the three mutants. This is notably the case for adenosine deaminase (Add) and the transcription factor PunR, known to activate the expression of the nucleoside transporter PunC[2]. Interestingly, the PurA^{L75D} mutant has high levels of hypoxanthine (hxan) and inosine (ins), two metabolites of the purine salvage pathway. This is logical considering that this strain has high IMP (imp) levels, which can be converted into hxan or ins through the nucleotide salvage pathway[3]. Overall, this dataset suggests that the three mutants are starving for purine nucleotides and try to compensate this starvation by upregulation of proteins responsible for synthesis and salvage of nucleotides from the medium.
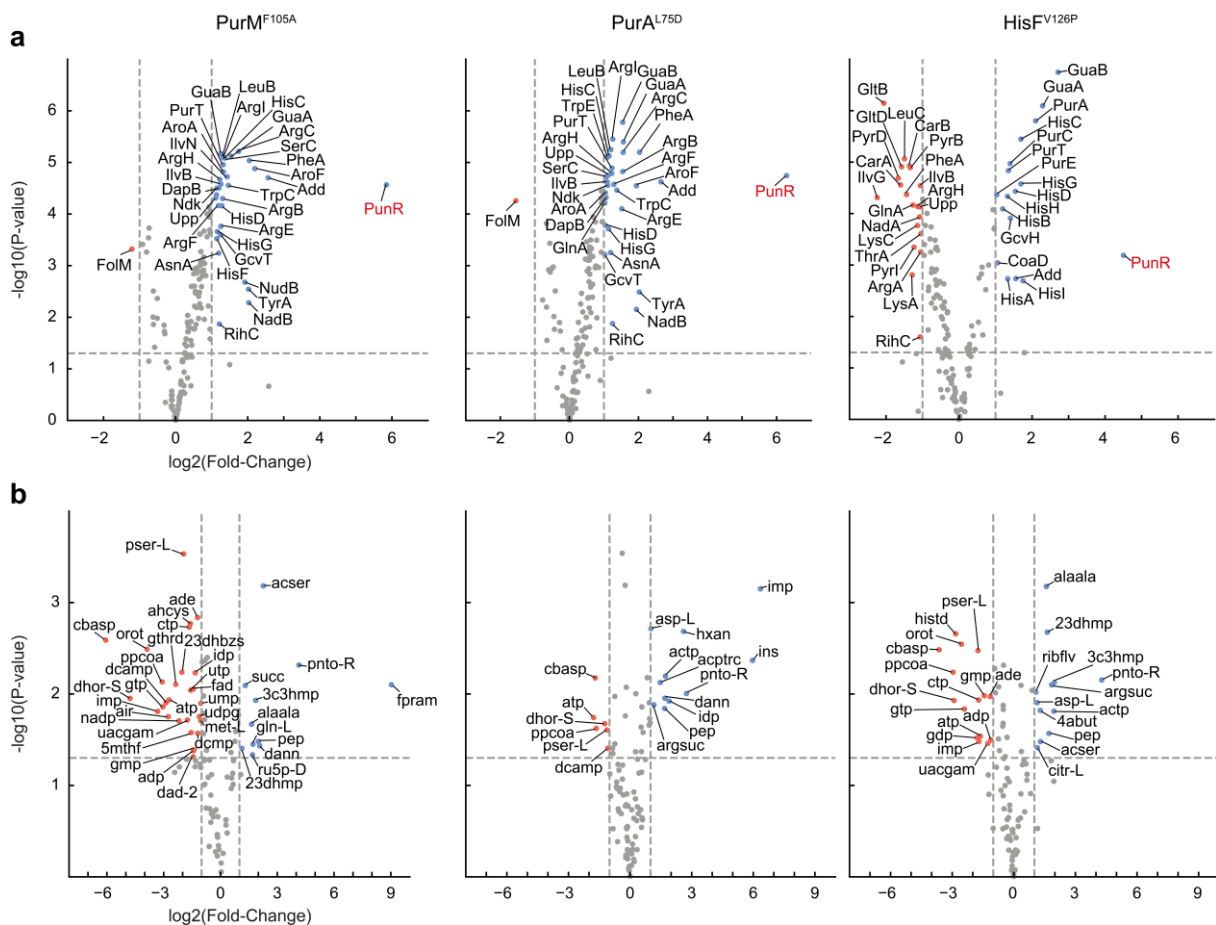
Figure 1: Metabolome and proteome comparison of the purine mutants. a, Volcano plots displaying protein level changes in the PurM^{F105A}, PurA^{L75D} and HisF^{V126P} mutants as compared to the non-edited control strain (n = 3). Only proteins of key pathways (purine and pyrimidine synthesis and salvage, folate synthesis, amino-acid synthesis) are shown. The transcription factor PunR is indicated in red. Dashed lines represent a threshold of log2(Fold-change) = 1 and -1 on the x-axis and a threshold of p-value of 0.05. **b,** Volcano plots displaying metabolite level changes in the PurM^{F105A}, PurA^{L75D} and HisF^{V126P} mutants as compared to the non-edited control strain (n = 3). This dataset is similar to the one showed in Chapter 2 but more metabolites are annotated.

All three mutants show decreases of the *de novo* pyrimidine pathway intermediates carbamoyl-L-aspartate (cbasp) and dihydroorotate (dhor-S). Orotate (orot) and CTP (ctp) levels are also low in the PurM^{F105A} and HisF^{V126P} mutants. The PurM^{F105A} additionally shows low UTP (utp) levels. However, the PurA^{L75D} mutant does not show significant level changes of *de novo* pyrimidine pathway end-products. Nevertheless, the *de novo* pyrimidine pathway is affected in all mutants. This could be caused by low ATP (atp) levels. Indeed, it has been previously shown that atp is an allosteric activator

of the PyrIB complex[4]. Hence, the three mutants starve for purine and pyrimidine nucleotides. This is further demonstrated by high levels of the pyrimidine salvage pathway enzymes Upp and RihC in the PurA^{L75D} and PurM^{F105A} mutants, although the HisF^{V126P} mutant showed oppositely decreased levels of these two enzymes.

The *de novo* pyrimidine pathway provides the nucleotide moiety for the peptidoglycan synthesis pathway intermediate UDP-*N*-acetyl-α-D-glucosamine (uacgam). Levels of uacgam are notably low in the PurM^{F105A} and HisF^{V126P} strains. Increased levels of the peptidoglycan synthesis pathway intermediate D-alanyl-D-alanine (alaala) are also observed in both strains. This indicates that the PurM^{F105A} and HisF^{V126P} mutants have an impaired peptidoglycan synthesis.

Could these two mutants have a slower peptidoglycan synthesis which may help in carbenicillin resistance? This hypothesis goes against the CRISPR screen results discussed in Chapter 2, where it was found that mutations in *de novo* pyrimidine pathway enzymes were rarely selected against carbenicillin. Furthermore, the PurA^{L75D} mutant does not show significant level changes in peptidoglycan synthesis pathway intermediates and has no significant decrease of *de novo* pyrimidine pathway end-products. The PurA^{L75D} mutant was the fastest growing of the three mutants, probably because its *de novo* pyrimidine and peptidoglycan synthesis pathways were less impaired. Since this mutant was also the most resistant of the three strains (see Chapter 2), it is difficult to link carbenicillin resistance with this metabolic phenotype. However, as the PurM^{F105A} and HisF^{V126P} mutants were more tolerant than the PurA^{L75D}, the impairment of peptidoglycan synthesis could play a role in decreasing carbenicillin lethality, which matches previous observations[5,6].

An important distinction is observable between the proteomes of the PurA^{L75D} and PurM^{F105A} mutants on one hand, and the HisF^{V126P} on the other hand. The HisF^{V126P} mutant displays low levels of many enzymes involved in amino-acid biosynthesis, which is the opposite of what is observed in the PurA^{L75D} and PurM^{F105A} mutants. As displayed by its low histidinol (histd) levels, the HisF^{V126P} mutant likely has a bottleneck in histidine synthesis, although histidine levels do not significantly decrease in this strain. The reason for the level decrease of other numerous amino-acid pathways enzymes is unclear and could be caused by multiple factors such as the alarmone ppGpp[7,8]. Nevertheless, the PurA^{L75D} and PurM^{F105A} mutants are both resistant to carbenicillin while not displaying the same proteome profile in amino-acid synthesis as

the HisF^{V126P} mutant. Intriguingly, the three mutants show altered levels of several amino-acid pathway intermediates such as O-phospho-serine (pser-L), pantothenate (pnto-R) and arginosuccinate (argsuc). It is unclear how these level changes are triggered and whether they influence carbenicillin resistance. Hypothesis related to these intermediates were not explored in this thesis.

PEP (pep) and Acetyl-P (actp) accumulate in the mutants. The increased levels of these two metabolites may be indicators that the mutants rely on fermentative pathways[9]. Indeed, atp levels have been shown to influence fermentation rates in *E. coli*[10]. The expression of several porins is regulated by acidic stress which could result from fermentation pathways usage[11]. This is the case for OmpF[12] which is responsible for carbenicillin transport to the periplasm[13]. The absence of OmpF from the proteomics dataset does not permit to reach better conclusions and transcriptomics may have been used to inform on *ompF* expression levels in the mutants.

The carbenicillin-sensitive PtsI^{I330P} mutant also had high pep levels (Chapter 2). However, this was likely due to a bottleneck in the Phosphotransferase system (PTS) and was unrelated to the pep level increase in the purine mutants. Levels of actp were low in that strain (log2FC = -1.753; p-value=0.005 – Chapter 2).

In conclusion, this dataset demonstrates that the three mutants rely on an array of strategies to compensate their respective bottlenecks, each with overlaps and differences. While the PurM^{F105A} displays numerous changes in metabolite levels, the HisF^{V126P} mutant shows a strong proteome response. Only the PurA^{L75D} strain has less perturbations in the levels of proteins and metabolites analysed, and was the fastest growing of the three mutants as well as the most resistant. Therefore, carbenicillin resistance is likely due to a trade-off between the benefits provided by a bottleneck in the *de novo* purine pathway and the resulting consequences on fitness.

Carbenicillin resistance could also be linked with a protein which had high levels in the three mutants. The transcription factor PunR fit this criterion and was appealing to propose a simple hypothesis. This will be explored in the next section.

An inconclusive investigation on the nucleoside transporter PunC

The transcription factor PunR is known to positively regulate the expression of the *punC* gene encoding for the nucleoside transporter PunC (**Fig. 2a**). Hence, PunC might be overexpressed by PunR and play a role in carbenicillin resistance. Interestingly, PunC is an inner membrane transporter, and carbenicillin locates in the periplasm where it binds penicillin binding proteins. Therefore, its role in carbenicillin resistance would not be trivial. Besides, PunC was not detected on the proteome dataset (**Fig. 1a**), so there was no direct proof that it was indeed highly expressed in the carbenicillin resistant mutants. The hypothesis was tested nonetheless.

If PunC had any effect on carbenicillin resistance, the suppression of its encoding gene should re-sensitise the purine and histidine mutants. Therefore, the *punC* gene was deleted on the PurA^{L75D} mutant genome (PurA^{L75D} Δ*punC)*. Carbenicillin resistance of the strain was tested using agar dilution (**Fig. 2b**). Conforming with the initial hypothesis, the resistance of the PurA^{L75D} Δ*punC* vanished to match that of the non-edited control strain. However, as it can be observed, a non-edited control Δ*punC* strain was not tested in this experiment. This did not permit to conclude if the abolition of resistance was due to the absence of PunC or a pleiotropic effect from the knock-out.
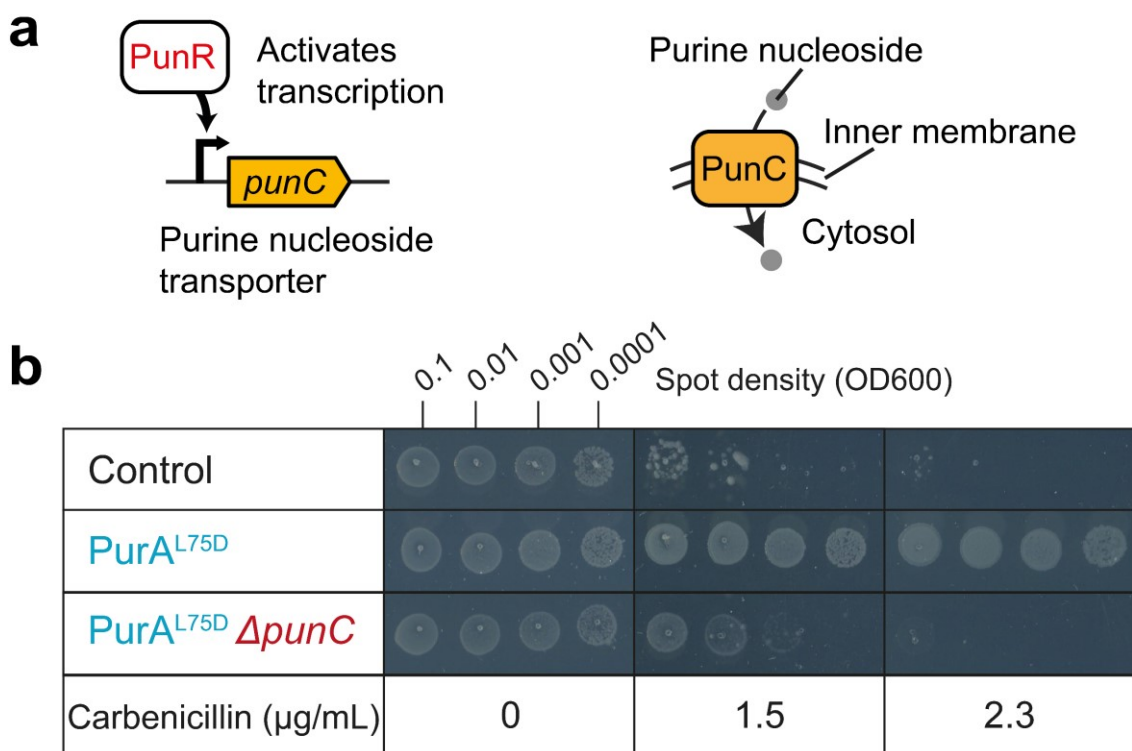
	Spot density (OD600) 0.1 / 0.01 / 0.001 / 0.0001		
Control			
PurA^{L75D}			
PurA^{L75D} Δ*punC*			
Carbenicillin (µg/mL)	0	1.5	2.3

Figure 2: The nucleotide transporter PunC is a potential mechanistic explanation for carbenicillin resistance. a, PunR, the transcription factor upregulated in the PurM^{F105A}, PurA^{L75D} and HisF^{V126P} mutants, regulates the expression of the nucleoside transporter PunC. **b,** Agar dilution assay with the PurA^{L75D} strain and the double mutant PurA^{L75D}Δ*punC* (shown is one of n = 2 replicates). Spots were done on the same plate per concentration, and scans of plates with different concentrations were assembled into a single figure using Adobe Illustrator.

To give additional proofs advocating for a role of *punC* in carbenicillin resistance, it was decided to construct multiple other strains. If PunC was responsible for carbenicillin resistance, its overexpression from a plasmid should induce resistance in sensitive strains. Modified versions of pTS40 (the DNA barcode plasmid) were generated (here referred to as pTS40-p10X). These plasmids carry an open reading frame permitting the constitutive expression of *punC*. The expression levels of *punC* were tuned by using different promoter strength (**Fig. 3a**). The Control Δ*punC* was cloned for this experiment and transformed with the pTS40-p10X variants. Four different strains were generated (PurA^{L75D} Δ*punC* p104, Control Δ*punC* p100, Control Δ*punC* p104 and Control Δ*punC* p107).

Unfortunately, none of the constructed strains displayed a resistance phenotype to carbenicillin (**Fig. 3b**). This could be due to a dysfunction of the open reading frame (*punC* is unproperly expressed), or deny a role for PunC in carbenicillin resistance. Most importantly, the Control Δ*punC* showed a lower carbenicillin minimal inhibitory concentration (MIC) than the non-edited control strain (**Fig. 3b**), which supports the pleiotropic effect hypothesis.

To investigate this further, the expression of *punC* was measured using real-time polymerase chain reaction (qPCR) to quantify *punC* messenger RNA (mRNA) levels (**Fig. 3c**). As hypothesised, the PurA^{L75D} mutant indeed showed 2-fold increased levels of *punC* mRNA as compared to the non-edited control strain (p-value<0.05), and both Δ*punC* strains displayed no expression of the mRNA, confirming the deletion of the *punC* gene from their genome. Hence, resistance could still be explained by higher *punC* expression in the mutants and the constructed pTS40-p10X plasmids might have not function properly. Besides, since the non-edited control expresses PunC, the increased sensitivity of the Control Δ*punC* might be caused by the absence of PunC in that strain. A final strategy was employed to decide whether or not to rule out the PunC hypothesis.
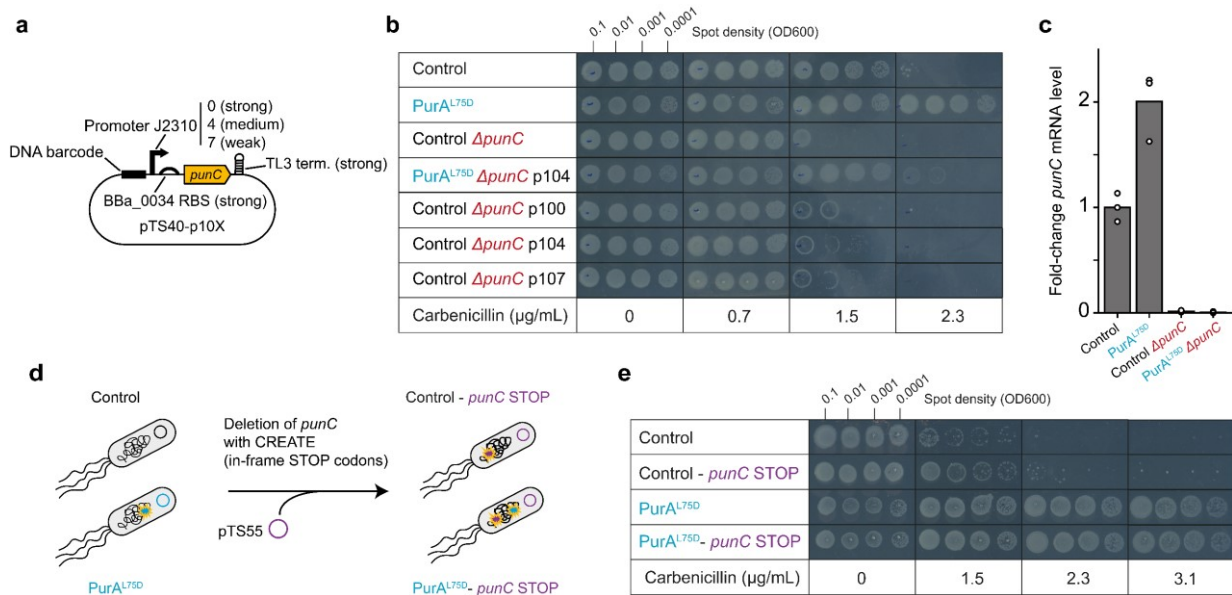
Figure 3: Failures in confirming the PunC hypothesis. a, Representation of the plasmids used in this study to overexpress PunC (pTS40-p10X). They are variants of the plasmid pTS40 and contain an open reading frame permitting the expression of *punC* with a strong ribosome binding site (RBS), a strong transcriptional terminator TL3, and three different promoter strengths: J23100 (strong), J23104 (medium) and J23107 (weak). **b,** Agar dilution assay on carbenicillin with various strains having a Δ*punC* and expressing PunC with the pTS40-p10X variants. The non-edited control strain and the PurA^{L75D} mutant are shown as controls for the experiment (n = 1). Spots were done on the same plate per concentration, and scans of plates with different concentrations were assembled into a single figure using Adobe Illustrator. **c,** *punC* mRNA levels in the non-edited control strain and the PurA^{L75D} mutant, with or without the deletion of *punC* in their respective genomes. Fold-changes are calculated as compared to the control average *punC* mRNA levels. (n = 3) **d,** Schematisation of the CREATE cloning method used to generate strains with a *punC* deletion. **e,** Agar dilution assay with the non-edited control strain and the PurA^{L75D} mutant and their *punC*-STOP variants on M9 agar with carbenicillin (n = 1).

Two new strains with *punC* deletions were generated using CREATE. This time, instead of relying on the complete deletion of the *punC* gene from *E. coli* genome, STOP codons were implemented in-frame of the *punC* gene at the second and eleventh residues. STOP codons lead to translational arrest upon being read by the ribosomal machinery. Two STOP codons were implemented to reduce chances of readthrough[14]. The cloning was performed in the non-edited control strain as well as in the PurA^{L75D} strain (**Fig. 3d**). The resulting strains were named Control - *punC* STOP and PurA^{L75D} - *punC* STOP. Carbenicillin resistance of these strains was tested using agar dilution assay. The strains had the same carbenicillin sensitivity as their variants without STOP codons (**Fig. 3e**). This further indicated that *punC* was not causing

carbenicillin resistance, and that the increased carbenicillin sensitivity in the Control Δ*punC* and PurA^{L75D} Δ*punC* strains was likely due to a pleiotropic effect.

What could be the explanation for the pleiotropic effect? One possibility is that the absence of the *punC* gene on *E. coli* genome perturbates the expression of neighbouring genes (a "polar effect"). For example, the *punC* gene is upstream of the *cfa* gene in *E. coli* BW25113 genome. This gene encodes for the protein Cyclopropane fatty acyl phospholipid synthase (CFA), involved in phospholipid synthesis. In theory, this is unlikely to happen as the Keio library has been crafted specifically for avoiding polar effect caused by gene deletion[15,16].

The results presented in Figure 3 are also not conclusive enough to fully dismiss the PunC hypothesis. Expression levels of PunC in the pTS40-p10X strains were never assessed. Unlike in the original Δ*punC* strains, expression levels of PunC were not measured in the *punC* STOP strains. This means the efficiency of this method to knock-out *punC* was not demonstrated.

All these limitations and uncertainties do not furnish clear answers to the original question, which was to assess why purine bottlenecks led to carbenicillin resistance. The next section proposes another strategy to answer this question.

Study of the impact of carbenicillin treatment on *E. coli* metabolome

Lethality of antibiotics have been associated with their potential metabolic side-effects, such as generation of ROS[17]. If carbenicillin indeed impacts *E. coli* metabolism, then resistance of the PurA^{L75D}, HisF^{V126P} and PurM^{F105A} mutants could be caused by a reduction of this impact due to their metabolic bottlenecks.

A workflow was designed to study this hypothesis (**Fig. 4a**). Both non-edited control strain and PurA^{L75D} mutant were incubated for one hour with high concentrations of carbenicillin (50 µg/mL, see Chapter 2). After 5, 30, and 60 minutes of treatment, metabolites were sampled and quantified. Treatment of 1 h at this concentration was enough to kill 46(± 32.8) % of the non-edited control strain population and 68(± 11.8) % of the PurA^{L75D} mutant population (Chapter 2). It was hypothesised that differences in metabolome changes between the PurA^{L75D} and non-edited control strain could explain the reduced carbenicillin lethality.

The data from this experiment are presented in Figures 4b, 4c and 4d. While Figures 4b and 4c show significant changes in the metabolome of each strain from 5 minutes to 60 minutes, Figure 4c compares the metabolome of both strains at similar treatment duration. Any metabolite that displays a strong level change in individual strains (**Fig. 4b and 4c**), and a stronger change in the non-edited control strain compared to the PurA^{L75D} strain over time (**Fig. 4d**) would be of interest for the starting hypothesis.

While carbenicillin treatment induced level decrease of most measured metabolites in both strains, many nucleosides and nucleotides had high level increases. For example, levels of adenosine (adn), inosine (ins), AMP (amp), cytidine (cytd), GMP (gmp) and guanosine (gsn) at least doubled in the control strain over the treatment duration (**Fig. 2b**). At similar time-points, the non-edited control strain accumulated amp, cytd, gmp and gsn at least two times faster than the PurA^{L75D} mutant (**Fig. 2d**). Interestingly, purine nucleotides atp, gtp, gtp and gtp had level decreases in both strains, and adp levels also decreased in the control strain (**Fig. 2b and 2c**). This seems to indicate that highly-phosphorylated nucleotides deplete while nucleosides monophosphates or nucleosides without phosphate accumulate during carbenicillin treatment.

Oppositely, a previous study showed decreased levels gmp, gsn and guanine in ampicillin-treated *E. coli*[18]. This effect was attributed to the generation of ROS because of elevated respiration caused by ampicillin. Decreased levels of nucleotide would be due the oxygenation of the guanine pool, which generates oxidised nucleotides that lethally incorporate into DNA and RNA. As this was not observed here, whether ROS play a role in carbenicillin lethality in the tested strains is still unclear. Ampicillin and carbenicillin might also have different metabolic consequences.

Since atp and adp levels drop and amp levels increase during carbenicillin treatment, the cells may have a destabilised adenylate energy charge (AEC). AEC is calculated with the formula [(atp) + ½ (adp)]/[(atp) + (adp) + (amp)] and represents the amount of metabolically available energy in a cell[19]. As such, it is intimately linked with growth rate[20]. As growth rates are tightly associated with beta-lactam lethality[5], destabilisation of the AEC via the *de novo* purine pathway could also be a defence mechanism in response to a perturbed peptidoglycan. However, no clear signal from peptidoglycan synthesis metabolites was detected in the present data set apart from alaala which depleted in the control strain (**Fig.4d**). AEC calculation relies on the determination of amp/adp/amp intracellular concentrations which was not performed for this dataset.
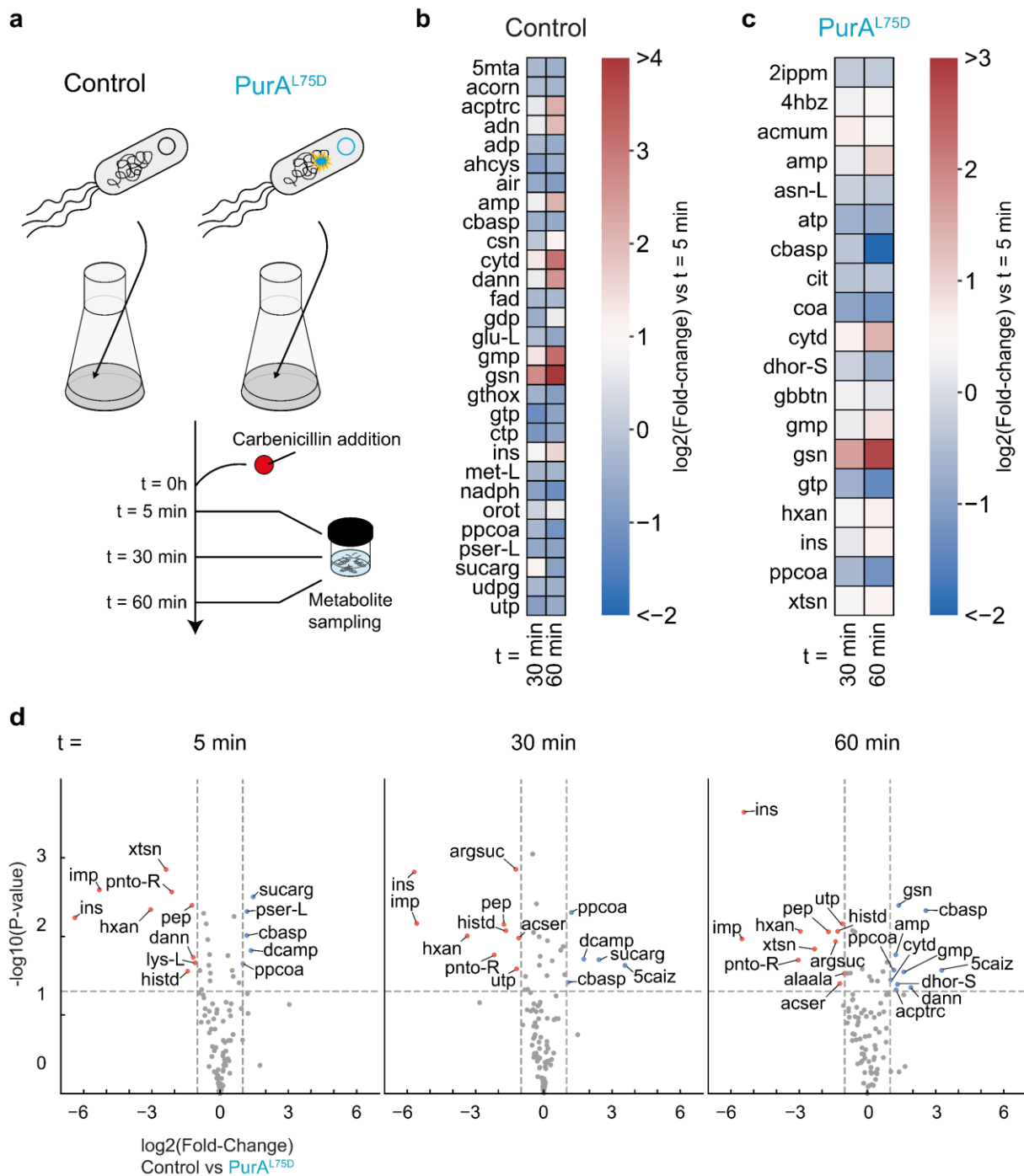
Figure 4: Metabolic consequences of carbenicillin treatment on *E. coli* metabolome. **a,** Schematisation of the experimental workflow. **b,** Metabolite level changes in the non-edited control strain after 30 minutes and 60 minutes of carbenicillin treatment as compared to 5 minutes (n = 3, all metabolites shown have p-value<0.05 for levels at t=60 min against t=5 min). **c,** Same as (b) but with the PurA^L75D mutant. **d,** Volcano plots showing metabolite changes of the non-edited control strain at different durations. Fold-changes are obtained by comparison of metabolite levels in the PurA^L75D strain at the same time-points (n = 3). Dashed lines represent a threshold of log2(Fold-change) = 1 and -1 on the x-axis and a threshold of p-value of 0.05.

Only few other measured metabolites accumulated in both strains. The control strain shows a wider variety of significant metabolite level decreases over treatment duration (18) than the PurA^{L75D} strain (9). This could be due to leakage because of membrane lysis, as the control population lyses faster than the mutant population. However, this would not explain why some nucleotides and nucleosides accumulate. Could they adhere to membrane easily than their highly phosphorylated alternatives?

One key limitation of the experimental set-up is that tolerance and not resistance was investigated. Because a high concentration of carbenicillin was used, both strains populations depleted, which does not allow to understand any resistance mechanism at play. Cell lysis and filamentation also led to complexified sampling of metabolites and may have blurred normalisation of cell biomass. One way to correct for these issues and study carbenicillin resistance would be to sample an *E. coli* population growing on agar supplemented with carbenicillin. However, metabolite sampling from biofilms suffers from population gradients which might affect metabolite levels[21]. Lower carbenicillin concentrations could have also been used.

In summary, carbenicillin treatment induces accumulation or depletion of multiple nucleotides and nucleosides which might destabilise the AEC. That this phenotype plays a role in carbenicillin tolerance and why carbenicillin affects the nucleotide and nucleoside pool remains unclear. The observed phenotype of the strains in response to carbenicillin contradicted previously published literature, which does not support the ROS hypothesis as explanation. The HisF^{V126P}, PurM^{F105A} and PurA^{L75D} mutants did not display resistance to H_2O_2 (**Fig. 5**), known to generate ROS in *E. coli*[18]. This hints that these strains are not resistant to oxidative stress. Since ROS were not measured in this thesis, discussing this hypothesis remains very challenging. The purine and histidine mutants might be sensitive to ROS, but shielded from carbenicillin-generated ROS if there were any.
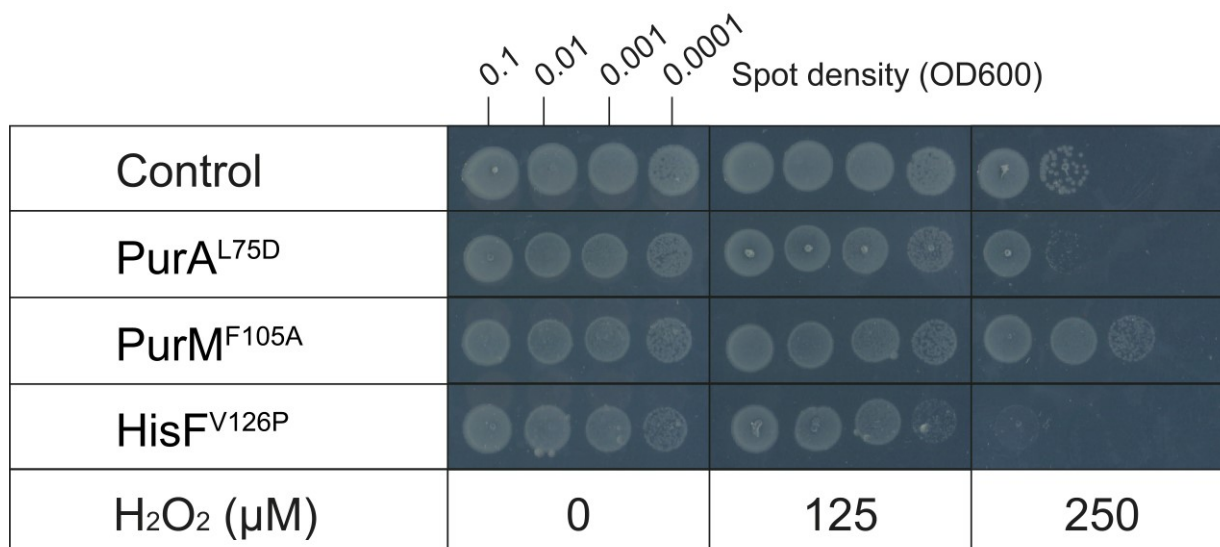
Figure 5: Histidine and purine mutants are not resistant to oxidative stress. Agar dilution assay with H_2O_2 with the non-edited control strain and the $PurA^{L75D}$, $PurM^{F105A}$ and $HisF^{V126P}$ mutants. n = 1. Spots were done on the same plate per concentration, and scans of plates with different concentrations were assembled into a single figure using Adobe Illustrator.

In Chapter 2, the carbenicillin tolerance of the $PurA^{L75D}$ strain was shown to be mainly caused by its slow-growth. However, the $LeuB^{I134P}$ strain was as tolerant as the $PurA^{L75D}$ strain while growing two times slower. This gives support to the AEC hypothesis. It is possible that the purine and histidine mutants, because they already have an altered *de novo* purine pathway, can manipulate their AEC easily and quickly in response to carbenicillin treatment, further decreasing their growth rates and improving their tolerance as opposed to a strain like $LeuB^{I134P}$ or the non-edited control which had a normally operating de novo purine pathway. This was never tested here but remains interesting.

In conclusion, this experiment had promising and interesting results to understand carbenicillin tolerance but did not help exploring carbenicillin resistance.

Strengthening of findings using 6-mercaptopurine

Parallels between laboratory and clinical *E. coli* strains are not trivial due to the diversity within and between *E. coli* phylogroups. This section describes experiments done to rule out hypothesis that could link purine metabolism and carbenicillin resistance to

unique features of the CREATE chassis *E. coli* BW25113: the carriage of two plasmids and the presence of a pyrimidine bottleneck in its genome. This was important to more reliably extrapolate findings made in Chapter 2 to other *E. coli* strains and was performed by using 6-mercaptopurine (6-MP).

6-MP is a cancer drug used to inhibit purine metabolism of leukaemia tumour cells and impair their proliferation[22] (**Fig. 6a**). It is also used to treat Crohn's disease, an inflammatory bowel disease[23]. In human cells, 6-MP is thought to be converted by the enzyme hypoxanthine phosphoribosyltransferase (Hpt in *E. coli*) into 6-thioinosine-5'-monophosphate and further metabolised into a myriad of nucleosides by other purine nucleotides salvage pathway enzymes[22]. These nucleosides act as competitive inhibitors for enzymes of the *de novo* purine pathway, although it is not clear which step of the pathway is inhibited. In *E. coli*, 6-MP has been shown to inhibit purine nucleotide synthesis[24]. It was assumed to be a direct inhibitor of PurF[25], the first enzyme of the *de novo* purine pathway, although no information was found to support that claim. Nevertheless, 6-MP offered an attractive alternative to CRISPRi (see Chapter 2) to study the relationship between *de novo* purine synthesis and carbenicillin is other *E. coli* strains.

Firstly, the effects of 6-MP on *E. coli* metabolism were investigated (**Fig. 6b and 6c**). Treatment of the non-edited control strain with 25 µM 6-MP indeed led to a metabolic phenotype highly similar to that of the purine mutants previously studied (**Fig. 1b**). *De novo* purine pathway end-products (adp, atp, gtp) had strong level decreases while the *de novo* pyrimidine pathway was also strongly affected, with low-levels of cbasp, orot and cmp/ctp. Interestingly, two *de novo* purine pathway intermediates (air and xmp) accumulated during 6-MP treatment. This seemed to indicate that the bottleneck induced by 6-MP was likely located in the gtp branch, through the inhibition of GuaA, of which xmp is the substrate (**Fig. 6a**). Interestingly, no metabolic bottleneck was detected at the PurF catalysed step since air levels were high. This contradicts previous statement in litterature[25].

Nevertheless, the data confirmed that 6-MP can indeed inhibit the *de novo* purine pathway of *E. coli*. The non-edited control strain was subjected to carbenicillin treatment during a broth dilution experiment (**Fig. 6d**). Adding 25 µM of 6-MP gave a fitness advantage against carbenicillin. The non-edited control strain was able to withstand carbenicillin treatment and grew at 2X MIC (end OD_{600} = 0.16), showing

resistance. As expected, 6-MP led to a growth rate decrease of 20%, likely due to *de novo* purine pathway inhibition (**Fig. 6e**).
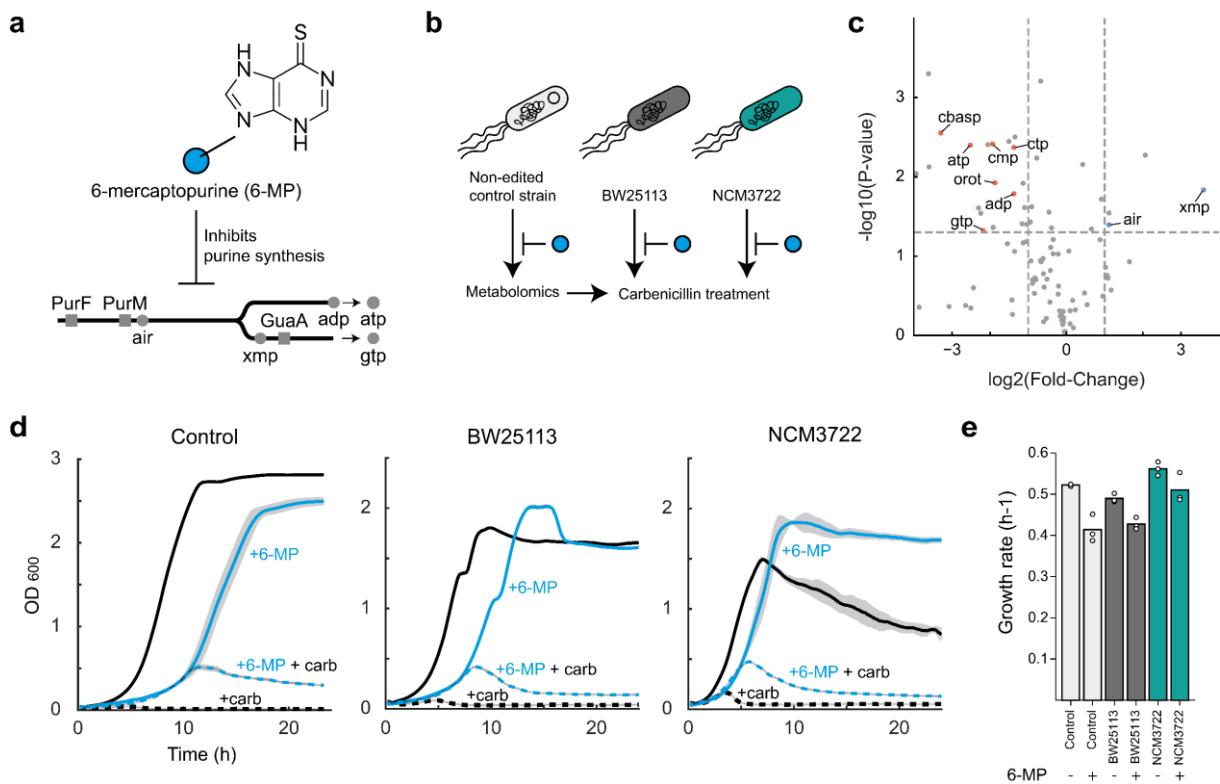

Figure 6: Treatment of *E. coli* with 6-mercaptopurine leads to low-level carbenicillin resistance. a, 6-mercaptopurine (6-MP) is a purine pathway inhibitor. Metabolites of the purine pathway as annotated in (c) are indicated. **b,** Representation of the experimental workflow with the non-edited control strain, the *E. coli* BW25113 wild-type (WT) strain and *E. coli* NCM2722 WT strain. **c,** Volcano plot showing metabolite changes in the non-edited control strain when incubated with 25 µM 6-MP. Fold-changes are obtained by comparison of metabolite levels of the untreated non-edited control strain. (n = 3 in both experiments). Dashed lines represent a threshold of log2(Fold-change) = 1 and -1 on the x-axis and a threshold of p-value of 0.05. **d,** Growth of the non-edited control, the *E. coli* BW25113 WT and *E. coli* NCM3722 WT strains with 25 µg/mL carbenicillin in M9 medium with or without supplementation of 25 µM 6-MP (n = 3). **e,** Growth rates of the three selected strains in M9 medium with or without supplementation of 25 µM 6-MP (n = 3). Same data as in (d).

This interesting result gave the opportunity to investigate two hypotheses. The first one involved the influence of the plasmids pTS40 and pTS41 on the resistance phenotype of the mutants generated with CREATE genome editing. Indeed, carrying plasmids can impose a metabolic burden on *E. coli* and affect its fitness[26]. Furthermore, kanamycin and chloramphenicol were systematically used in cultivation mediums of strains carrying pTS40 and pTS41 to maintain population homogeneity. Could plasmid metabolic burden and the presence of other antibiotics influence carbenicillin resistance?

Another hypothesis revolved around the *de novo* pyrimidine pathway defect present in the genome of *E. coli* K-12 strains like BW25113. Indeed, this strain suffers from a frameshift mutation in the gene *rph* (named *rph-1* allele), which decreases the expression of the downstream gene *pyrE* as a polar effect[27,28]. This has been shown to result in the expression increases of *de novo* pyrimidine pathway enzymes and a growth defect in minimal medium due to pyrimidine starvation[27]. The link between the *de novo* purine pathway and the *de novo* pyrimidine pathway has been explored in this thesis chapter. Hence, concerns may be raised on the impact of the *rph* frame-shift in carbenicillin resistance of the purine and histidine mutants.

To investigate both hypotheses, two strains were subjected to simultaneous 6-MP and carbenicillin treatment. These two strains were *E. coli* BW25113 WT (lacking pTS40 and pTS1), and *E. coli* NCM3722 WT, which is a K-12 derivative without the *rph* frame-shift mutation[29]. Both strains showed similar growth phenotypes as the non-edited control strain when subjected to the carbenicillin and 6-MP treatment (**Fig. 6d**). However, 6-MP induced a 13% and 10% growth rate decrease in BW25113 WT and NCM3722 WT respectively, which was lower than in the non-edited control strain (20%, **Fig. 6e**). Therefore, plasmid burden might impact the robustness of the non-edited control strain against nucleotide perturbation. Interestingly, NCM3722 WT had a higher growth rate (0.56 h-1 ± 0.014) than both BW25113 strains (0.49 ± 0.009 for WT and 0.52 ± 0.0021 for the non-edited control), which matches published literature[27].

Nevertheless, 6-MP treatment led to low-level resistance against carbenicillin in all three tested strains, which indicated that the presence of plasmid burden and the *rph* frame-shift mutation does not impact the link between the *de novo* purine pathway and carbenicillin. Interestingly, if *E. coli* strains can be broadly affected by 6-MP, then a patient under 6-MP treatment might have higher chances of acquiring β-lactam

resistant *E. coli* strains in its microbiota. Furthermore, the gut microbiota has been shown to be associated with Chron's disease, as bacteria can play a role in inflammation although they are usually not treated with β-lactams[30].

This conclusion remains highly speculative and this study has multiple caveats. First, only broth dilution assays were used to determine the MICs instead of agar dilution assays. Broth dilution assays have the considerable disadvantage of furnishing results that are not always conclusive, especially with β-lactams which induce filamentation of cells and affect OD_{600} reading[31]. For example, the OD_{600} increases observed during carbenicillin and 6-MP treatments might not entirely be the result of cell division but also filamentation (**Fig. 6d**). Whether the effect of 6-MP on growth rates was responsible for the observed resistance instead of its inhibition activity was also not tested. Since the "resistance by slow growth" hypothesis was ruled-out in Chapter 2, it is unlikely that this is correct. However, this could have been tested by using another molecule like *N*-(phenyl)thioacetamide-linked 1,2,3-triazoles which inhibits CysK and cysteine synthesis[32] although effects on *de novo* purine synthesis should be assessed first.

The number of *E. coli* strains used in this section was very limited so general conclusions are weak. Using agar dilution and a larger panel of *E. coli* strains or other bacterial species should give much more informative results. Metabolomics was not performed on the *E. coli* BW25113 WT and *E. coli* NCM3722 WT strains. Therefore, the effect of 6-MP on these strains can only be hypothesised from the metabolome of the non-edited control strain.

Given these limitations, this dataset was encouraging regarding the relevance of the carbenicillin resistance phenotype of the purine and histidine mutants, which was its primary objective. Furthermore, the dataset furnishes a solid foundation for a more complete study which could examine the effects of drugs on the metabolome of *E. coli* and other microbiota members, and how this in turn affects antibiotic resistance during treatment to complete existing knowledge[33].

Conclusion

This chapter, although exposing uncomplete investigations with substantial limitations, offers an interesting complement to Chapter 2. Unfortunately, the elucidation of the mechanism linking carbenicillin and *de novo* purine synthesis could not be achieved. Instead, carbenicillin tolerance was better addressed with the chosen experimental designs. New hypothesis (peptidoglycan bottleneck and AEC) which could complement the current model (carbenicillin tolerance with slow-growth) were formulated. Furthermore, using 6-MP permitted to strengthen the relevance of the carbenicillin-purine link and justified previous characterisation efforts.

Given the observations made in Chapter 2 and the present chapter, it is very likely that a **local** perturbation of the *de novo* purine pathway leads to a **specialised** response which induces low-level carbenicillin resistance. Carbenicillin resistance of the purine and histidine mutants is unlikely linked with a general mechanism such as the generation of ROS since it was constrained to carbenicillin and aztreonam and not to meropenem or gentamicin (Chapter 2). Hence, it is very possible that the observed resistance is linked to the decreased expression (two-fold would be enough) of a carbenicillin high affinity-porin of the outer membrane like OmpF, as suggested in this text and in Chapter 2. Therefore, transcriptomics should be performed to the PurA^{L75D}, PurM^{F105A} and HisF^{V126P} mutants to investigate this hypothesis, since both metabolomics and proteomics failed to give a definitive answer to the originally asked question.

Bibliography

1.   Donati, S. *et al.* Multi-omics Analysis of CRISPRi-Knockdowns Identifies Mechanisms that Buffer Decreases of Enzymes in *E. coli* Metabolism. *Cell Systems* **12**, 56-67.e6 (2021).

2.   Rodionova, I. A. *et al.* Identification of a transcription factor, PunR, that regulates the purine and purine nucleoside transporter punC in *E. coli*. *Commun Biol* **4**, 991 (2021).

3.   Kanehisa, M. & Goto, S. KEGG: kyoto encyclopedia of genes and genomes. *Nucleic Acids Res* **28**, 27–30 (2000).

4.   Helmstaedt, K., Krappmann, S. & Braus, G. H. Allosteric Regulation of Catalytic Activity: *Escherichia coli* Aspartate Transcarbamoylase versus Yeast Chorismate Mutase. *Microbiol Mol Biol Rev* **65**, 404–421 (2001).

5.   Lee, A. J. *et al.* Robust, linear correlations between growth rates and β-lactam-mediated lysis rates. *Proc Natl Acad Sci U S A* **115**, 4069–4074 (2018).

6.   Cho, H., Uehara, T. & Bernhardt, T. G. Beta-Lactam Antibiotics Induce a Lethal Malfunctioning of the Bacterial Cell Wall Synthesis Machinery. *Cell* **159**, 1300–1311 (2014).

7.   Traxler, M. F. *et al.* The global, ppGpp-mediated stringent response to amino acid starvation in *Escherichia coli*. *Molecular Microbiology* **68**, 1128–1148 (2008).

8.   Gourse, R. L. *et al.* Transcriptional Responses to ppGpp and DksA. *Annu. Rev. Microbiol.* **72**, 163–184 (2018).

9.   Clark, D. P. The fermentation pathways of *Escherichia coli*. *FEMS Microbiol Rev* **5**, 223–234 (1989).

10.   Boecker, S. *et al.* Deciphering the physiological response of *Escherichia coli* under high ATP demand. *Mol Syst Biol* **17**, e10504 (2021).

11.   Russell, J. B. & Diez-Gonzalez, F. The effects of fermentation acids on bacterial growth. *Adv Microb Physiol* **39**, 205–234 (1998).

12.   Yoshida, T., Qin, L., Egger, L. A. & Inouye, M. Transcription Regulation of ompF and ompC by a Single Transcription Factor, OmpR. *Journal of Biological Chemistry* **281**, 17114–17123 (2006).

13.   Prajapati, J. D., Kleinekathöfer, U. & Winterhalter, M. How to Enter a Bacterium: Bacterial Porins and the Permeation of Antibiotics. *Chem. Rev.* **121**, 5158–5192 (2021).

14.   Fan, Y. *et al.* Heterogeneity of Stop Codon Readthrough in Single Bacterial Cells and Implications for Population Fitness. *Mol Cell* **67**, 826-836.e5 (2017).

15.   Baba, T. *et al.* Construction of *Escherichia coli* K-12 in-frame, single-gene knockout mutants: the Keio collection. *Mol Syst Biol* **2**, (2006).

16.   Mateus, A. *et al.* Transcriptional and Post-Transcriptional Polar Effects in Bacterial Gene Deletion Libraries. *mSystems* **6**, e0081321 (2021).

17.   Dwyer, D. J., Collins, J. J. & Walker, G. C. Unraveling the physiological complexities of antibiotic lethality. *Annu Rev Pharmacol Toxicol* **55**, 313–332 (2015).

18.   Belenky, P. *et al.* Bactericidal Antibiotics Induce Toxic Metabolic Perturbations that Lead to Cellular Damage. *Cell Reports* **13**, 968–980 (2015).

19.   Chapman, A. G., Fall, L. & Atkinson, D. E. Adenylate energy charge in *Escherichia coli* during growth and starvation. *J Bacteriol* **108**, 1072–1086 (1971).

20.   Swedes, J. S., Sedo, R. J. & Atkinson, D. E. Relation of growth and protein synthesis to the adenylate energy charge in an adenine-requiring mutant of *Escherichia coli*. *J Biol Chem* **250**, 6930–6938 (1975).

21.   Díaz-Pascual, F. *et al.* Spatial alanine metabolism determines local growth dynamics of *Escherichia coli* colonies. *eLife* **10**, e70794 (2021).

22.   Lennard, L. The clinical pharmacology of 6-mercaptopurine. *Eur J Clin Pharmacol* **43**, 329–339 (1992).

23.   Cuffari, C., Théorêt, Y., Latour, S. & Seidman, G. 6-Mercaptopurine metabolism in Crohn's disease: correlation with efficacy and toxicity. *Gut* **39**, 401–406 (1996).

24.   Bolton, E. T. & Mandel, H. G. The effects of 6-mercaptopurine on biosynthesis in *Escherichia coli*. *J Biol Chem* **227**, 833–844 (1957).

25.   Yang, J. H. *et al.* A White-Box Machine Learning Approach for Revealing Antibiotic Mechanisms of Action. *Cell* **177**, 1649-1661.e9 (2019).

26.   Silva, F., Queiroz, J. A. & Domingues, F. C. Evaluating metabolic stress and plasmid stability in plasmid DNA production by *Escherichia coli*. *Biotechnology Advances* **30**, 691–708 (2012).

27.   Jensen, K. F. The *Escherichia coli* K-12 'wild types' W3110 and MG1655 have an rph frameshift mutation that leads to pyrimidine starvation due to low pyrE expression levels. *J Bacteriol* **175**, 3401–3407 (1993).

28.   Grenier, F., Matteau, D., Baby, V. & Rodrigue, S. Complete Genome Sequence of *Escherichia coli* BW25113. *Genome Announc* **2**, e01038-14 (2014).

29.   Brown, S. D. & Jun, S. Complete Genome Sequence of *Escherichia coli* NCM3722. *Genome Announc* **3**, e00879-15 (2015).

30.   Scribano, M. L. & Prantera, C. Use of antibiotics in the treatment of Crohn's disease. *World J Gastroenterol* **19**, 648–653 (2013).

31.   Fredborg, M. *et al.* Automated image analysis for quantification of filamentous bacteria. *BMC Microbiol* **15**, 255 (2015).

32.   Wallace, M. J. *et al.* Discovery and Characterization of the Antimetabolite Action of Thioacetamide-Linked 1,2,3-Triazoles as Disruptors of Cysteine Biosynthesis in Gram-Negative Bacteria. *ACS Infect. Dis.* **6**, 467–478 (2020).

33.   Maier, L. *et al.* Extensive impact of non-antibiotic drugs on human gut bacteria. *Nature* **555**, 623–628 (2018).

34.   Cherepanov, P. P. & Wackernagel, W. Gene disruption in *Escherichia coli*: TcR and KmR cassettes with the option of Flp-catalyzed excision of the antibiotic-resistance determinant. *Gene* **158**, 9–14 (1995).

35.   García-Nafría, J., Watson, J. F. & Greger, I. H. IVA cloning: A single-tube universal cloning system exploiting bacterial In Vivo Assembly. *Sci Rep* **6**, 27459 (2016).

36.   Cetnar, D. P. & Salis, H. M. Systematic Quantification of Sequence and Structural Determinants Controlling mRNA stability in Bacterial Operons. *ACS Synth. Biol.* **10**, 318–332 (2021).

37.   Naville, M., Ghuillot-Gaudeffroy, A., Marchais, A. & Gautheret, D. ARNold: A web tool for the prediction of Rho-independent transcription terminators. *RNA Biology* **8**, 11–13 (2011).

Material and methods:

Strains

The non-edited control strain and PurA[L75D] mutant were used to construct the Control *punC* STOP and PurA[L75D] *punC* STOP variants. Strain JW1652-1 Δ*punC* from the Keio collection[36] was used to construct the Control Δ*punC* and PurA[L75D] Δ*punC* strains. Strains *E. coli* BW25113 and *E. coli* NCM3722 were used for the 6-mercaptopurine experiments. One Shot™ TOP10 *E. coli* (Thermo Fisher #C404010) was used for intermediate cloning.

Cultivation media

Refer to Chapter 2. When needed, 6-Mercaptopurine monohydrate (Merck # 852678-1G-A) was supplemented to the culture medium at final concentration 25 µM.

Growth rate calculation

Refer to Chapter 2.

Metabolomics (non and dynamic)

Non-dynamic metabolomics presented in Figures 1a, 4d and 6c was performed as described in Chapter 2. The dataset presented in Figure 1a is the same as in Chapter 2.

For dynamic metabolomics, strains were cultivated in 4 mL LB for 8 h at 37°C and 220 rotations per minutes (RPM) from glycerol stocks. LB precultures were used to inoculate shake flasks with 50 mL M9 medium and incubated overnight at 37°C and 220 RPM. The next day, OD_{600} of the pre-culture shake flasks was quantified and normalised to 0.25 if cells were in exponential phase (0.2-0.8). If necessary, cells were reinoculated in M9 medium to obtain exponentially growing cultures. The pre-culture shake flasks were then split into three shake flasks with each 10 mL of culture and carbenicillin was added at final concentration 50 µg/mL. Cells were incubated at 37°C and 220 RPM for one hour. Metabolites sampling was done 5 minutes, 30 minutes, and 1 hour after carbenicillin addition with the same method as previously described.

Proteomics measurement

Precultures in 4 mL LB were inoculated from glycerol stocks for 8h at 37°C 220 rpm shaking and transferred to M9 medium for overnight incubation at 37°C and 220 RPM. M9 pre-cultures in exponential phase were used to inoculate shake flasks containing 10 mL of M9 medium with a starting OD_{600} of 0.1. Strains were cultivated in triplicates until OD_{600} reached 0.25-0.6. An equivalent of $OD_{600} = 0.8$ was transferred to pre-chilled 2 mL tubes. Cells were centrifugated at maximum speed for 10 minutes at 4°C. Supernatant was discarded and pellets were resuspended with ice-cold PBS. This washing step was repeated and pellets were stored at -80°C until further processing.

For proteome measurement, *E. coli* cells pellets were resuspended in 300 µL lysis buffer (0.5% sodium lauroyl sarcosinate (SLS), 100 mM ammonium bicarbonate) and heated for 15 min at 90°C. Proteins were reduced with 5 mM Tris(2-carboxyethyl) phosphine (Thermo Fischer Scientific) at 90°C for 15 min and alkylated using 10 mM iodoacetamid (Sigma Aldrich) at 20°C for 30 min in the dark. The totally extracted protein material was digested with 1 µg of trypsin (Serva) at 30°C overnight. After digestion, SLS was precipitated by adding a final concentration of 1.5% trifluoroacetic acid (TFA, Thermo Fischer Scientific). Peptides were desalted by using C18 solid phase extraction cartridges (Macherey-Nagel). Cartridges were prepared by adding

acetonitrile (ACN), followed by equilibration with 0.1% TFA. Peptides were loaded on equilibrated cartridges, washed with 5% ACN and 0.1% TFA containing buffer and finally eluted with 50% ACN and 0.1% TFA, and finally dried. Dried peptides were reconstituted in 0.1% Trifluoroacetic acid and then analysed using liquid-chromatography-mass spectrometry carried out on a Exploris 480 instrument connected to an Ultimate 3000 RSLC nano and a nanospray flex ion source (all Thermo Scientific). Peptide separation was performed on a reverse phase HPLC column (75 µm x 42 cm) packed in-house with C18 resin (2.4 µm; Dr. Maisch). The following separating gradient was used: 98% solvent A (0.15% formic acid) and 6% solvent B (99.85% acetonitrile, 0.15% formic acid) to 35% solvent B over 30 minutes at a flow rate of 300 nl/min. MS raw data was acquired on an Exploris 480 (Thermo Scientific) in data independent acquisition mode with a method adopted from [41]. In short, Spray voltage were set to 2.0 kV and heated capillary temperature at 275 °C. For DIA experiments full MS resolutions were set to 120.000 at m/z 200 and full MS, AGC (Automatic Gain Control) target was 300% with an IT of 50 ms. Mass range was set to 350–1400. AGC target value for fragment spectra was set at 3000%. 45 windows of 14 Da were used with an overlap of 1 Da. Resolution was set to 15,000 and IT to 22 ms. Stepped HCD collision energy of 25, 27.5, 30 % was used. MS1 data was acquired in profile, MS2 DIA data in centroid mode.

Analysis of DIA data was performed using DIA-NN version 1.8 [42] with a *E. coli* uniprot protein database. Full tryptic digest was allowed with two missed cleavage sites, and oxidized methionines and carbamidomethylated cysteins. Match between runs and remove likely interferences were enabled. The neural network classifier was set to the single-pass mode, and protein inference was based on genes. Quantification strategy was set to any LC (high accuracy). Cross-run normalization was set to RT-dependent. Library generation was set to smart profiling. DIA-NN outputs were further evaluated using the SafeQuant[43,28] script modified to process DIA-NN outputs.

Statistical analysis

Refer to Chapter 2.

Quantification of mRNA with qPCR

Sampling of RNA was performed with the same method as indicated for proteome sampling. However, 1 OD_{600} was sampled and PBS washing was not performed. Cell pellets were directly stored at -80°C until further processing.

RNA isolation was performed using the Quick-RNA Fungal/Bacterial Miniprep Kit (Zymo Research # R2014). RNA concentration and purity were then quantified using a NanoDrop (Thermo Fisher). A total of 5 µg of RNA was then diluted in ddH2O for each sample and subjected to DNAse digestion using DNAse I (Roche # 05952077103) and RNasin (Promega # N2511). RNA was then amplified with qPCR using the QuantiFast SYBR® Green RT-PCR Kit (Qiagen # 204156) and the following primers:

qPCRrplRFw: 5' - GGACACGACCATGATATTGG – 3'

qPCRrplRRev: 5' – TCTGGTAGCTGCTTCTACTG – 3'

qPCRpunCFw: 5' - GTTTCTGATTGGTGGTTATGG – 3'

qPCRpunCRev: 5' - AGGGTAGATCGCGCCATTG – 3'

Levels of *punC* mRNA were normalised by the levels of *rplR* mRNA for each sample.

Cloning of *punC* deletion strains (Δ*punC* and *punC*-STOP)

To generate the Control Δ*punC* and PurA[L75D] Δ*punC strains,* the kanamycin cassette of strain JW1651-1 Δ*punC* was cured by transforming pCP20 using electroporation[34]. Colonies were picked and cultivated for 20 h in LB medium at 43°C. Strains were then streaked on LB agar with no antibiotics and incubated overnight at 43°C. Multiple colonies were then picked and streaked on LB agar with either kanamycin, carbenicillin or no antibiotics, and incubated at 37°C overnight. Colonies with no resistance against carbenicillin and kanamycin and visible on LB agar were picked for colony PCR of the *punC* gene. PCR amplicons were sent for sequencing and strains harbouring the FRT scars and absence of the kanamycin resistance cassette were cultivated and stored at -80°C for further editing using the CRISPR-based genome editing method as described above.

Cloning of the Control - *punC* STOP and PurA[L75D] - *punC* STOP was performed using the same CREATE methodology as presented in Chapter 1 and 2. The non-edited

control strain and PurA^{L75D} mutants were transformed with pTS55, which is identical to pTS40 but with a spectinomycin resistance cassette. The pTS55 plasmids were assembled using the same cloning method as for assembling pTS40 plasmids. Oligonucleotide sequences contained a *punC* protospacer (5'-AGAGAATATACATGCAACCT-3') and a homology arm for the *punC* genomic region of *E. coli* BW25113 with STOP codons insertions at second residue and mutation to STOP codon at eleventh (after insertion, TGG→TGA) residue of the *punC* protein. Transformants were selected on LB agar plates with chloramphenicol, spectinomycin and aTc.

Cloning or pTS40-p10X plasmids

The plasmids pTS40-p10X variants were cloned by assembling multiple DNA sequences of various origins. The coding sequence of *punC* (spanning from native RBS to terminator; 1734156 bp to 1735523 bp of BW25113 genome) was amplified from the genome of *E. coli* BW25113 and subsequently inserted into pTS40 using IVA cloning[35]. Native RBS and terminators were respectively identified using RBS calculator[36] and ARNold[37]. Terminator sequence TL3 was amplified from pTS41 and inserted downstream of the *punC* STOP codon in pTS40. Then, promoters were added upstream of the *punC* coding sequence using IVA cloning. RBS sequence BBa_0034 was added in replacement of the *punC* native RBS.

Agar dilution assays

Refer to Chapter 2. Spot assays for ROS testing were done using M9 agar supplemented with liquid H_2O_2 (Sigma-Aldritch # H1009).

Broth dilution assays

Precultures in 4 mL LB were inoculated from glycerol stocks for 8 h at 37°C 220 RPM shaking and transferred to M9 medium for overnight incubation at 37°C and 220 RPM. M9 pre-cultures in exponential phase were used to inoculate 96-well plates at starting OD_{600} <0.05. Carbenicillin was added to the cultivation medium at concentration 25 μg/mL when needed. 6-MP was also added at concentrations ranging from 6.25 μM to 100 μM following a dilution gradient. Incubation was performed for 24 h at 37°C. Various plate readers were used (BioTek Epoch, and Tecan Infinite 200 Pro). Therefore, OD_{600} values were corrected based on former calibration experiments.

Supplements

Strain	25 µM 6-MP	Growth rate (h^{-1})
Control	-	0,52 ± 0,0021
Control	+	0,41 ± 0,027
E. coli BW25113 WT	-	0,49 ± 0,009
E. coli BW25113 WT	+	0,43 ± 0,012
E. coli NCM3722 WT	-	0,56 ± 0,014
E. coli NCM3722 WT	+	0,51 ± 0,03

Table 1: Growth rates values as shown in Figure 6e

BiGG	Metabolite name	BiGG	Metabolite name
23dhbzs	2,3-dihydroxybenzoylserine	glc-D	D-Glucose
23dhmp	(R)-2,3-Dihydroxy-3-methylpentanoate	gln-L	L-Glutamine
26dap-LL	LL-2,6-Diaminoheptanedioate	glu-L	L-Glutamate
2ippm	2-Isopropylmaleate	gly	Glycine
3c3hmp	3-Carboxy-3-hydroxy-4-methylpentanoate	glyc3p	Glycerol 3-phosphate
3c4mop	3-Carboxy-4-methyl-2-oxopentanoate	gmp	GMP
4abut	4-Aminobutanoate	gsn	Guanosine
4hbz	4-Hydroxybenzoate	gthox	Oxidized glutathione
5mta	5-Methylthioadenosine	gthrd	Reduced glutathione
5mthf	5-Methyltetrahydrofolate	gtp	GTP
accoa	Acetyl-CoA	gua	Guanine
acmum	N-Acetylmuramate	his-L	L-Histidine
acorn	N2-Acetyl-L-ornithine	histd	L-Histidinol
acptrc	N-Acetylputrescine	hom-L	L-Homoserine
acser	O-Acetyl-L-serine	hxan	Hypoxanthine
actp	Acetyl phosphate	idp	IDP

ade	Adenine	imp	IMP
adn	Adenosine	ins	Inosine
adp	ADP	mal-L	L-Malate
ahcys	S-Adenosyl-L-homocysteine	met-L	L-Methionine
air	5-amino-1-(5-phospho-D-ribosyl)imidazole	nad	Nicotinamide adenine dinucleotide
alaala	D-Alanyl-D-alanine	nadp	Nicotinamide adenine dinucleotide phosphate
ala-L	L-Alanine	nadph	Nicotinamide adenine dinucleotide phosphate - reduced
amet	S-Adenosyl-L-methionine	orot	Orotate
amp	AMP	pep	Phosphoenolpyruvate
arg-L	L-Arginine	phe-L	L-Phenylalanine
argsuc	N(omega)-(L-Arginino)succinate	pheme	Protoheme
asn-L	L-Asparagine	pnto-R	(R)-Pantothenate
asp-L	L-Aspartate	ppcoa	Propanoyl-CoA
atp	ATP	prbatp	1-(5-Phosphoribosyl)-ATP
cbasp	N-Carbamoyl-L-aspartate	pro-L	L-Proline
cit	Citrate	pser-L	O-Phospho-L-serine
citr-L	L-Citrulline	pyam5p	Pyridoxamine 5-phosphate
cmp	CMP	pydam	Pyridoxamine
coa	Coenzyme A	ribflv	Riboflavin
csn	Cytosine	ru5p-D	D-Ribulose 5-phosphate
ctp	CTP	ser-L	L-Serine
cytd	Cytidine	sucarg	N2-Succinyl-L-arginine
dad-2	Deoxyadenosine	succ	Succinate
dann	7,8-Diaminononanoate	sucglu	N2-Succinyl-L-glutamate
dcamp	Adenylosuccinate	suchms	O-Succinyl-L-homoserine
dcmp	dCMP	trp-L	L-Tryptophan
dhap	Dihydroxyacetone phosphate	tyr-L	L-Tyrosine
dhor-S	(S)-Dihydroorotate	uacgam	UDP-N-acetyl-D-glucosamine
fad	Flavin adenine dinucleotide oxidized	udpg	UDPglucose
fdp	D-Fructose 1,6-bisphosphate	ump	UMP
fpram	2-(Formamido)-N1-(5-phospho-D-ribosyl)acetamidine	urea	Urea
gbbtn	gamma-butyrobetaine	utp	UTP
gdp	GDP	val-L	L-Valine
		xtsn	Xanthosine

Table 2: Metabolite abbreviations used in this chapter.

Conclusion of the thesis

The question asked at the beginning of this thesis was the following: **Do mutations in metabolic genes of *E. coli* have a general impact on antibiotic resistance?**

Across this thesis, it seems clear that metabolic mutations do not have a general effect on antibiotic resistance. Instead, metabolism-mediated resistance tends to be specific to each antibiotic.

The CRISPR library introduced in Chapter 1 has been very important for this thesis. Indeed, the thousands of metabolic mutants showed non-overlapping resistance phenotypes against either of carbenicillin or gentamicin in Chapter 2. The specificity of metabolic mutations was further demonstrated by showing that mutants resistant to gentamicin were not resistant to carbenicillin and vice-versa. Carbenicillin-resistant mutants were even sensitive to another β-lactam (meropenem). Most importantly, the metabolic mutations in the resistant mutants were shown to cause metabolic bottlenecks that are responsible for the observed resistance phenotype.

As re-cloned resistant mutants were successfully proven to be resistant toward their respective antibiotics, the CRISPR screen results could be used with confidence to adopt more general conclusions. The screen notably informed that low and reduced fitness does not confer a general advantage against carbenicillin or gentamicin. This was further tested by using a slow-growth control mutant, and clearly exemplified by the high sensitivity of the carbenicillin resistant mutants against gentamicin despite their slow growth. Surely, slow growth did confer carbenicillin tolerance, hinting that both resistance and tolerance may involve different factors. Tolerance against gentamicin or other antibiotics was never tested which did not allow to explore this hypothesis further.

Nevertheless, the specific metabolism-antibiotic link is of high interest since a multitude of *E. coli* clinical isolates were shown to have various metabolic bottlenecks. One of them, a UPEC strain (EC-249), has a *de novo* purine pathway metabolic bottleneck that conferred carbenicillin-sulbactam tolerance. However, EC-249 was unsuccessfully grown on agar medium, so its resistance could not be tested properly, indicating that the extrapolation of Chapter 2 results obtained from a laboratory *E. coli* strain (BW25113) to clinical *E. coli* strain was not trivial. Nevertheless, this study opens the

way to a myriad of possibilities for exploration of the role of metabolic bottlenecks in clinical bacterial isolates in antibiotic resistance.

For example, libraries of clinical *E. coli* isolates with metabolic mutations and an implemented barcoding system could be generated. Pooling these clinical barcoded strains and subjecting them to antibiotic treatments might furnish an even better picture than what was shown in Chapter 2. Ideally, much more antibiotics should be used than just carbenicillin and gentamicin, and focus should be made toward antibiotics used in the clinic, like the last resort β-lactams meropenem and imipenem. It is accepted that *in vitro* and *in vivo* cultivation conditions are very different. Subjecting such library to a treatment in a gnotobiotic mice might also be very interesting, although new technical challenges may arise regarding the sampling of the strains and their identification.

Future studies must also investigate the mechanistic link between specific metabolic bottleneck and the antibiotic they confer resistance to. Since metabolic bottlenecks provide low-level resistance, it may be technically challenging to show this link, as demonstrated in Chapter 3. It is very possible that most metabolic mutations confer an advantage because of undirect consequences in antibiotic transport towards their targets. This might explain the specificity of metabolic bottlenecks, since transport may differ between antibiotics of the same of different classes, as demonstrated clearly by the differences of resistance phenotypes between carbenicillin, meropenem, and gentamicin.

As a conclusion, the author of this thesis thinks that the originally asked question was successfully answered and that this work provides exciting new opportunities to understand antibiotic resistance.